SPUTTERING OF INSULATORS IN THE ELECTRONIC STOPPING REGION

Thesis by

Joseph Edward Griffith

In Partial Fulfillment of the Requirements

for the Degree of

Doctor of Philosophy

California Institute of Technology

Pasadena, California

1979

(Submitted May 7, 1979)

For our knowledge is imperfect, and our prophecy is imperfect; but when the perfect comes, the imperfect will pass away. When I was a child, I spoke like a child, I thought like a child, I reasoned like a child; when I became a man, I gave up childish ways. For now we see through a glass darkly, but then face to face.

I Corinthians 13.9-12

ACKNOWLEDGMENTS

Many have made important contributions to this effort, but I have space to name only a special few. Foremost among them is Tom Tombrello, whose sound advice and unwavering support made it possible to push on through month after month of initially disappointing results. Don Burnett facilitated the track work through generous donations of time and equipment. A number of crucial ideas arose out of discussions with enthusiastic colleagues. Jon Melvin, Ziggy Switkowski, Pete Haff, Jim Mayer, Marc-A. Nicholet and John Poate all made useful suggestions.

Several students helped in the execution of the experiments. In performing the microprobe runs for me, Tim Benjamin and John Jones always gave more than was requested. Sharon Streight analyzed one of the sticking fraction runs for her senior thesis at Occidental College. Mari Weller graciously shared her expertise in helping with the Rutherford backscattering run. Bob Weller's contribution was profound. He participated fully in the sticking fraction, low energy yield and energy spectrum experiments, and I share all credit with him for these projects.

Finally, I dedicate this dissertation to my parents and my sister, whose love shaped this work by shaping me.

ABSTRACT

Using track detectors we have measured sputtering yields induced by MeV light ions incident on a uranium containing glass, UO_2 and UF_4. No deviation from the behavior predicted by the Sigmund theory was detected in the glass or the UO_2. The same was true for UF_4 bombarded with ^4He at 1 MeV and with ^{16}O and ^{20}Ne at 100 keV. In contrast to this, 4.75 MeV $^{19}F(+2)$ sputters uranium from UF_4 with a yield of 5.6 ± 1.0, which is about 3 orders of magnitude larger than expected from the Sigmund theory. The energy dependence of the yield indicates that it is generated by electronic rather than nuclear stopping processes. The yield depends on the charge state of the incident fluorine but not on the target temperature. We have also measured the energy spectrum of the uranium sputtered from the UF_4. Ion explosions, thermal spikes, chemical rearrangement and induced desorption are considered as possible explanations for the anomalous yields.

TABLE OF CONTENTS

TABLE OF CONTENTS (Cont.)

I. INTRODUCTION

A nonrelativistic charged particle passing through a solid loses energy in two ways. It may collide with individual electrons and thus experience what we call electronic stopping. Or it may undergo nuclear stopping by colliding with nuclei. The relative importance of the two mechanisms depends on the energy of the incident particle. Furthermore, the mechanism that dominates determines how the solid will dissipate the deposited energy.

At energies below a few tens of kilovolts nuclear stopping dominates. The incident particle collides with the nuclei via a screened Coulomb interaction, which results in very little electronic excitation. An atom struck by the particle is called a primary recoil. The primary recoil can itself be quite energetic, sometimes receiving many hundreds of electron volts. It collides with other atoms, which in turn collide with still more. Eventually, the kinetic energy of the primary recoil will be shared by a multitude of low energy atoms called a cascade. If the cascade is generated close enough to the surface of the solid some of these low energy atoms may reach it and escape into space. In that event, we say that the solid has been sputtered. The sputtering yield, S, is defined as the number of atoms that escape per incident particle. We speak loosely here: the escaping objects may not be atoms but molecules or ions. In addition, we may want to restrict our attention to only one type of atom in the solid and thus describe a partial sputtering yield. A widely used theory of sputtering based on this picture has been developed from neutron transport theory by Sigmund and his coworkers. It will provide the bench mark against which we will

compare the exotic forms of sputtering to be encountered later.

At higher energies the electronic stopping power begins to dominate and eventually becomes orders of magnitude larger than the nuclear stopping power. Much of the deposited energy serves to ionize the constituent atoms, producing energetic free electrons. The fraction ionized directly by the incident particle is called the primary ionization, J. For us, this will be the most important component of the electronic stopping power. Since electrons do not efficiently transfer momentum to nuclei, one might expect that little of the energy would appear as nuclear kinetic energy. In insulators, however, an extraordinary phenomenon sometimes appears.

Consider an insulator and an etchant that is capable of slowly dissolving it. For instance, mica and concentrated hydrofluoric acid are a combination we will encounter many times in what follows. If a particle with a sufficiently large ionization rate, such as a fission fragment, penetrates the mica it will leave in its wake a badly damaged lattice. We know this because the hydrofluoric acid will preferentially attack the region around the flight path thousands of times faster than it dissolves the undamaged lattice. After a few minutes of etching, a hole with a volume of several cubic microns will have formed around the flight path. Under an optical microscope the hole appears as a tiny track, which is what we call it.

The mechanism by which tracks form is still controversial. Experiments in which latent, unetched tracks are erased by high temperature annealing suggest that the atoms in the lattice have been violently jostled out of their original positions. Yet we said earlier

that little atomic movement is expected in the electronic stopping region. One attempt to resolve this dilemma is known as the ion explosion model, proposed by Fleischer, Price and Walker (1975). In it the ionized atoms remain charged long enough for Coulomb repulsion to propel them into interstitial positions. They suggest that in metals, which do not produce tracks, the electron refilling time is too short to allow the mechanism to take effect. Though we will discuss the model in more detail later, it will be useful mainly for heuristic purposes: precise calculations and reliable predictions are not yet possible.

In spite of the model's limitations, Peter Haff was able to use it to make a prediction (Haff 1976). He reasoned that if the ions do acquire considerable kinetic energy from Coulomb repulsion, then they should produce the same effect that the primary recoils produce in the nuclear stopping region. That is the ion explosion should generate a cascade, which should in turn produce a sputtering yield that may be exceptionally large. Furthermore, the behavior of the yield would differ drastically from that produced by the Sigmund mechanism. Haff sputtering would exhibit a peak in the electronic stopping region rather than in the nuclear stopping region, and it would appear only in insulators. At the time the prediction was made, no exceptionally high energy sputtering data for insulators existed, so we designed a series of experiments to test the hypothesis. This dissertation is a description of those experiments.

Experimental verification of the prediction might at first thought seem straightforward. It is not. One of the cardinal requirements for a correct sputtering measurement is that the sputtered surface

be atomically clean. Unfortunately, even at 10^{-9} torr many surfaces at room temperature will absorb a monolayer of gas from the residual atmosphere in which they sit. At low energies the sputtering action itself may be used to keep the surface clean if one employs a sufficiently intense beam. This trick does not work at the high energies necessary for testing the Haff hypothesis. At several MeV the beam carries so much heat that it will evaporate the target long before the sputtering rate becomes sufficient to clean the surface. As we shall see, that heat can be turned to our advantage if it is applied in a controlled manner to a restricted class of targets. Learning to do this properly required some trial and error; our initial attempts were not entirely successful. Nevertheless, the data from those early experiments are instructive and will be discussed in detail.

Our first experiments used targets consisting of soda-lime glass that had been doped with enriched uranyl nitrate. Two considerations motivated this choice. The first is that soda-lime glass is a well known track detector, which will produce tracks when irradiated with heavy ions as light as fluorine. Since fluorine was the beam we wanted to use, the glass was a natural choice. The second factor involves the method by which we detect the sputtered atoms. As reported in the thesis by Ron Gregg (1977), mica track detectors can be used to measure sputtering yields for targets containing ^{235}U. By adding a small amount of ^{235}U to the glass we hoped to monitor its sputtering behavior. Unfortunately, the data from this target quickly told us that surface contamination was

influencing the yield. Irradiations at relatively high beam currents revealed "sputtering yields" much smaller than anticipated by Haff. The complexity of the glass, however, made it difficult to interpret the results in an unambiguous way. For instance, electron microprobe studies of the beam spot indicated that the glass was losing large amounts of sodium due to excessive heating of the target. We corrected for this by reducing the beam current, which caused the yield to drop to unmeasurable levels. The beam current dependent yields were a strong indication that the cooler target surface was also a dirtier surface.

The contamination problem with the glass targets proved to be insurmountable, so we tried uranium oxide targets next. Though no one had ever seen tracks in uranium oxide, it has a relatively high resistivity, which suggested that it might exhibit the desired phenomenon. There are indications that surface contamination also had some influence on the uranium oxide yields, but the data are good enough to show that no mechanism of the type envisioned by Haff operates in it. This result was by no means conclusive since a loophole existed. After performing the experiment we learned that even small deviations from stoichiometry in uranium oxide can cause the resistivity to plummet (Ishii et al. 1970). Since we did not have precise control over the composition of our target, we had no assurance that the resistivity was actually high enough to allow the Haff mechanism to operate. For this reason we switched to uranium tetrafluoride targets.

Fluorine at 4.75 MeV sputters UF_4 with a yield three orders of magnitude larger than the Sigmund theory predicts. Furthermore,

the yield exhibits a peak in the electronic stopping region where the Sigmund theory says that it should be monotonically decreasing. The behavior of this target is especially fortuitous because UF_4 apparently does not tightly bind gas molecules to its surface. Consequently, gentle heating allowed us to overcome the contamination problem. The data show that the sputtering yield is independent of target temperature between 70°C and 170°C for pressures in the 10^{-9} torr range. This not only suggests that the target is free of contamination but also that if thermal spikes are producing the high yield, then the temperature of the spikes must be very high. The thermal spike model is one of several alternative explanations for the anomalously high yield. We will discuss them along with the Haff model in the next section.

Before proceeding to the theoretical part of this dissertation, we make one final note. In all of the sputtering experiments described here, the sputtered particles were collected on catcher foils. The sputtered particles impinge on the foil's surface with energies in the few eV range. To calculate the sputtering yield from the experiment one must know how many of the sputtered particles bounced off the catcher foil. Theoretical calculations are not yet feasible, so we measured the sticking fraction. Within the context of this thesis, it is needed only as a catcher foil calibration. The measurement is, however, important in its own right, so we will present a few results that extend beyond the immediate goal of determining uranium sputtering yields.

II. THEORY

The collision cascade of the Sigmund and Haff models is one of several mechanisms that can eject atoms from a surface under bombardment. Thermal spikes, stimulated desorption and chemical rearrangement are also conceivably capable of producing sputtering. Therefore, the deviation of the UF_4 sputtering yield from the Sigmund prediction does not in itself confirm Haff's hypothesis. Having found the enhanced yield, we had to design a set of experiments capable of discriminating among the various possibilities. To understand the strategies we adopted, one must know the essential characteristics of each candidate. In this section we will sketch those characteristics. Only the Haff model will be discussed in detail. At the end of this section we will present the standard statistical mechanical arguments that are applied to surface coverage phenomena, so the reader can understand the technique used to keep the target surface clean.

Since we have adopted the Sigmund theory as our bench mark, we now present the formulas necessary for calculating the sputtering yield in that theory. For derivations it is best to consult Sigmund's papers (1969 and 1972). We consider an incident particle with atomic number Z_1 and atomic mass A_1 impinging on a monatomic target with atomic number Z_2 and mass A_2. The target has number density N ($Å^{-3}$). We denote the surface binding energy by U (eV), which is usually taken to be the sublimation energy of the bulk material. The interaction of two Thomas-Fermi atoms is characterized by a screening radius,

$$a = a_o(.885)(Z_1^{2/3} + Z_2^{2/3})^{-1/2}$$

where a_o is the Bohr radius, .5292 Å. It is convenient to define a reduced energy,

$$\epsilon = \frac{aA_2 E}{Z_1 Z_2 e^2 (A_1 + A_2)}$$

where e is the electronic charge and E is the laboratory energy of the incident particle. In the Sigmund theory the sputtering yield is proportional to the nuclear stopping cross section, $S_n(\epsilon) = \int T d\sigma$ where σ is the cross section for a collision transferring energy T to the struck particle. A compact empirical fit to some results from the Lindhard theory of stopping has been given by Winterbon et al. (1970):

$$S_n(\epsilon) = \frac{9}{8\epsilon}[\ln(x+r) - x/r]$$

where $r = (1+x^2)^{1/2}$, $x = (2\lambda'\epsilon^{4/3})^{1/3}$ and $\lambda' = 1.309$. This is related to the nuclear stopping power, $\left.\frac{dE}{dX}\right|_n$, by (Lindhard et al. 1968)

$$\left.\frac{dE}{dX}\right|_n = 4\pi \frac{N a Z_1 Z_2 e^2 A_1}{A_1 + A_2} S_n(\epsilon) .$$

Finally, Sigmund expresses the sputtering yield with the formula

$$S(E) = \frac{.042\ \text{Å}^{-2}}{U} \alpha(A_2/A_1) \frac{1}{N} \left.\frac{dE}{dX}\right|_n \frac{1}{\cos\psi} \qquad (2.1)$$

where ψ is the angle of the beam with respect to the target normal, and the dimensionless function $\alpha(A_2/A_1)$ is given by Andersen and Bay (1975). The α function is independent of ϵ only for $\epsilon < 1$,

where the electronic stopping is negligible (Sigmund et al. 1971). At energies corresponding to $\epsilon > 10$, the behavior of α is poorly understood.

A simple prescription for treating binary targets has been developed by Haff and Switkowski (1976). Suppose the target consists of two types of atoms, a and b, with abundances n_a and n_b such that $n_a + n_b = 1$. Then the sputtering yield of a, $S_{\overline{ab}}$, is expressed

$$S_{\overline{ab}} = n_a(n_a S_a + n_b S_b)$$

where S_a and S_b are calculated from Eq. 2.1. The expression for $S_{a\overline{b}}$ is similar. Their analysis applies only if the atoms leave the surface individually. If the sputtered particles appear as molecules or molecular fragments, then the expression would need to be modified.

Sigmund's theory also makes precise predictions concerning the energy spectrum of the sputtered particles. The spectrum, which is common to all collision cascade models including Haff's, is distinctly different from those of the other mechanisms we will consider. It peaks at one half the surface binding energy and falls as E^{-2} at high energies. A typical example of such a spectrum is shown in Fig. 1 taken from R.A. Weller's thesis (1978). In our discussion of the Haff model, we will present an explicit functional form for the energy spectrum.

The crucial difference between the Sigmund and Haff models is in the mechanism that initiates the cascade. Recall that in the electronic stopping region most of the energy lost by an incident ion is

deposited directly into the electrons. Many of these electrons are excited into continuum states, leaving behind ions in the lattices. This situation can generate an ion explosion if two conditions are fulfilled. First, enough ions must be produced so that most of them have an ionized neighbor. This establishes a strong electrostatic potential between the ions, which will, if given time, convert into kinetic energy. The second condition is that the free electrons in the target do not recombine with the ions so quickly that they do not have enough time to start moving. The time required is believed to be about 10^{-14} seconds. Apparently, this refilling time is controlled by the bulk resistivity of the material, since tracks form only in materials with high electrical resistivity ($\rho \geq 2000$ Ω-cm) (Fleischer et al. 1975). Thus, we do not expect to see deviations from the Sigmund prediction due to this mechanism at high incident energies in metals and semiconductors.

The method by which Haff made these notions precise is a derivative of the theoretical approach to sputtering taken by Thompson (Thompson 1968 and Haff 1976a). We begin with an equation from Thompson's paper. Let $\Phi(E,\theta)$ be the flux of particles emerging from the sputtered surface with energy E and angle θ with respect to the surface normal. If the incoming beam is perpendicular to the surface, then we have

$$\Phi(E,\theta) = \frac{d\cos\theta}{4\pi(1+U/E)^3 E^2}\,\eta \int_{E+U}^{\infty} E_a\, q(E_a)\, dE_a$$

where d is the interatomic spacing and U is the surface binding energy. A detailed discussion of the factors in the integral can be

found in Thompson's paper. We merely need to know that the integral expresses the energy deposited as primary recoils by the beam per unit time per unit volume. The factor η, which is approximately 0.5, is the efficiency with which that energy is converted into displacement damage. Haff replaces η times the integral with $f\ \overline{\Delta E}/\lambda_b$ where f is the incident flux, $\overline{\Delta E}$ is the average energy of a primary recoil and λ_b is the mean free path to produce a primary recoil. Now $\Phi(E,\theta)/f$ is the sputtering yield,

$$S(E,\theta) = \frac{d}{\lambda_b} \frac{\overline{\Delta E}}{(1+U/E)^3 E^2} \frac{\cos\theta}{4\pi} .$$

This expression explicitly displays the energy spectrum and the angular distribution of the sputtered particles produced by a collision cascade. If we integrate over E, we get

$$S(\theta) = \frac{d}{\lambda_b} \frac{\overline{\Delta E}}{2U} \frac{\cos\theta}{4\pi}$$

and integration over $d\Omega$ gives

$$S = \frac{1}{8} \frac{d}{\lambda_b} \frac{\overline{\Delta E}}{U} .$$

So far, we have made no assumption concerning how $\overline{\Delta E}$ is transferred to a primary recoil. The formula applies to both the Sigmund and Haff mechanisms, and it is the manner in which $\overline{\Delta E}$ is computed that distinguishes the two approaches. Haff takes $\overline{\Delta E}$ to be the kinetic energy produced by the Coulomb repulsion between two ions sitting side by side in the lattice. If the two ions have the same mass, then each acquires $\frac{1}{2}\overline{\Delta E}$. Haff also requires that exactly one pair is produced per lattice spacing, which implies that

$\lambda_b = \frac{d}{2}$. Realistically, one expects the number of ions per lattice spacing to vary with J. If one allows this number to float with J, however, difficulties arise in attempting to calculate the average charge $\overline{\Delta n}$ of each ion. So we have

$$S = \frac{1}{8} \frac{\overline{\Delta E}}{U} \tag{2.2}$$

for a beam incident perpendicular to the surface. To calculate $\overline{\Delta E}$ we take

$$\overline{\Delta E}(R(t_e)) = (\overline{\Delta n}\ e)^2 \left(\frac{1}{d} - \frac{1}{R(t_e)}\right) \tag{2.3}$$

where $R(t_e)$ is the distance between the ions when the electronic refilling quenches the process. $\overline{\Delta n}$ is fixed at

$$\overline{\Delta n} = \frac{d}{2} \frac{J}{\overline{T}} \tag{2.4}$$

where $\overline{T}$ is the average energy expended by the incident particle to produce a free electron. This formula for $\overline{\Delta n}$ is a manifestation of Haff's demand that exactly two ions be formed per lattice spacing. Implicit in this assumption is the existence of a threshold: we must have $J \geq \overline{T}/d$ to trigger the explosion. It suggests that light ions may never have sufficient ionizing power to induce this type of sputtering, just as they are incapable of forming tracks in many insulators. Substituting Eq. 2.3 and Eq. 2.4 into Eq. 2.2 we get

$$S = \frac{1}{32} \frac{e^2}{U} \left(\frac{1}{d} - \frac{1}{R(t_e)}\right) \frac{d^2}{\overline{T}^2} J^2 \tag{2.5}$$

At this point it is instructive to estimate some of the numbers predicted by these equations. The functional dependence of J^2

with respect to energy is shown in Fig. 2. But the magnitude of J is not well known, so we estimate it by setting $J = dE/dx\big|_e$. J will be discussed in greater detail below. For 5 MeV ^{19}F incident on UF_4, $\frac{dE}{dx}\Big|_e \approx 300$ eV/Å. We take $T = KZ_t$, where K is the Bloch constant (≈ 10 eV) and $\overline{Z}_t$ is the average atomic number of the target. For this case, $\overline{T} = 256$ eV. In UF_4 the U-F bond length is 2.3 Å (Larson et al. 1964), which is the value we will use for d. Substituting these numbers into Eq. 2.4 gives

$$\overline{\Delta n} = 1.4 \ .$$

To estimate $\overline{\Delta E}$ we set $R(t_e) = \infty$, which implies

$$\overline{\Delta E} = 11 \text{ eV} \ .$$

One worries that this is rather low relative to the displacement energy of an atom in the lattice. Haff suggests that the high degree of excitation in the neighborhood of the ion reduces the displacement energy considerably. Nevertheless, the primary recoil energies cannot be much greater than the lattice binding energies. One likely consequence of this is a significant distortion of the energy spectrum above a few electron volts; it would fall off more rapidly than our equations predict. Furthermore, sputtered particles would be produced only by events occurring very close to the surface, and the behavior of those particles would be strongly influenced by the structure of the crystal lattice at the surface. Finally, taking U = 3 eV, which is the sublimation energy, we get

$$S = 0.5 \text{ at } 5 \text{ MeV} \ .$$

This value should be considered a lower bound, because it is possible

that the excitation in the lattice also reduces the surface binding energy. A reduction in the surface binding energy not only increases the predicted yield but also shifts the peak in the energy spectrum.

According to Eq. 2.5, the dependence of S on the energy is determined by J, which we take to be $\overline{Z}^2 J_p$. $\overline{Z}$ is the effective charge of the incident ion, and J_p is the primary ionization rate of a bare proton. For $\overline{Z}$ we use an expression due to Heckman et al. (1963):

$$\overline{Z} = Z\left[1 - 10^{-\frac{1}{3}(137\beta/Z^{0.55})}\right]$$

Z being the ion's atomic number and $\beta = v/c$. We display $\overline{Z}$ for fluorine in Fig. 3. Reliable theoretical estimates for J_p are not available, since the energy regime of interest is well below that in which the Born approximation is valid. Experimentally determined ionization cross sections for protons and electrons in various gases are available from the work of Schram et al. (1965 and 1966) and De Heer et al. (1966). All of the ionization curves have roughly the same shape, so we have arbitrarily chosen the argon data as an illustration. The electron data have been scaled to the proton energy equivalent to the electron's velocity: $E_p = \frac{m_p}{m_e} E_e$ where E_p = protron energy, E_e = electron energy, m_p = proton mass and m_e = electron mass. The data can be fit to a curve of the form

$$J_p = \frac{A}{E_p} \ln(BE_p) .$$

A least square analysis gives $B = 4.5 \times 10^{-3}$/keV. In Fig. 4 we compare the functional form to the data, and in Fig. 5 we show $\overline{Z}^2 J_p$. The Haff model predicts that the sputtering yield should

follow J^2 if the incident ion strikes the surface in the equilibrium charge state. In practice, the ion usually enters the solid with a charge that may be two to four units below the equilibrium value. The path length needed to equilibrate the ion's charge is not known. But if it exceeds a few monolayers, the yield will be reduced because the ion explosions occurring close to the surface have the strongest influence on the yield. Furthermore, S should increase as the charge state of the incident beam increases.

The ion explosion's dependence on the electronic component of the stopping power sharply differentiates it from the Sigmund mechanism. That contrast does not necessarily exist, however, between the ion explosion and thermal spike models. Thermal spikes have been theoretically linked to both the nuclear stopping power and the electronic stopping power. The former mechanism has been most actively pursued by Kelly (1977), while the latter has been recently explored by Davies et al. (1979) in frozen gas targets. In essence, they argue that the energy of a primary recoil, whether it be an entire atom or an individual electron, eventually degrades to an energy distribution approximating thermal equilibrium in a small region around the incident ion's path. The spike is believed to reach quasi-equilibrium in about 10^{-11} seconds. The elevated temperature produced at the target surface, which could be as high as $10,000^{\circ}K$, allows some of the atoms to evaporate. Unfortunately, severe problems arise when one attempts to theoretically estimate the sputtering yield. Little is known about the thermal conductivity in the excited region. Even less is known about the spatial distribution of the deposited energy, making it difficult to calculate the

temperature at the surface. Due to these limitations we will make only a few qualitative statements on thermal spike behavior.

At the core of most thermal spike models lies the assumption that the flux of sublimed atoms can be described by simple kinetic theory coupled with the Clausius-Clapeyron expression for the vapor pressure. Thus, S is proportional to $\exp(U/kT)/T^{\frac{1}{2}}$, where T is the sum of the target temperature and the temperature increase due to the spike. U is the sublimation energy as before. The dependence on the initial target temperature can be very strong within a few hundred degrees of the melting point of the target. Furthermore, the sputtered atoms exhibit an energy distribution characteristic of an equilibrated Maxwell-Boltzman gas: $S(E) \propto E^{\frac{1}{2}}\exp(-E/kT)$, where E is the energy of the sputtered atom. This distribution has been seen in the sputtering of gold at high temperatures by Chapman et al. (1972). The angular distribution would be proportional to $\cos\theta$ irrespective of the direction of the incident beam. Unfortunately, no precise statement can be made concerning the dependence of S on the stopping power.

Another potential sputtering mechanism, which follows the electronic stopping power, is known as stimulated desorption. The mechanism we have in mind is an analogue of the Frank-Condon process used to describe the dissociation of molecules. Fig. 6 illustrates it. An atom or molecule on the surface of the target is promoted from its ground state to an antibonding state or an excited bonding state. If the final energy is greater than the zero energy of the final state, then the potential of the final state will propel the

particle out to infinity. The energy distribution of the desorbed particles will depend on the shapes of the initial wavefunction and the final potential curve. Energies up to several electron volts are possible. Since this is a purely surface phenomenon, it would be sensitive to the initial charge state of the incident ion. It would not, however, be sensitive to the mass of the incident particle: energetic electrons initiate this process with high efficiency (Menzel 1975).

The final mechanism we consider is chemical sputtering. This contingency could arise in the UF_4 targets, because uranium is known to form several different fluorides. Presumably, the new molecule would appear due to the disruption and rearrangement caused by the incident ion. After migrating to the surface, it would escape into space with low energy. Chemical effects could also enhance other mechanisms if they tended to change the stoichiometry at the surface by preferentially removing either uranium or fluorine. The least ambiguous way to test for chemical sputtering is to look at the sputtered particles with a mass spectrometer to see if the yield is dominated by a single molecular species. In lieu of that, anomalous sputtering behavior in the nuclear stopping region, which normally would be adequately described by the Sigmund theory, is the most likely indicator of chemically induced erosion.

In the next section we will describe the apparatus used to explore the mechanisms that produce sputtering in the electronic stopping region. As explained in the introduction, working in this energy regime poses some problems. In particular, we had to adopt a new

approach to maintaining a clean surface. The technique used was motivated by certain general properties of the adsorption isotherms that describe the coverage of a surface equilibrated with a gas at pressure p and temperature T. As a concrete example, we will consider the Langmuir isotherm, which is applicable to localized adsorption of monatomic gases at up to one monolayer coverage. Derivations can be found in Hill (1960).

Let $\theta(p, T)$ be the fraction of the surface covered, where $0 < \theta < 1$. For the Langmuir isotherm we have

$$\theta(p, T) = \frac{\chi(T)p}{1+\chi(T)p}$$

where $\chi(T) = q(T)e^{-U/kT}e^{\mu^{\circ}(T)/kT}$ $(U<0)$. $\mu^{\circ}(T)$ is the chemical potential of the gas, and $q(T)$ is the partition function for an atom in a three-dimensional harmonic oscillator well. The factor $\exp(-U/kT)$ is common to all isotherms. It arises from the requirement that we have a consistent energy scale for both the atom at infinity and the atom in the potential well at the surface. Thus, when we calculate the partition function of the bound atom, we must add the surface binding energy U to the bound state energies so as to place zero energy at the top of the well. If U is small enough ($\lesssim$ 1eV), this factor supplies us with a powerful lever with which we can pry contaminant molecules from the surface. At very low pressures, θ is approximately proportional to $p \exp(-U/kT)$. Under the right conditions we gain far more by heating the target than by improving the vacuum.

Unfortunately, we cannot explicitly calculate the surface coverage

in our experiment, because we do not know the binding energies of the most common contaminants (H_2 and CO) to the targets we will use. In addition, we have none of the standard surface analysis tools, so we must fall back on more general arguments. The technique we will adopt in the UF_4 experiments will be to measure the sputtering yield as a function of target temperature. The isotherm tells us how the yield should behave. At low temperature, the surface will probably be contaminated, so S will be low. As the temperature increases, the surface will become cleaner so that S will rise until the surface contamination is negligible. For the clean surface, S should be constant with temperature (if the sputtering mechanism allows) until the temperature becomes high enough for thermal spike effects to set in. This behavior is demonstrated in Fig. 7 for several different pressures. The argument must be used with great care, because a pitfall exists. One of the contaminants could bind so tightly to the surface that it does not come off until the target begins to evaporate. To check for this we can perform some low energy sputtering experiments on the targets so that sputter cleaning can be used. The low energy runs will allow us to compare yields obtained from a heat cleaned target with those from a sputter cleaned target. If the results agree, then we can be certain that the heated target is clean.

III. EXPERIMENTS

A. GENERAL TECHNIQUES

The experiments we performed in our exploration of high energy sputtering fall into four types. Fig. 8 illustrates them schematically. We began with high energy yield measurements in which the sputtered uranium atoms were collected on cylindrical aluminum catcher foils. To check for target surface contamination, we performed some low energy yield measurements using the same catcher foil configuration. To calibrate the catcher foils, we measured sticking fractions using a double catcher arrangement in which some sputtered uranium atoms bounced off a primary foil onto a cylindrical secondary foil. Finally, we measured the energy distribution produced by our high energy mechanism with the apparatus developed by R.A. Weller (1978). In the next few sections we will discuss some general features of these experiments. We begin by describing the vacuum chambers and accelerators used in the irradiations.

1. Hardware

We used the Caltech tandem accelerator to perform the high energy measurements. In most of the runs, we employed ^{19}F beams with energies from 1.16 MeV to 28.5 MeV and charge states ranging from +2 to +5. Stable beam currents between 1 nanoamp and 1 microamp were readily obtainable. In two additional runs, we used ^{4}He beams at energies from 0.5 MeV to 2.0 MeV. The energies were determined by a 90^{o} bending magnet coupled with an Alpha Scientific, Inc. Model 3193 NMR gaussmeter, which allowed us to set beam energies accurate to within a few kilovolts. The

beams for the low energy experiments were provided by a 150 kV duoplasmatron ion source. The beam energy is determined by the potential produced with a Deltaray Model L150-5-ARD power supply. This power supply was calibrated by R.A. Weller in 1975 using a precision voltage divider. Because no calibrations have been performed since then, we do not claim to know the energy to better than 5%. Fortunately, the experiments performed with the 150 kV ion source do not require extremely accurate beam energies.

The beam lines for both accelerators were kept at pressures between 10^{-6} torr and 10^{-7} torr with oil diffusion pumps. The liquid nitrogen cold traps above these pumps were filled a few hours before each run to minimize the hydrocarbon partial pressure. Even so, the vacuum was very dirty relative to the conditions that had to be maintained in the target chamber. To isolate the targets from this dirty vacuum, a liquid nitrogen cooled in-line cold trap 16" long and with 7/16" inner diameter was placed between the beam line and the ultrahigh vacuum (UHV) system containing the target. Furthermore, a copper or gold seal straight-through valve was used to completely isolate the UHV chamber from the rest of the system except when beam was on target. With the straight-through valve closed, base pressures better than 10^{-9} torr were usually obtained. Typical pressures during the runs were about 10^{-8} torr, though this did depend somewhat on the type and intensity of the beam, which was the main gas load on the system.

Several different target chamber configurations were used during the experiments. We defer until later discussion of the specific

details. At this point we will discuss the components, which were used as a mix-and-match ensemble to construct the chambers. For a detailed discussion of our ultrahigh vacuum technique, the reader should consult the thesis by Ron Gregg (1977).

The vacuum pumps were the heart of each system, and the chambers were designed around them so as to minimize the pumping impedance between pump and target. Two of the pumps were titanium sublimation pumps. The first was a small Varian model rated at 50 l/s, while the second was a 500 l/s Ion Equipment COV-500. The latter was supplemented with a 25 l/s ion pump, which is the second type of pump we used. In addition to the 25 l/s pump, we had an 11 l/s Ultek D-I ion pump and a 60 l/s Ultek D-I ion pump. We employed the 60 l/s pump in a unique manner, suggested by Jon Melvin. The central chamber of the pump was cleared of obstructions, so we could shoot the beam through it. Thus, we were able to place this pump between the target and the in-line cold trap. To be certain that the magnets in the pump would not steer the beam, we measured the field in the pump chamber with a Bell, Inc. Model 240 gaussmeter. The field did not exceed 30 gauss in the central region of the chamber. No problems have been encountered in steering even light beams through the pump. Finally, molecular sieve sorption pumps were used to obtain pressures of about 1 micron of Hg, so the ion pumps could be started.

The striking fraction runs were performed in a large chamber described in the Gregg thesis. All of the other experiments were done in standard 1-3/8" I.D. stainless steel crosses. All connections were made with Con-Flat flanges and OFHC copper gaskets.

All valves leading into the UHV section of the chambers had either OFHC copper or gold seals. Other commercially made components used included a bellows, windows and an electrical feedthrough. Any pieces built specifically for this project were constructed from the following materials: stainless steel, copper, Corning machinable glass ceramic, alumina ceramic, mica, tantalum, tungsten, sapphire and aluminum. Be-Cu snap rings and chromel-constantan thermocouples were also used. The targets themselves consisted of soda-lime glass, UO_2 and UF_4. Owing to the fragility of some of the targets, the system was never baked at temperatures above 200°C. Consequently, pump down time for the UHV systems was about one week.

2. Track Detector Method

All of the targets described here contained ^{235}U. Uranium containing targets were employed, so we could exploit the phenomenon mentioned in the introduction: a fission fragment from ^{235}U can produce a track in mica, which is observable under an optical microscope after the mica has been etched. In practice, we collected sputtered ^{235}U on high purity aluminum, which was then tightly pressed against a clean mica surface. On a second mica we placed a standard glass containing a known concentration of ^{235}U. After irradiating them together with neutrons, we etched both micas and determined the fission track densities. Thus, we could compare the amount of ^{235}U on the catcher with that in the standard.

We performed the neutron irradiations at the UCLA Nuclear Energy Laboratory in their R-1 reactor. Two ports of the reactor

were used. For neutron fluences of $10^{15}/cm^2$ - $10^{16}/cm^2$, we placed the samples in the center vertical access hole. The thermal column was used when fluences of $10^{13}/cm^2$ - $10^{14}/cm^2$ were desired. The energy spectrum of the neutrons has been determined by the reactor staff. In the vertical hole, the neutron flux is approximately 56% epithermal, 44% thermal and 0.4% fast, while in the thermal column we have 99% thermal and 1% epithermal. A typical irradiation lasted 1-2 hours. The samples could not be handled for about a week after each irradiation due to the activity induced in the micas.

The mica used was muscovite supplied by the Perfection Mica Co. in 1-1/2" x 2" rectangles. A clean surface was prepared by cleaving the micas with a scalpel so that the surfaces exposed to the catcher foil touched nothing but that catcher. The catcher was sandwiched between the two halves of the cleaved mica. The sandwiches were stacked in a small lucite holder. A sandwich containing the standard glasses was placed on top of the stack, which was then clamped down with a piece of lucite and two nylon screws. Two standard glasses spaced a few centimeters apart were used for the irradiations in the center vertical hole. This precaution was taken because the neutron flux spatial gradient is small in a region of the hole only 5" in length. To be certain that we were always in that region, the track densities produced by the two identical glasses were compared after each irradiation. In no irradiation did we find any evidence to indicate that the micas had been exposed to an inhomogeneous flux.

Two types of standard glasses were used in the experiments. For irradiations in the thermal column, we used a glass containing

0.10% by weight UO_3 from a pre-war source. This was custom made by Corning Glass Works. The concentration of uranium oxide in the glass was determined by weighing the initial ingredients and assuming that no losses occurred during melting. For irradiations in the center vertical hole, we used Standard Reference Material No. 612 (NBS-612) from the National Bureau of Standards. The ^{235}U concentration of the glass was determined by isotope dilution. The calculations used to infer neutron fluences from the standards have been reproduced in Appendix A. In this appendix we also present the results from an irradiation in which the two types of glass were exposed to the same neutron flux. Since the NBS-612 glass is by far the more thoroughly studied of the two, we wanted to see how the 0.10% glass compared with it. Both glasses were prepared for irradiation in the same manner. After being cut with a diamond saw, they were polished with 1 micron alumina powder. They were then rinsed in dilute nitric acid followed by methanol. Since less than one ^{235}U atom in 10^6 fissioned in each irradiation, they could be reused indefinitely. The nitric acid and methanol rinses were occasionally repeated to maintain cleanliness.

Approximately one week after each run, the micas from both the catchers and the standards were etched in 48% hydrofluoric acid. A typical etch was performed at 22°C for about 20 minutes. Since the appearance of the tracks is rather insensitive to small variations in the etching conditions, no special effort was made to keep those conditions uniform. We will assume that the etch reveals the tracks with 100% efficiency (Fleischer et al. 1975). After rinsing and drying, the micas were taped to a microscope slide for observation.

The microscope used for scanning is an exquisite instrument built by Leitz Wetzlar (serial number 646120). It has stage micrometers, which allow one to reproducibly position the mica along both axes to within a few tens of microns. A reference point was established on each mica by scratching a small cross on the surface with a scalpel. To determine track densities, we must be able to count the tracks within a square of known size. The boundaries of the square were determined by a grid on an eyepiece reticle. For each objective lens of the microscope, the area covered by the grid was determined with a Unitron objective micrometer with 10 micron spacing between the lines. The objective micrometer was also used to check the accuracy of the stage micrometer along the x-axis of the stage (see Fig. 9).

Since the track densities encountered were never more than a few times $10^6/cm^2$, transmitted light was used to count them. With the exception of two sticking fraction runs, all tracks for this thesis were counted by the author. Though every track counted was a fission fragment track in mica, there were differences in the track populations encountered. Tracks from a catcher foil were all produced by uranium atoms sitting at the surface of the mica. Thus, the tracks were all of about the same length ($\sim$ 10 microns). The tracks from the standard glass, however, were produced by uranium atoms distributed throughout a glass matrix. Consequently, their lengths varied from about 10 microns to zero. As we note in Appendix A, this difference influences the precision with which the two uranium surface concentrations can be compared.

3. Charge Integration

The track detectors allow us to determine the number of uranium atoms that leave the target during an experiment. In a sputtering yield measurement, we must also count the beam particles entering the target. We accomplish this by using a current integrator to monitor the flow of electrons into the target induced by the positively charged beam. For an accurate measurement, one must know that all electrons entering or leaving the target do so through the integrator. Great care was required, since beam currents down to 1 nanoamp were employed.

Several mechanisms can lead to incorrectly determined currents. First of all, when the beam strikes the target, it can knock several electrons out into space. The same happens when the beam strikes collimators upstream, which sprays excess electrons onto the target. Furthermore, the ion pumps produce free electrons that can get to the target. Heated surfaces can boil off electrons that might reach the target. Finally, if the target is not properly insulated, leakage through the insulator can produce erroneous readings.

In Fig. 10 we show the chamber configuration used for the UF_4 yield measurements. The yield experiments on glass and UO_2 differed in that we did not use the heater and thermocouple. Note that two current meters are shown. The "house" meter was used to help focus and steer the beam through the .12" hole in the tantalum collimator. Once the beam had been threaded through the hole onto the target, we maximized the target current while minimizing the collimator current. A typical collimator current during the run was a few tenths of a nanoamp. A +300 V bias was maintained on the

collimator to keep electrons from spraying onto the target and to suck up any electrons drifting down from the ion pump. A tantalum disk with a 1/2" hole was placed 2.5" down stream from the collimator to catch any electrons that might escape its attractive field. To protect the target from electrons in the 11 l/s ion pump, a strong horseshoe magnet was used, though experience indicated that it was not necessary.

The target-catcher foil combination was designed to act as a Faraday cage. They were electrically connected outside the chamber so that electrons lost from the target would be collected by the catcher. Both were kept at +300 V bias. The thermocouple and heater were insulated from the target with alumina ceramic and sapphire. With bias on target the leakage currents to the target were negligible. The heater proved to be troublesome at high temperatures, since the target bias attracted electrons boiling off the hot tungsten wire. The current integrator used, a Brookhaven Instruments Corporation Model 1000, was capable of balancing out this current at target temperatures up to 200°C, but the integrator had to be reset every time the target temperature was changed.

To be certain that the integration was working properly, some tests were performed with 2.5 nanoamps of fluorine on target. The beam was fluctuating with an amplitude of about 0.2 nanoamps, so we could not detect changes in the current smaller than 0.1 nanoamps. Doubling the bias voltages and turning off the ion pumps did not affect the current reading. A strong magnet had no influence on the current except between the target and collimator, where there seemed to be an increase of about 0.1 nanoamps. Removing the bias

from the target doubled the current reading. Even at the lowest beam currents, we believe that the current integration was good to about 5%.

One problem remains. Any beam striking the catcher foil will be detected as beam on target. Should beam particles be lost to the catcher foil, the measured sputtering yield would be too low. An aiming error of 1/16" will cause the problem to appear. To guard against this, the chamber was carefully aligned using a telescope mounted at the tandem's switching magnet. After alignment the chamber was rigidly clamped in place. At the end of each irradiation, the beam spot was carefully examined and found to be perfectly round. Nevertheless, there are some indications that a few of the UF_4 runs were affected. We will discuss them later.

4. Data Analysis

As we stated earlier, the track detectors allow us to determine the number of atoms sputtered from the target during bombardment. In this section, we will describe the calculations that allow us to make that determination. The arguments we will present apply to both the yield and sticking fraction experiments. Recall that in these experiments the catcher (or secondary) foils are wrapped about the target in a cylindrical geometry. We will imagine the thin cylinder to be a segment of the hemisphere generated by rotating the cylinder about the target normal. Let R be the radius of the hemisphere, and let θ be the angle relative to the target normal (see Fig. 9). In effect, θ denotes the direction of a sputtered particle as it leaves the target. We will describe the angular distribution of the sputtered

particles with the functional form

$$f(\theta) = A \cos^B \theta .$$

To determine the total number of particles, we integrate $f(\theta)$ over the hemisphere:

$$\text{Total} = \int_0^{\pi/2} (A \cos^B \theta)(2\pi R^2 \sin \theta \, d\theta) \qquad (3.1)$$

$$= 2\pi R^2 \frac{A}{B+1}$$

In the yield experiments, $R = 1.43$ cm or $2\pi R^2 = 12.85$ cm^2; in the sticking fraction experiments, $R = 1.27$ cm or $2\pi R^2 = 10.13$ cm^2. Of course, this analysis does not apply when the sputtered particle distribution is not symmetric about the target normal. In general, we can exploit this symmetry only when the incident beam is perpendicular to the target.

The data appear in raw form as a map of the number of tracks counted at a given magnification versus position along a data band on the mica detector (see Fig. 9). Before we can fit the numbers to the form $A \cos^B \theta$, we must convert the positions along the x-axis into angles. Since we know the radius, we only need to know the position corresponding to some given angle, say $\theta = 0$. Two methods for finding this point are available. In the first, we determine the left and right hand boundaries of the band and let $\theta = 0$ be the midpoint between them. In the second, we fit the data to $A \cos^B \theta$ using a series of zero points spaced .01 cm apart and choose the zero point resulting in the smallest χ^2. The latter method was the one we adopted. For data bands 4.5 cm long, the average discrepancy

between the two methods was 0.1 cm.

The parameters A and B were determined by applying a weighted least squares analysis (Bevington 1969) to the expression

$$\ln N(\theta) = \ln A + B \ln \cos \theta$$

where $N(\theta)$ is the number of tracks counted at angle θ. The track counts follow a Poisson distribution with variance N. In the weighted least squares routine, we must use the variance of ln N, which is in this case 1/N. A computer program based on Bevington's treatment of the weighted least squares analysis was used to compute A and B along with the standard deviations of A and B. In addition, the program generated the χ^2 for the fit. We will present results from this program when we discuss the specific experiments.

At this point, A is merely the number of tracks at $\theta = 0$. To use A we must convert it into a density of uranium atoms. The first step in the conversion is to compute the area covered by these tracks. That comes from the area covered by the reticle grid and from the number of frames scanned at each value of x on the mica. Now we have the track density, which we can convert into a ^{235}U density using the neutron fluence from the standard glasses as explained in Appendix A. Finally, we obtain the uranium density by dividing the ^{235}U density by the atomic abundance of the ^{235}U in the target. In most cases the isotopic composition of our targets had been altered, so we depended on our supplier, Oak Ridge National Laboratory, to give us the relevant numbers. Having converted A into the number density of uranium atoms at $\theta = 0$, we can now apply Eq. 3.1 to obtain the total number of uranium atoms sputtered.

From the charge integration we know the number of incident atoms, so we divide this into the total number of uranium atoms to give us the partial yield S(U). A small correction to this number remains to be made; we will discuss it at the end of the section on errors.

5. Errors

From time to time in the previous sections and in Appendix A we have described errors that can enter into our measurements. No effort will be made to recount them here. We will, however, remind the reader of the most serious one, which is the 20% uncertainty in the neutron fluence due to poor knowledge of the range of a fission fragment in glass. In the neutron fluence determination we can claim far greater precision than accuracy. The precision of this measurement is determined by two factors. The first is the number of tracks counted on the mica for the standard glass. In most cases we counted between one and two thousand tracks giving us a standard deviation of 3% or less. The other factor is counting errors by the observer, a problem much more difficult to quantify. Spot checks by the author indicated that track counts were reproducible to within about 2%.

The source of error we want to concentrate on in this section is of an entirely different nature. Recall that the radii of our catcher and secondary foils are less than 1.5 cm. Consequently, significant errors could appear if the beam spot is as much as 0.1 cm off center. Misalignments of this magnitude turned out to be unavoidable, so we wrote a computer program to numerically study the behavior of the data when such displacements occur. The geometry of the

analysis is illustrated in Fig. 11. We simulated a beam spot with a rectangular grid of 25 equally weighted source points. Each source point produced an imaginary flux of sputtered particles with angular distribution $\cos^{B_o} \varphi$. In all cases quoted here, B_o equals 1 and L = W (see Fig. 11). For a given point on the catcher foil, the response produced by a source point is proportional to

$$\frac{(\cos^{B_o} \varphi)(\cos \alpha)}{R^2}$$

The definitions of R and α can be determined from the figure. A two-dimensional Simpson's rule routine was used to sum the contributions from the entire grid. The program performed this calculation for 21 equally spaced points on the catcher foil and then fit those points to the functional form $A \cos^B \theta$ using a least squares routine. In this way we were able to study the behavior of A and B as a function of beam spot size and displacement vector $\vec{D}$. By specifying $\vec{D}$ we could displace the beam spot along all three axes.

In Table 1 we exhibit some of the results from the program. The numbers have been normalized to give A/(B+1) = 1.0 for a 0.5mm square beam spot that is exactly centered. All cases correspond to the same amount of material leaving the beam spot. The most important conclusion to be drawn from the results is that while B is sometimes sensitive to alignment errors, A/(B+1) is not. In particular, note the behavior with respect to displacements along the z-axis ($D_z < 0$ implies the target is too far from the catcher). We have reason to believe that the target in the UF_4 runs was displaced about 1mm from center in the negative z direction. Thus a sputtered

angular distribution with $B_0 = 1$ would be detected as a distribution with $B = 0.75$. Indeed, the measured angular distributions tended to fall between $B = 0.7$ and $B = 0.8$. Even with this error, however, the calculated yield will be wrong by only 1%. This correction is so small we will not include it in the data analysis. In Figs. 12 and 13 we show a pair of angular distributions computed by the program.

At the end of the last section, we alluded to a correction that would be made to the data. That correction arises from the following consideration. Imagine a sputtered uranium atom approaching the catcher foil. It most likely has an energy in the low eV range (Weller 1978). We ask, "What is the probability that it will stick to the catcher's surface?" We must know the answer to calculate the sputtering yield. Since no reliable theory describing this situation exists, we initiated a program to measure the sticking probability. We will describe it in the next section.

B. STICKING FRACTION EXPERIMENTS

1. Introduction

Our sticking fraction (or trapping probability) measurements were initially motivated by the work of Close and Yarwood (1967), who studied the trapping of low energy noble gas atoms on tungsten surfaces. Their data indicated that the trapping efficiencies fell drastically at energies below a few hundred electron volts. Though we suspected that this behavior was peculiar to the noble gases, their paper undermined our belief that low energy uranium atoms stuck to aluminum oxide surfaces with unit probability. Our fears were reinforced by the papers of Hurkmans et al. (1976, 1976a,

1977) and Overbosch et al. (1977) in which the trapping of alkali metals on hot tungsten surfaces was experimentally explored. Though the behavior of the alkali metal atoms was different from that of the noble gases, they too demonstrated that trapping probabilities could be much less than one at energies relevant to our own experiments.

To remedy the situation we undertook the series of sticking fraction experiments illustrated in Figs. 8 and 14. Since the primary aim of this effort was to calibrate our catcher foils, the criteria for a correct experiment were different from those usually demanded in a surface scattering experiment. For instance, our catchers are exposed to a flux of uranium with the energy distribution shown in Fig. 1. Consequently, we used an unanalyzed beam of sputtered particles rather than the customary monoenergetic beam. Furthermore, during a sputtering experiment the catcher foil surfaces are contaminated with gases from the vacuum, so initially at least we made no special effort to clean our primary foils. To have done so might have produced misleading results.

Without the extraordinary sensitivity afforded us by our track technique, the experiment would have been much more difficult for the following reason. If the sticking probability is close to 1, which was the case, we must severely limit the fluence to which the primary foil may be exposed. If the accumulation of uranium on the primary foil exceeds, say, 0.1 monolayers, then the probability that an incoming uranium will strike a uranium rather than a substrate atom becomes unacceptably large. Therefore, we always limited the uranium fluence on the primary to less than $5 \times 10^{13}/cm^2$. This implies that the uranium surface density on the secondary was very

small.

Perhaps, even 0.1 monolayers on the primary foil is too much. We must consider the possibility that the uranium atoms reaching the secondary do not do so by merely bouncing off the primary. Conceivably, they could be atoms that stuck to the primary but were subsequently resputtered by incoming uranium atoms or even argon atoms backscattering from the uranium foil. Fortunately, two simple tests allow us to check for this possibility. In the first, we perform a normal sticking fraction run using a ^{235}U foil to produce the sputtered uranium beam. Then we immediately repeat the run using the same catcher foils but with a ^{238}U foil to produce the sputtered beam. Our track detectors are blind to ^{238}U, so this second run will have no influence on the final result unless the incident beam resputters ^{235}U already on the primary.

The second test is conceptually similar to the first, but in this one we measure the sticking fraction as a function of the ^{235}U fluence on the primary. Suppose that the incoming uranium atoms are resputtering uranium from the primary with an effective yield $\overline{S}$. The number of uranium atoms resputtered will be

(fluence of U atoms)(average surface coverage)($\overline{S}$) .

The average surface coverage during the run is 1/2 of the final coverage and is proportional to the fluence of uranium atoms. Thus, the fraction not sticking to the primary will be proportional to the fluence of uranium atoms on the primary if all of the atoms reaching the secondary do so through resputtering. Similar arguments can be made if backscattered argon is causing the resputtering. We will

present results from both tests later.

2. Data Analysis

We will quote our results in terms of the fraction f of uranium atoms that do not stick to the primary foil. To see how we determine f, consider N atoms incident on the primary. (1 - f) N of these stick, while fN atoms strike an imaginary hemisphere with radius equal to that of the secondary foil. Of these fN atoms, (1 - f)fN stick to the hemisphere. Since f will turn out to be small, we will not worry about the fate of those atoms not sticking to the secondary. Now we take the ratio of the number on the hemisphere to that on the primary:

$$\frac{\text{atoms on hemisphere}}{\text{atoms on primary}} = \frac{(1 - f)fN}{(1 - f)N} = f \ .$$

From our analysis leading to Eq. 3.1, we know how to calculate the number of atoms on the hemisphere. We must now determine the number of atoms on the primary. The sputtered uranium beam incident on the primary is collimated by a hole 0.4 cm in diameter. The resulting beam spot produces a uniform track density on its associated mica except at the rim of the spot, where the track density gradually falls to zero over a distance of about 0.1 cm. To find the area of the spot, we use the stage micrometer of the microscope to determine a set of about 20 points on the rim where the track density has fallen to approximately 1/2 of the value in the interior of the spot. A typical error in determining the radial position of such a point is about .01 cm, which translated into errors of up to 10% in the area. In practice, we expect to do much better than

10%, since randomly fluctuating errors about the 1/2-density radius should tend to cancel. To calculate the area of the spot, we choose a point close to the center and compute the distances $r(\theta)$ to the 20 points. We then numerically evaluate the integral

$$\frac{1}{2}\int_0^{2\pi} r^2(\theta)\,d\theta \ .$$

The value obtained is stable against changes in the position of the center point. With the area in hand, we can determine the total number of uranium atoms in the spot by counting a few thousand tracks in the interior. This, along with the number of uranium atoms on the hemisphere, immediately gives us the sticking fraction.

In addition to the error in the spot area, one other possible source of error is worthy of note. Due to the very high density of ^{235}U in the primary spot, we must irradiate it with neutrons in the reactor's thermal column rather than in the center vertical hole, where the secondary goes. Consequently, we compare the primary against the 0.10% glass and the secondary against NBS-612. In Appendix A we show that the two standards agree very well. Furthermore, since we eventually consider only the ratio of the neutron fluences, the uncertainty in the fission fragment range does not plague us. Thus, the only errors from the neutron fluence determinations are the usual 3% errors due to counting statistics.

3. The Experiments

The sticking fraction experiments were performed in the chamber shown in Fig. 15. Two schematic views of the configuration inside the chamber are shown in Fig. 14. The heater shown in

the figure was used in only two of the runs; in all of the others the primary foil sat at room temperature. Surface contamination problems motivated our use of the heater. As we explained at the end of the theory section, even with base pressures in the 10^{-9} torr range one expects to find a monolayer of gas adsorbed on most surfaces. Since heating can desorb much of this gas, we wanted to see if heating the primary foil to 150°C would affect the sticking fraction. The heat was provided by passing about 1-1/2 amps through a thin tantalum foil. We measured the temperature with a chromel-constantan thermocouple connected to an Intersil ICL7106 millivolt meter. In lieu of a reference thermocouple, we measured the room temperature with a mercury thermometer and took that to be the temperature corresponding to 0.0 mV. The temperature reading was accurate to within 2°C.

In each run we could perform two independent measurements by mounting two primary-secondary assemblies (we call them cages) on a cylinder 2.5" in diameter. The sputtered uranium atoms were produced by irradiating an enriched uranium foil (93% ^{235}U) with argon. The uranium foils were cleaned with concentrated nitric acid and rinsed with acetone shortly before loading them into the UHV chamber. No sputter cleaning was performed. By using two uranium foils along with shields we could irradiate the cages independently. During the runs the argon beam was the main gas load on the system: typical pressures were a few times 10^{-8} torr. Base pressures in the chamber before each run were usually a few times 10^{-9} torr.

In all cases the secondary was high purity aluminum foil supplied by Ventron Alfa. This same foil was used for the primary

in five runs. Due to the high purity of the foil, we did not attempt to clean it before loading it into the cages. In one run, freshly cleaved mica was used as a primary. Two runs employed primaries consisting of aluminum evaporated onto a mica substrate, and two runs employed similar primaries consisting of evaporated gold. The evaporations were performed in a bell jar pumped with a liquid nitrogen chilled baffle and an oil diffusion pump. Typical pressures were about 10^{-6} torr.

The results from these experiments are shown in Table 2. The precision achieved in our measurement of f, the fraction not sticking, can be inferred from the scatter in the four Al foil runs using 80 keV argon: $2.42 \pm .33\%$, which corresponds to a 14% error. The fluctuations in B are larger than expected and difficult to explain, though they may be due to warping of the primary foils. Note that f does not scale with the uranium surface density on the primary. Furthermore, the run in which the primary was also irradiated with sputtered ^{238}U did not produce an anomalous result. Thus, we may conclude that the uranium residing on the secondary foil did not get there through re-sputtering. All but two of the values for f lie in the 2% to 3% range. This may indicate that surface contamination controls the sticking probability. The mechanisms producing the two excursions out of this range are not understood. The low value of f for the heated gold may be due to the high mass of the substrate atoms. The low value resulting from the 40 keV argon run is unexplained. Three representative angular distributions are displayed in Figs. 16, 17 and 18.

Much of our difficulty in interpreting these numbers arises from the absence of an adequate theoretical description of the interaction. Several reasonably successful theories for surface scattering exist, but they apply only when the incident atom is lighter than the surface atoms. In that case, the interaction with the surface can be described in terms of a single binary collision. The mass ratio with which we are dealing makes the picture much more complicated. Unless some sort of collective action occurs, the heavy uranium atom must undergo multiple scattering just to turn around.

C. EXPERIMENTS WITH GLASS TARGETS

1. Target Preparation

Of the track detectors usable in a UHV system, common soda-lime glass has one of the lowest thresholds for track registration. In addition, it is a system that is easy to manipulate; through simple procedures, we can dope the glass with controlled quantities of uranium. These glasses are, however, complicated, and many aspects of their behavior are poorly understood. These complexities finally proved to be overwhelming. But in struggling with them, we discovered some features of the targets' behavior under bombardment that are intriguing.

To produce the target, we selected a Gold Seal microscope slide and ground it into a fine powder with a sapphire mortar and pestle. A uranyl nitrate solution was prepared by dissolving 45 mg of enriched uranium (93.32% by weight ^{235}U) in 0.5 ml of 70% HNO_3. An unknown fraction of the uranium had oxidized, which introduced an error of no more than 10% into the uranium concentration determination.

100 μl of this solution was injected into .75 g of the glass, which was then stirred and baked to drive off the water. The mixture was sealed in a platinum capsule and baked at 1500°C for 14 hours to insure complete mixing. During this time a small hole developed in the capsule allowing about a third of the glass to ooze out and be lost. After quenching, the glass was annealed at 600°C for over 8 hours before opening the capsule. One large piece was obtained, which was cut and polished with alumina to form a target surface with dimensions 0.5 cm by 0.3 cm. If we assume that no losses occurred during baking, then the glass is about 1.1% ^{235}U by weight or approximately 0.3% atomic.

After the glass was finished, Tim Benjamin and John Jones performed some electron microprobe analyses of the glass. They employed a 15 keV electron beam with a current of 5 nanoamps. For a given spot, the duration of each irradiation was 200 seconds. At this energy, the microprobe samples the top 2-3 microns of the glass. At first, beam spots 30 microns in diameter were chosen, but the data indicated that the electron beam was driving out over 90% of the sodium oxide. Expanding the beam spot size to 50 microns alleviated the problem. In Table 3 we show the results from one of the runs.

2. Results

The sputtering yield experiments were performed in the chamber shown in Figs. 19 and 20. In Figs. 21 and 22 we show the catcher foil holder, which allowed us to perform three sputtering runs without breaking vacuum. The catcher foil shown in the picture was for

an incident beam normal to the target surface ($\psi = 0^{o}$). In most of our glass experiments, we set $\psi = 45^{o}$. The holder was also rotated 45^{o}, so $\theta = 0^{o}$ still corresponded to the center of the catcher foil. The holes in the catcher foil were shifted accordingly. Since the target could not be moved, all three of the runs were performed on the same beam spot. At the end of each set of runs, the target was polished to expose a fresh surface. The initial runs were performed with fluorine beams at energies ranging from 2 MeV to 20 MeV and at beam currents of about 20 particle nanoamps. In some cases the beam power exceeded 3 watts/cm^{2}. Since the target was a good thermal insulator, it could not efficiently dissipate the heat generated. The heating produced some dramatic effects. The beam spot became powdery, and a raised annulus around the spot indicated that the glass had flowed. As we can see from Table 3, the microprobe studies reveal preferential loss of sodium, which means that it is evaporating or diffusing away from the beam spot.

The angular distributions of the sputtered uranium atoms do not, however, indicate that the uranium evaporated. In Figs. 23 and 24 we show angular distributions from two of the high current runs. In all cases, $\theta = 0^{o}$ corresponds to the target normal. Note that these distributions peak at about 45^{o} relative to the normal, which is 90^{o} with respect to the beam. Evaporation could not produce such a distribution. A further surprise is the sharpness of the angular distribution produced by such a rough surface. For comparison, we display in Fig. 25 an angular distribution produced by a slightly oxidized pre-war uranium foil irradiated at $\psi = 45^{o}$. The

surface of the foil was not nearly as rough as that of the glass after irradiation, but the angular distribution produced by it is similar. Finally, in Fig. 26 we show the angular distribution from a 10 MeV run on the glass target. In this case the beam current was only 5 nanoamps. Note that the peak is not as sharp. Other experimenters have also observed such shifts in the angular distributions of sputtered particles produced by irradiation at oblique incidence. But the magnitude of the forward shift tends to decrease as the beam energy increases (Oechsner 1975).

Since the targets were irradiated at $\psi = 45^{o}$, we cannot compute the total sputtering yield. Nevertheless, we can compare the uranium densities at the peaks of the various angular distributions. The data are shown in Table 4. In the table we compare the results from the glass with the ^{235}U yield from the uranium foil, which contains .72% ^{235}U. Total sputtering yields for uranium foils will be quoted in the next section, and we will see that no anomalously high yields were detected. Thus, we may conclude that the yields from the glass targets are not exceptional either.

Clearly, the only parameter strongly influencing the yields from the glass is the beam current. In fact, some irradiations of the glass targets were performed at normal incidence with beam currents below 5 nanoamps. No uranium above background was detected on the catcher foils. Thermal effects provide the only mechanism through which the beam current can control the yield. If the uranium atoms were being sputtered by thermal spikes, then high currents would enhance the yield by increasing the target temperature. Yet, we

have argued that the shape of the angular distributions precludes this. On the other hand, if surface contamination were suppressing the sputtering, then high currents could increase the yield by keeping the surface clean. In section II we pointed out that high temperatures can desorb contaminant gases from a target surface. In this case, such cleansing action would be aided by the flux of sodium evaporating from the surface. Therefore, we conclude that the glass surface was probably contaminated during our sputtering runs.

D. EXPERIMENTS WITH UO_2 TARGETS

1. Target Preparation

The most convenient alternative to the glass targets was UO_2. As a binary compound, it escapes many of the complications inherent in the glass. Furthermore, its high melting point allowed us to use intense beams without evaporating its constituents. Of course, it is not a known track detector. Nevertheless, at $400^{\circ}K$ it has an electrical resistivity of about 4×10^4 Ω-cm (Ishii et al. 1970), which is over an order of magnitude greater than the generally accepted minimum resistivity for track registration. Unfortunately, Ishii and his coworkers demonstrated that even tiny deviations from stoichiometry can cause the resistivity to drop by orders of magnitude. Whereas we were not equipped to monitor the uranium-oxygen ratio to the required precision, the results would provide a good test of the ion explosion idea only if the anticipated anomaly were seen. We can explain away the ion explosion's failure to appear by invoking a nonstoichiometric uranium-oxygen ratio.

In all of the runs, the target consisted of an oxide layer on a

cold rolled uranium foil. A picture of the surface of such a foil can be found in the Gregg thesis (1977). Before preparing the oxide layer we always cleaned the foil by etching it in concentrated nitric acid and then rinsing it in distilled water and acetone. The manner in which we prepared the oxide changed as we learned more about the system. Practically all of what we know about the oxidation of uranium comes from the work of Flint, Polling and Charlesby (1954).

In several runs with a natural uranium target, we wanted the oxide layer to be as thin as possible, so we loaded it into the UHV system and began pumping within 30 minutes of removing it from the rinse. Since no color change occurred, the oxide layer was less than 500 Å thick (Flint et al. 1954). In several other early runs we simply let an enriched foil sit out in air at room temperature for a few days. The pale brown color it developed indicates that the oxide layer was about 500 Å thick. An oxide layer formed in this manner does not protect the uranium from further oxidation, which means that the layer is not continuous. A continuous protective layer will form, however, if the oxidation occurs at elevated temperatures. Based on Flint's results, we decided to produce 700 Å thick layers by heating the foil in air at 100°C for 20 minutes. The resulting oxide layer was a beautiful deep blue. We performed no surface analysis on the samples, so we cannot guarantee the purity or the stiochiometry of the targets. Even if the uranium-oxygen ratio had been exactly what we desired, it probably would have changed under bombardment.

2. Results

All of the runs were performed using the chamber and catcher

foil holder shown in Figs. 19 through 22. All results quoted in this section are for beams incident at $\psi = 0^{o}$ (normal incidence). The results are displayed in Table 5. In Table 6 we show some results from a Sigmund theory calculation using the expression for binary sputtering from Haff and Switkowski (1976). One should bear in mind that we have stretched the Sigmund theory to energies far higher than intended by its author. For instance, the behavior of the α function has been explored to values of ε no higher than 10 (Sigmund et al. 1971), while in this calculation we encountered ε values greater than 10^{3}. Lacking an explicit expression for α, we somewhat arbitrarily set it equal to 0.1. For the binding energy U we chose 5.4 eV, the sublimation energy of uranium metal.

In view of the uncertainties involved, the agreement between the Sigmund numbers and the thick oxide yields is astonishing. Though the numbers fluctuate considerably, several general trends are apparent. First of all, the yields tend to decrease as the oxide thickness increases. In fact, the yields from the thinnest layers are just a factor of two below those expected for pure uranium from the Sigmund theory. We suspect that the collision cascades in the thin oxide layers were depleted in oxygen, which would account for this behavior. Furthermore, there seems to be no dependence on the heating from the beam: the largest yield (.04) appeared in the run with the lowest beam power (.14 watts/cm^{2}). Finally, the yield decreases with increasing energy as expected from the Sigmund theory. The yields show no sign of exotic effects from the ion explosion mechanism.

E. EXPERIMENTS ON UF_4

In contrast to the glass and oxide targets, which gave us nothing but trouble, our uranium tetrafluoride targets proved to be ideally suited to studying the exotic sputtering processes for which we had been searching. The reward for this choice was two-fold. This compound's extraordinary properties allowed us to overcome the usual technical difficulties associated with sputtering yield measurements. In addition, the target displayed an unexpected richness and subtlety in its behavior under ion bombardment. The rather extensive experiments described in the next few sections only begin to reveal the sputtering phenomenon that we have discovered, and the identity of the mechanism involved still eludes us. Nevertheless, not all of our experiments were immediately directed toward uncovering that identity. To be certain that our numbers were not misleading us, some technical issues had to be resolved. These issues arose partly because UF_4 is an unfamiliar substance--especially in this context. To help acquaint the reader with UF_4 and the other uranium fluorides, we have assembled some information on their physical and chemical properties in Appendix B.

1. Target Preparation

In vacuum, UF_4 melts without decomposing at 1309°K (Rand and Kubaschewski 1963). It also vaporizes nondestructively (Hildenbrand 1976), which opens up the possibility of utilizing it as a thin film. By evaporating a few thousand angstroms of UF_4 onto a highly polished copper backing, we immediately solve several problems. Being an excellent thermal and electrical insulator, it would cause

serious complications due to heating and charging if irradiated in bulk form. The close proximity of a conducting substrate mitigates both problems. Furthermore, by evaporating onto a polished surface we achieve a smooth UF_4 surface without having to polish or otherwise sully the UF_4 itself. The evaporation can, however, introduce problems of its own.

When considering the use of evaporated targets for sputtering, we must keep in mind the experiments of Andersen and Bay (1972) with evaporated Cu targets. They found that gaseous contaminants incorporated into the target during deposition can suppress the measured yield by over a factor of two. At 5×10^{-7} torr, the pressure at which their evaporations were performed, the flux of molecules striking the surface exceeds $10^{14}/cm^2$-s. To reduce the contamination to a few percent, one must deposit nearly 10 monolayers every second. They obtained acceptable results from 10,000 Å layers, which were deposited in 5-10 minutes. They also discovered that the evaporated films tended to expel the foreign moelcules when exposed to UHV conditions--even at room temperature. In performing our own evaporations, we strove to reproduce the conditions achieved by Andersen and Bay.

We obtained anhydrous UF_4 in powdered form from two suppliers. A batch from Ventron Alfa was of unknown isotopic content. We used it for a Rutherford backscattering experiment to be described later. Oak Ridge National Laboratory supplied a highly enriched batch (93.08 atomic % ^{235}U) for use in all of the sputtering experiments. For evaporation, the powder was loaded into a tantalum boat consisting of a sealed tube with a small hole in the middle. The boat could

be heated to nearly white heat by passing up to 100 amps through it. Of course, separate boats were maintained for the two batches to avoid diluting the enriched uranium.

The evaporations were performed in a Veeco VE-775 vacuum system incorporating an oil diffusion pump with a liquid nitrogen chilled baffle. The vacuum chamber was equipped with a Sloan crystal oscillator for monitoring the mass density of UF_4 deposited and with a shutter for controlling the duration of the evaporation. The pressure in the chamber was measured with an ion gauge. After loading the boat and the copper target into the chamber, we allowed it to pump down overnight with the baffle at room temperature. During this time, the tantalum boat was heated in the vacuum with a 40 amp current to help outgas the UF_4, which is slightly hygroscopic. On the following day the baffle was chilled, which made the pressure fall to about 5×10^{-7} torr within a few hours. The current through the boat was gradually increased until it could be maintained at 80 amps without significantly degrading the vacuum. We began evaporation by opening the shutter. In less than 2 minutes we would deposit about 2,000 Å of UF_4 onto the copper at pressures that rarely exceeded 10^{-6} torr. We terminated the evaporations by quickly closing the shutter.

Assuming that the gas incident on the target stuck with unit efficiency, we calculated that most of the evaporations produced films with less than 10% contamination. One unusually poor run resulted in an estimated contamination of 42%, but this film did not produce results at variance with the other targets. This is probably owing

to our handling of the targets after evaporation. Immediately after removing the target from the bell jar, we loaded it into the UHV system and started pumping. The targets' exposure to atmospheric pressure always lasted less than an hour. Once the chamber pressure was below 10^{-7} torr, heating tapes were used to elevate the target temperature to about 200°C. It was baked for a week at this temperature as the pressure fell to below 2×10^{-9} torr. We believe that the target cleaned itself by outgassing during the baking, and the consistency of the results obtained bears this out.

2. Rutherford Backscattering Experiment

To be certain that our evaporated films were really UF_4, we measured the uranium to fluorine ratio in one of our films using backscattering. For these runs we did not evaporate onto a copper backing, because the copper would have hidden our fluorine signal. Instead, we evaporated 22 $\mu g/cm^2$ UF_4 onto a 9 $\mu g/cm^2$ self supporting carbon foil. We used ^4He at 1.8 MeV and 2.0 MeV incident energy for the analysis. Applying Bragg's rule, we estimate from Ziegler's tables (1977) that a 2.0 MeV ^4He ion loses about 5 keV passing through 22 $\mu g/cm^2$ of UF_4. Since this is small relative to the incident energy, we will calculate all scattering cross sections at the incident energy.

To calculate the uranium-fluorine ratio from the data, we must know the differential scattering cross section in the lab, $\left.\frac{d\sigma}{d\omega}\right|_{lab}$. For ^4He scattering from ^{238}U at 2 MeV, electronic screening causes the cross section to deviate from the Rutherford value by about 2%. Consequently, we will calculate the cross sections in the

Lindhard theory. The computation was performed with an HP-67 programmable calculator. For derivations the reader should consult Lindhard et al. (1968) and Marion (1970). Now we must define some notation.

Consider an ion with mass A_1 and atomic number Z_1 incident on an atom with mass A_2 and atomic number Z_2. Let θ be the center of mass scattering angle, and let ψ be the lab scattering angle. In Section II we defined the parameters a (screening length), ϵ (reduced energy) and λ' (fitting parameter). Let $\eta = \epsilon \sin(\theta/2)$. Now we apply a fit to the Lindhard scaling function due to Weissmann and Sigmund (1973):

$$f(\eta) = \lambda' \eta^{1/3} [1 + (2\lambda')^{2/3} \eta^{8/3}]^{-3/2} .$$

In the center of mass frame we have

$$\frac{d\sigma}{d\omega}(\theta)\Big|_{cm} = \frac{a^2 \epsilon^2}{8} \frac{f(\eta)}{\eta^3} .$$

To convert this into the lab frame, we note that

$$\theta = \sin^{-1}(x \sin \psi) + \psi$$

where $x = A_1 / A_2$. We may now apply the formula

$$\frac{d\sigma}{d\omega}(\psi)\Big|_{lab} = \left[\frac{d\sigma}{d\omega} (\sin^{-1}(x \sin \psi) + \psi)\Big|_{cm} \right] \left[\frac{(x \cos \psi + \sqrt{1 - x^2 \sin^2 \psi})^2}{\sqrt{1 - x^2 \sin^2 \psi}} \right]$$

To complete the analysis we will need one more result. The final energy E_f of the scattered ion is related to its initial energy E_o by the expression $E_f = KE_o$, where

$$K(\psi) = \frac{A_1^2}{(A_1 + A_2)^2} \left[\cos\psi + (x^{-2} - \sin^2\psi)^{1/2}\right]^2 .$$

Our experiments were performed at $\psi = 135^\circ$ and 150°. In Table 7 we show the computed values for $\frac{d\sigma}{d\omega}(\psi)\Big|_{lab}$ and KE_0 for these angles.

An ORTEC surface barrier detector (Model No. BA-17-50-100; Serial No. 17-744I) was used to detect the backscattered alphas. The detector's bias was +60 volts. A collimator with a 1/4" diameter hole was mounted on the face of the detector; its distance from the target was 4.31". We calibrated the detector with a ^{212}Pb source, which emits alphas at 6.051 MeV, 6.090 MeV and 8.785 MeV. The full width at half maximum of the 6.051 MeV and 8.785 MeV peaks was 19 keV. We used the same foil for all four runs. With 5 nanoamps of ^{4}He(+1) on target, each run lasted a little less than 20 minutes.

The results from the runs are shown in Table 8. We exhibit a sample spectrum in Fig. 27. To obtain the fluorine-uranium ratio, we used the expression

$$\frac{\text{F atoms}}{\text{U atoms}} = \frac{\text{F counts} / \left.\frac{d\sigma}{d\omega}\right|_F}{\text{U counts} / \left.\frac{d\sigma}{d\omega}\right|_U} .$$

We have a 2% statistical uncertainty in the fluorine counts and, perhaps, 1% uncertainties from the background subtractions and screened cross section calculations. Thus, the variation from the expected value of 4.0 is within experimental error. Since the ratio seems to decrease as the distance of closest approach decreases, we may be getting a small systematic error from inelastic channels in the

scattering from fluorine.

3. Low Energy Sputtering of UF_4

Low energy sputtering yield measurements allow us to answer two important questions relating to the high energy experiments. The first is technical; the second is fundamental. We turn to the technical issue now, reserving the fundamental one for the end of this section.

As we noted in Section I, high energy beams cannot be used to sputter clean a target surface due to the heat they deposit in the substrate. Low current sputter cleaning is ineffective, even at 10^{-9} torr, because it cannot remove contaminant molecules from the surface as rapidly as they arrive at the surface from the residual atmosphere in the chamber. Consequently, we depend on careful control of the surface temperature to maintain the cleanliness necessary for an accurate yield measurement. Our arguments in Section II indicate that this approach works only if UF_4 does not bind gas molecules to its surface too strongly. We have no a priori knowledge of the bond strengths involved, but we can test the effectiveness of our technique with low energy sputtering. The strategy adopted for the test is simple. First, we perform a sputtering run with low beam current at 100 keV on a target that has been processed in the same way that the targets for the high energy runs are processed. After this run, we increase the beam current to sputter clean the target, removing a few monolayers in a few minutes. Immediately after the cleaning is completed, we perform a second sputtering run. If the measured yields from the two runs agree, then we may be

assured that the targets used in the high energy experiments were clean.

The chamber used in these runs is shown in Fig. 28. It is similar to the configuration used for the high energy runs. The differences are due to its being mounted on the sputtering leg of the 150 kV ion source. In particular, the 50 l/s sublimator was added to help counteract the heavy gas load from the high current beams. The current integration technique was described in Section III. A. 3 (see Fig. 10). The target was identical to that used in the high energy measurements.

The target is shown in Figs. 29 and 30. The UF_4 film is on the polished surface of the Cu block. (Note that in the photograph the reflection of the support post can be seen.) The beam current is collected from the stainless steel support post with a feedthrough wire not visible in either figure. Embedded in the copper is a chromel-constantan thermocouple. The thermocouple junction sits in a small cavity directly behind the point where the beam hits. As with the sticking fraction experiments, the temperature was monitored with an Intersil millivolt meter. The tungsten heater is a coil sandwiched between two sapphire disks. Both the thermocouple and the heater are electrically insulated from the copper. Recall that the catcher foil holder shown in Figs. 21 and 22 has a spring at one end. When hooked to the feedthrough, it allows current to be collected from the catcher foil also. The holder mounts onto a bellows, which allows us to fully retract the catcher foil during the cleaning runs. The tungsten heater could be used to raise the target temperature to about 200°C. Above that temperature two undesirable

effects set in. Electrons from the hot wire spoiled the current integration, and the UF_4 film tended to peel from the copper surface at temperatures above 250°C. To be certain that sublimation of the UF_4 is not a problem at these temperatures, we performed a simple test. We exposed a catcher foil to the target when it was at temperatures ranging from 210°C to 240°C. The exposure lasted one hour, which is over ten times longer than the duration of a typical sputtering run. We found no uranium above background on the catcher foil. In all of the low energy runs, the target temperature was 163°C.

The thickness of the UF_4 film was about 2000 Å. Using a computer program dubbed "LSS-10" (Johnson and Gibbons 1969) we computed the projected range of 100 keV ^{16}O in UF_4. The oxygen penetrates about 1500 Å into the film with a standard deviation in the projected range of 640 Å. Though using lower energies gives greater sputtering yields, we chose 100 keV as the energy for all of the low energy runs, because lower energies would allow the incident beam particles to accumulate too close to the surface. The runs were performed in two sets, each beginning with a fresh target. By the end of each set, the accumulated dose from the irradiations was about 2.2×10^{16} ions/cm^2.

Now we detail the history of the two sets of runs. In Table 9 we list the runs in chronological order and display the relevant numbers. In the first set we intended to use an ^{16}O beam but discovered later that the magnet calibration was wrong by one mass unit. The problem was corrected before we ran the second set. Fortunately, the beam type is not a crucial element in the test. The very first run (I-1) was performed under the conditions used in

the high energy experiments. Note that very little material was removed from the surface during this run. After completing it we performed the first cleaning run, which lasted for about 7 minutes. With the intense beam in the chamber, the pressure rose to 7.5×10^{-8} torr. Assuming that this was predominately N_2, we estimate that the flux of molecules striking the surface was 3×10^{13} / cm^2-s. Given a uranium yield of .15 and a fluorine yield of .60, we were removing about 8×10^{13} atoms/cm^2-s from the target, so we were fulfilling the conditions necessary for producing a clean surface. When the cleaning run was complete, we chopped the beam, moved the catcher foil into position and immediately started the yield measurement. At high beam current the yield measurement lasted only 2 seconds. The elapsed time between the cessation of the cleaning run and the end of the data run was 22 seconds. This may not have been quick enough, since it is comparable to the time required to reform a monolayer of gas on the surface--if the sticking fraction of the molecules is close to one. We will comment on this possibility below. All of the subsequent runs were at high beam currents, and they were handled in a similar manner.

The yields determined from the first set of runs demonstrated that our heated target produces results in good agreement with a target cleaned in a more traditional manner (see Table 9). But because of the uncertainty about surface contamination accumulating between the cleaning and data runs, we performed the second set using ^{16}O and ^{20}Ne. The strategy here was to check the effectiveness of our sputter cleaning technique by determining the ratio of the yields from the ^{16}O and ^{20}Ne irradiations. The Sigmund theory

produces very accurate estimates for such ratios. If the theoretical and experimental numbers agree, then we may be confident that our technique is producing accurate numbers. From Table 9 we see that for the ^{16}O beam we found S(U) = 0.17 and for the ^{20}Ne beam we found S(U) = 0.26. Thus, the experimental ratio is 1.53. From the Sigmund theory we obtain a ratio of 1.46. Since the experimental ratio is subject to an uncertainty of 10-20%, the agreement is better than we had a right to expect.

We may now use the experimental numbers to estimate the effective surface binding energy encountered by uranium and fluorine atoms leaving the UF_4 surface. In the computation we will use the so-called inelastic α function, which was calculated with electronic stopping taken into consideration (Andersen and Bay 1975). With a binding energy of 2.5 eV, the Sigmund theory numbers can be brought into agreement with the yields determined using the ^{16}O and ^{20}Ne beams. Recall that the sublimation energy of UF_4 is 3.2 eV (see Appendix B).

We now turn our argument around and claim that these results demonstrate that the Sigmund theory provides an excellent description of the low energy sputtering mechanism in UF_4, which brings up the fundamental point we mentioned at the beginning. In the next section we will examine some sputtering yields in the electronic stopping region that definitely do not fit into the Sigmund picture of sputtering. Since we believe that the anomalous sputtering is due to electronic energy loss mechanisms, we expect that sputtering of UF_4 will behave normally at energies where the electronic stopping is not dominant. And so it does.

4. High Energy Sputtering of UF_4

According to the Sigmund theory a 4.75 MeV ^{19}F ion striking the surface of a UF_4 target should sputter uranium with a yield of 7×10^{-3} (we chose $\alpha = 0.1$ and U = 2.5 eV). In Table 10 we display our experimentally determined sputtering yields. The experimental yield corresponding to the conditions just described is about three orders of magnitude larger than the Sigmund theory prediction. Clearly, some new mechanism is involved. To help reveal its identity, we explored the variation in the yield as a function of several variables: the energy of the incident ion, the charge state of the incident ion, the mass of the incident ion, the target temperature, the pressure in the vacuum chamber and the number density of ions implanted into the target.

The experiments were performed in the chamber shown in Figs. 19 and 20. The target was the one illustrated in Figs. 29 and 30. We have already described the details of the target and how it was prepared. Recall that the thickness of the UF_4 films used was about 2000 Å. A 1 MeV ^{19}F ion will in most cases penetrate the film and stop after traveling over 5000 Å into the copper substrate. Furthermore, the total dose implanted into the beam spot was usually very small. Consequently, we do not believe that any significant amount of fluorine from the beam accumulated in the UF_4 film. The catcher foil holder shown in Figs. 21 and 22 could be used for three runs without breaking vacuum. The target was immobile, so the same beam spot was used for all three irradiations. A fresh target was prepared for

each new catcher foil. After most of the irradiations, the beam spot was not visible when the target was removed from the chamber. One hour exposure to air, however, always caused a perfectly round spot to appear. This led us to believe that the chamber was well aligned. Nevertheless, over the course of seven sets of runs we noticed that one catcher foil position was producing results consistently low by about 20%, which would occur if the beam were hitting the catcher foil. We threw out the seven data points involved and realigned the chamber. The anomaly disappeared. These seven points were the only ones discarded.

To demonstrate the quality of the angular distributions obtained, we display a representative one in Fig. 31. It was probably flattened by target misalignment (see Section III.A).

We will discuss the temperature and pressure dependence of the yield first, because it bears on the accuracy of the data. The results are shown in Table 11. Beam powers ranging from 0.3 watts/cm^2 to 0.03 watts/cm^2 were employed for the 19 MeV and 9.5 MeV runs. We expect no significant heating from the beam, since the copper's conductivity suppresses hot spots. In fact, no variation in the yield with beam power was observed. We can see that the yield is stable from 70°C to 170°C. The 19 MeV points at 40°C and 210°C suggest the behavior illustrated in Fig. 7, but the variation is not large enough to be conclusive. Three additional 19 MeV runs are tabulated in Table 12. These were not included with the others, because of the rather extreme conditions under which they were executed. The beam power for these was

over 3 watts/cm^2. Note that the pressures are much higher than quoted for the other runs. The low yield from the run conducted at 1.5×10^{-7} torr indicates that pressures this high will result in surface contamination -- even at 205°C. We believe that the same is true for the run performed at 37°C. But even with these large excursions from our usual conditions, the yield was stable to within a factor of 2.

One additional comparison between Tables 11 and 12 is fruitful. Note that in the runs displayed in Table 12 the amount of material removed from the surface is two orders of magnitude greater than in the other 19 MeV runs. In addition, the 19 MeV runs in Table 11 vary in the amount of material removed by a factor of 4 but show no significant variation in the yield. In other words, we can discern no dose dependence in the yield. Now that we have established that our data are not being influenced by temperature, pressure or dose, we may turn to the variables concerning more fundamental aspects of the sputtering process.

The most striking feature of the yield is its energy dependence, which is displayed in Fig. 32 along with an electronic stopping power curve from Northcliffe and Schilling (1970). Unfortunately, the energy dependence cannot be decoupled from an apparent incident charge state effect, which we show for the 4.75 MeV and 9.5 MeV points. So far, the charge state effect is not firmly established, but we have reason to expect it to occur if the ion explosion is producing the sputtering (see Section II). At a given energy the tandem accelerator does not allow much latitude in

choosing the incident charge state. In particular, the machine does not permit us to easily irradiate the target with ions whose charge is close to the equilibrium value (see Fig. 3). An additional complication arises from our ignorance of the behavior of the charge state as the ion penetrates the target surface. The distance necessary to equilibrate the charge is not known. Furthermore, the incident ion ejects 5-10 electrons out into space when it strikes the surface. We do not know what effect this has on the ion or the sputtering mechanism. In any event, the dependence of the sputtering mechanism on the electronic stopping power (or some component of the electronic stopping power such as the primary ionization rate) is evident. At energies above 9.5 MeV the square of the primary ionization rate provides a better fit to the data than the electronic stopping power (see Fig. 2), but it also does not decrease as steeply as the data.

Our final test involved the dependence of the yield on the mass of the projectile. We irradiated the target with ^{4}He(+1) at 4 MeV, 2 MeV and 1 MeV. If the sputtering behaves as predicted by the Haff model, we expect the yield to be the fluorine yield reduced by the ratio of the effective charges to the fourth power:

$$S_{He}(U) = S_F(U)\left(\frac{\overline{Z}(He)}{\overline{Z}(F)}\right)^4 .$$

At 1 MeV this expression predicts a yield of 8×10^{-2}. An estimate of the yield from the Sigmund theory, with $\alpha = 0.1$ and $U = 2.5$ eV, gives us $S(U) = 3 \times 10^{-4}$ at 1 MeV. We established

the ^{4}He fluence for the experiment using the Haff prediction rather than the Sigmund prediction, and the track density produced by the catcher foil was just measurable. The signal-to-noise ratio was about one. From this we obtained a crude estimate for the yield at 1 MeV, which was $S(U) = 2 \times 10^{-4}$. The data were not good enough to allow us to determine the energy dependence of the yield, but the magnitude of the results suggests that the ^{4}He induced sputtering is mediated by the Sigmund mechanism.

5. Energy Spectrum Determination

Time-of-flight experiments have proved to be powerful probes of the mechanisms that produce sputtering (Thompson 1968 and Weller and Tombrello 1978). Since the high energy yield measurements described in the previous section are incapable of discriminating between cascade and thermal spike processes, we adapted the apparatus designed by Weller (1978) to our high energy experiment in an attempt to decide the issue. Though the energy spectrum determination was successful, we will see that the results were inconclusive. But the experiment was not in vain. Characteristically, the UF_4 behaved in a surprising manner.

In both of the runs performed, we used a 4.74 MeV $^{19}F(+2)$ beam transported into the North 10^o leg of the Caltech tandem. The chamber used is shown in Fig. 33. Fortunately, only minor modifications of Weller's apparatus were required, so we refer the reader to his thesis for most of the details. Beam chopping was provided with a set of plates between the tandem tank and the

90° analyzing magnet. As before, the collector wheel rotated at 500 rev/sec, and the radius of the collector was 5.08 cm. The pressure in the motor chamber during the runs was always below 10^{-6} torr.

Since long runs resulting in high fluences were required, we redesigned the UF_4 target. The target surface consisted of a UF_4 film about 5000 Å thick that was evaporated onto a polished copper backing. The film was evaporated and baked under the same conditions used for the other UF_4 targets (see Section III.E.3). The target assembly was mounted on a bellows with 2 cm travel. By moving the target during the run, we limited the fluence on any spot of the film to less than $5 \times 10^{16}/cm^2$. Since the design precluded an internal heater and thermocouple, we heated the target externally with heating tapes and estimated the temperature with a surface thermometer. We performed the first run at a target temperature of $170^{\circ}C$ and the second run at a temperature of $75^{\circ}C$. In both runs the chamber pressure was about 10^{-8} torr with the beam on target. There were two very important differences between the two runs. In the first run we biased the target at +300 V to suppress electrons, while in the second the target was not biased. Furthermore, in the first run we employed a collector wheel with two slots, while in the second the wheel had only one slot.

The analysis of the data was performed in the manner described by Weller (1978). In the first run the distance ℓ between target and wheel was 74.8 cm, so the relationship between E and z is

$$E = 880.35 \text{ eV}/z^2 \ . \qquad \text{(Run I)}$$

E is the energy of the sputtered particles. z is a dimensionless parameter related to the travel time t required for a sputtered particle to reach the wheel:

$$z = (2.80 \times 10^{-5}/\text{sec})t \ .$$

For the second run ℓ = 87.2 cm, so

$$E = 1196.4 \text{ eV}/z^2 \ . \qquad \text{(Run II)}$$

For the arrival time spectra we plot the track density on the wheel (arbitrarily normalized) versus z. We display these in Figs. 34 and 35. For the energy spectra we plot the track density (again arbitrarily normalized) times z^3 versus the sputtered particle energy E (see Figs. 36 and 37).

The difference between the two sets of data is striking--especially when we compare the arrival time spectra. We believe that the difference is due to the target bias. Any sputtered particles that were positively charged would be accelerated by the +300 V bias, which would cause the yield to pile up at low z. Recall that in the first run we employed a wheel with two slots, so we see two identical spectra in the plot. If we assume that the particles in the two sharp peaks were accelerated by the bias, we obtain a charged fraction of 47%. This is extraordinarily high given that Sigmund sputtering rarely produces charged fractions of more than a few percent. It is not surprising, however, in view

of the ionizing power of the incident beam.

We believe that the true energy spectrum of the sputtered uranium is represented by the yield from the second run. Note that the energy spectrum has a kink at about 5 eV. This means that the data at energies above 5 eV are probably not reliable, since the enhancement at high energies may be caused by extremely low energy particles from the beam pulse during the previous revolution of the wheel. On the other hand, the data at energies below 5 eV are of high quality. In Figs. 38 and 39 we show two fits to the data below 5 eV. Remember that we are attempting to discriminate between thermal and cascade phenomena. Consequently, the first fit takes the Maxwell-Boltzmann form

$$1.7 \times 10^{7} \; E^{\frac{1}{2}} \exp(-E/.62 \text{ eV})$$

corresponding to a temperature of 7000°K. The second fit is a three parameter fit to the functional form expected from a cascade (see Weller 1978 and Section II):

$$3.1 \times 10^{8} \; \frac{E}{(E + 1.2 \text{ eV})^{6.1}} \; .$$

We will comment on the significance of these fits in the next section.

IV. DISCUSSION

With the data in hand, we may again consider the relative merits of the sputtering models presented in Section II. Our goal was to amass sufficient evidence to allow us to unambiguously determine the identity of the mechanism producing the high yields in UF_4. We begin by assessing the extent to which we have attained that goal. Having done so, we will see that some deficiencies remain, so we will propose a few additional experiments to remedy them.

Several of the contenders may be quickly eliminated. From our earlier discussions we know that the Sigmund theory cannot describe the sputtering behavior of UF_4 in the electronic stopping region, though it works well at lower energies. The success of the Sigmund theory at low energies indicates that chemical rearrangement is not producing the anomalous yields. If chemical effects were influencing the high energy yields, we would see some manifestation of them in the violent disturbances induced by the low energy bombardment. One slightly worrisome point concerning chemical sputtering remains to be tested, however. The anomalous yield was seen only when bombarding a fluoride target with fluorine. We will comment on this later. Finally, the very low yields obtained from the high energy ^4He irradiations demonstrate that induced desorption is not important here. Had such a mechanism been available, the ^4He would surely have triggered it.

Only the thermal spike and ion explosion mechanisms remain serious candidates, and the data do not allow us to choose between them. The energy dependence of the yield from UF_4 can be fit to either model, and so can the mass dependence. From the energy spectrum data, one might argue that the thermal spike mechanism is favored, since the temperature obtained is reasonable while the parameters obtained from the cascade fit are not. Yet, this is not a cogent argument, because we know that the energy of the primary recoils produced by an ion explosion should be unusually low. In addition, the high degree of ionization at the surface could significantly lower the surface binding energy. Therefore, we expect the energy spectrum produced by such a weak cascade to deviate from the shape illustrated in Fig. 1. Moreover, the charge state dependence of the yield tends to undermine the argument in favor of the thermal spike picture. Though one might aver that the unequilibrated charge state influences the rate of heat deposition at the surface, it is difficult to imagine that the region along the ion's path could support the induced temperature gradients long enough to influence the evaporation rate from the spike. Clearly, more experimental work is needed.

Before proposing some new experiments to resolve the ion explosion versus thermal spike issue, we must turn our attention to a few loose ends remaining from the experiments just completed. To finally put our worries about chemical effects to rest, two experiments are needed. The first is a low energy yield determination with a fluorine beam on UF_4; the second is a high energy

yield determination with a neon beam on UF_4. The mass dependence of the yield also needs further study: experiments employing ^{12}C and ^{35}Cl beams would be informative. Finally, the statistics for the charge state effect need to be improved with a few additional runs. We will probably perform these in an improved chamber with tighter tolerances for the target position and with a larger catcher foil radius. This would allow us to determine the angular distributions with greater accuracy.

The experiment with the highest priority will only require a trivial modification of the current apparatus. Recall that the glass and UO_2 irradiations performed at 45^o incidence produced angular distributions that peaked at 90^o relative to the beam direction. Though this was probably due to the Sigmund mechanism, we suspect that the ion explosion would behave similarly but for a different reason. In the ion explosion the coulomb repulsion is likely to propel the primary recoils radially outward from the incident ion's path. Such an effect could not come from a thermal spike, because the equilibration process occurs so slowly that the spike will not remember the direction from which the ion came. So we propose to irradiate a UF_4 target with high energy ^{19}F incident at 45^o. If the angular distribution deviates from a cosine peaked at the target normal, we may be assured that thermal processes are not at work.

The success of our Rutherford backscattering technique suggests one last experiment on UF_4. We could sputter a target similar to the self supporting foil used for the uranium-fluorine ratio

determination. By monitoring the ratio, we could experimentally determine the fluorine sputtering yield relative to the uranium yield. If the ratio changes, we will know that the UF_4 is not leaving the surface as a complete molecule.

Naturally, one wonders if the mechanism operating in UF_4 at high energies will appear in other insulators. Biersack and Santner (1976) have sputtered KCl and found yields that follow the electronic stopping power. But, unlike the UF_4 sputtering, the KCl yields exhibit an exponential dependence on the target temperature, which indicates that alkali halide sputtering is mediated by a different mechanism. Brown et al. (1978) have studied the sputtering of ice by light ions with energies in the MeV range. They found very high yields, which seem to behave in a manner similar to that of the UF_4. Unfortunately, the extraordinary difficulties encountered in working with such a target have precluded a comprehensive set of experiments. Surprisingly, a low energy sputtering experiment on SiO_2 performed by Ahn et al. (1975) has uncovered an effect that may be related to our high energy mechanism. They found that simultaneous bombardment with 1 keV Xe and 3.5 keV electrons produced a substantially higher yield than with Xe alone. Though they attempted to explain the enhanced yield with an induced desorption model, one should not exclude the possibility that the electronic excitation induced by the electron beam is triggering some component of the mechanism found at high energies. In particular, the electron beam may be reducing the surface binding energy. A similar effect has been invoked by

Thompson and Johar (1979) to explain anomalies found in sputtering by polyatomic ions. They suggest that the disruption produced by the nuclear stopping power decreases the binding energy.

As these clues accumulate we begin to realize that the primitive theories presented in Section II do not encompass all of the phenomena associated with high energy sputtering. For instance, none of them allow for binding energies that may be influenced by the dynamics of the sputtering mechanism. Whether minor modifications of one of the current models will result in an adequate description is not yet clear. But we suspect that substantial advances in our ability to describe disordered systems will be required before a comprehensive theory will emerge.

Appendix A - Standard Glasses Used for Neutron Irradiation

Two techniques can be employed when using a uranium containing standard glass to determine neutron fluences. We can etch the latent fission fragment tracks in the glass itself, or we can etch latent tracks in a piece of mica that was firmly pressed against the glass during the irradiation. In our experiments, we have adopted the latter approach, since it allows us to reuse the glass. Ron Gregg has compared results from the two approaches and found them to be in agreement (Gregg 1977).

With either technique, one must know the range of a fission fragment in the glass matrix. Unfortunately, the uncertainty in this number is quite large. Two values have been quoted. The first, $r = 2.24 \times 10^{-3} g/cm^2$, is due to Haines, and it is discussed in detail by Gregg (1977). The second, $r = 2.91 \times 10^{-3} g/cm^2$, was quoted by Carpenter (1972) in his measurement of the U concentration in NBS-612 with the track technique. Using this range, Carpenter obtained a value for the U concentration that deviated less than 2% from the values obtained with mass spectrometric analyses. Though this result makes the Carpenter number rather attractive, we will adopt the value used in the Gregg thesis: $r = 2.24 \times 10^{-3} g/cm^2$. We will apply it to both standard glasses, even though their compositions differ slightly (see Table 14). Even if the true range of the fission fragment were accurately known, a further problem would arise due to difficulties in counting etch pits from fragments that penetrate only a micron or less into the mica. The threshold for detecting very shallow pits varies among

observers, and a given observer will not necessarily detect the pits consistently. Thus, we can measure the neutron flux with an accuracy no better than about 20%.

Given the range of a fission fragment, we can calculate the effective number of ^{235}U atoms per square centimeter available in the glass. The appropriate formula is

$$^{235}U/cm^2 = \frac{r}{2}\left[\frac{(\text{wt. fraction U})(6.022 \times 10^{23})}{238.03}\right][\text{isotope fraction } ^{235}U].$$

The factor of $\frac{1}{2}$ arises from geometrical considerations: only $\frac{1}{4}$ of the fission fragments produced within r of the surface travel in a direction allowing them to penetrate the surface. Remember that each fission event produces two fragments. In Table 13 we display the relevant numbers for NBS-612 and the 0.10% Corning glass. The numbers for the Corning glass are based on a UO_3 weight fraction of 10^{-3}. We used a molecular weight of 286.03.

With the ^{235}U surface density in hand, we can calculate the number density of tracks from a given neutron fluence.

$$\text{tracks}/cm^2 = (\text{neutrons}/cm^2)(^{235}U/cm^2)\,\sigma$$

σ is the thermal neutron fission cross section, which we take to be $582 \times 10^{-24} cm^2$. In Table 13 we also quote the reciprocal of $\sigma(^{235}U/cm^2)$, which gives us the number of neutrons per track.

The NBS-612 glass has been thoroughly studied by the National Bureau of Standards. In addition to the Carpenter measurement, two independent isotope dilution studies produced

numbers differing by only 0.1% (Carpenter 1972). No such studies have been performed on the Corning glass. To check the accuracy of the 0.10% glass, we irradiated it together with the NBS-612 glass in the UCLA Reactor thermal column. Owing to the low track density from the NBS glass, its mica was etched for 80 minutes in 48% HF rather than the normal 20 minutes for the 0.10% glass. We do not believe that this introduced a significant error into the measurement. The track densities obtained were

$$\text{NBS-612:} \quad 1.94 \pm .07 \times 10^{4}/\text{cm}^2$$

$$\text{Corning 0.10\%:} \quad 1.31 \pm .04 \times 10^{6}/\text{cm}^2 .$$

The ratio of these densities is $1.48 \pm .10 \times 10^{-2}$. From Table 13 we predict a ratio of 1.49×10^{-2}, so we can accept the numbers quoted by Corning.

Appendix B - Selected Chemical and Physical Properties of Uranium Fluorides

Six fluorides of uranium are known: UF_3, UF_4, $UF_{4.25}$, $UF_{4.5}$, UF_5 and UF_6. We will discuss UF_3, UF_4 and UF_6, with most of our effort directed toward UF_4. Unless explicitly noted, all information quoted here is from Katz and Rabinowitch (1951) or Rand and Kubaschewski (1963). For the heat of formation at 25°C we use the notation H_{298}. Energies will be expressed in calories or kilocalories; the reader should note that 1 eV/atom corresponds to 23.07 kcal/mole. A list of important chemical reactions involving uranium fluorides has been compiled by Steunenberg and Vogel (1961).

UF_3

This compound forms deep red-violet crystals with an orthorhombic unit cell. At 1000°C it may be prepared with the reaction $2UF_4 + H_2 \rightleftharpoons 2UF_3 + 2HF$. At this temperature it also disproportionates: $4UF_3 \rightleftharpoons 3UF_4 + U$. Both reactions proceed at a negligible rate below 900°C. Its preparation from UF_4 requires extremely pure UF_4, which may be obtained by sublimating it in high vacuum. $H_{298} = -345 \pm 10$ kcal/mole.

UF_4

UF_4 is an insulator with ionic bonds (Ellis 1976). It forms brilliant green crystals with a monoclinic unit cell. The molecular volume is 77.5 $Å^3$, and the U-F bond distances in the

lattice are 2.249 Å - 2.318 Å (Larson et al. 1964). It may be formed with the reaction $UO_2 + 4HF \rightleftharpoons UF_4 + 2H_2O$. H_{298} = -450 ± 5 kcal/mole. It is stable in air to 200°C and in O_2 to 800°C. It can hydrate to $UF_4(2.5H_2O)$ with a heat of -9 ± 2 kcal/mole, but the water may be expelled by heating in vacuum at 200°C for 24 hours.

UF_4 melts at 1309°K. Its vapor pressure obeys the expression

$$p(\text{torr}) = 760 \exp(-\Delta G/RT)$$

where

$$\Delta G(\text{cal/mole}) = 75,100 - 90.3T + 13.8T \log_{10} T$$

and R = 1.986 cal/°K. At 100°C p = 7×10^{-30} torr, and at 200°C p = 7×10^{-21} torr.

The electrical resistivity of sintered UF_4 pellets has been measured by Reynolds and Middleton (1952). They quote a value of 10^8 Ω-cm, but the purity of the sample is not known. The thermal conductivity of fused UF_4 at 60°C is 5×10^{-3} cal/sec-cm-°K = 2×10^{-2} watt/cm-°K (Steunenberg and Vogel 1961). The thermal diffusion coefficient is 8×10^{-3} cm²/sec.

UF_6

UF_6 may be prepared with the reaction $UF_4 + F_2 \rightleftharpoons UF_6$, which proceeds slowly at temperatures below 250°C. H_{298} = -511.5 kcal/mole. UF_6 melts at 337.2°K and sublimes at 330°K.

REFERENCES

Ahn, J., Perleberg, C.R., Wilcox, D.L., Coburn, J.W. and Winters, H.F., 1975, J. Appl. Phys. 46, 4581.

Andersen, H.H. and Bay, H., 1972, Rad. Eff. 13, 67.
1975, J. Appl. Phys. 46, 2416.

Bevington, P.R., 1969, Data Reduction and Data Analysis for the Physical Sciences (McGraw-Hill, New York), pp. 92-118.

Biersack, J.P. and Santner, E., 1976, Nucl. Instr. Meth. 132, 229.

Brown, W.L., Lanzerotti, L.J., Poate, J.M. and Augustyniak, W.M., 1978, Phys. Rev. Lett. 40, 1027.

Carpenter, B.S., 1972, Anal. Chem. 44, 600.

Chapman, G.E., Farmery, B.W., Thompson, M.W. and Wilson, I.H., 1972, Rad. Eff. 13, 121.

Close, K.J. and Yarwood, J., 1967, Brit. J. Appl. Phys. 18, 1593.

Davies, J.A., L'Ecuyer, J., Matsunami, N., Ollerhead, R. and Bøttiger, J., 1979, to be published.

De Heer, F.J., Schutten, J. and Moustafa, H., 1966, Physica 32, 1766.

Ellis, W.P., 1976, Surface Sci. 61, 37.

Fleischer, R., Price, P. and Walker, R., 1975, Nuclear Tracks in Solids (University of California Press, Berkeley), pp. 3-105.

Flint, O., Polling, J.J. and Charlesby, A., 1954, Acta Met. 2, 698.

Gregg, R., 1977, Ph.D. Thesis, California Institute of Technology.

Haff, P.K., 1976, Appl. Phys. Lett. 29, 473.
1976a, "Notes and Comments on Sputtering", Caltech preprint BAP-7, unpublished.

Haff, P.K. and Switkowski, Z.E., 1976, Appl. Phys. Lett. 29, 549.

Heckman, H.H., Hubbard, E.L. and Simon, W.G., 1963, Phys. Rev. 129, 1240.

Hildenbrand, D.L., 1976, Los Alamos Scientific Laboratory Technical Report No. PYU-4822.

Hill, T.L., 1960, An Introduction to Statistical Thermodynamics (Addison-Wesley, Reading, Massachusetts), pp. 124-140.

Hurkmans, A., Overbosch, E.G., Olander, D.R. and Los, J., 1976, Surface Sci. 54, 154.

Hurkmans, A., Overbosch, E.G. and Los, J., 1976a, Surface Sci. 59, 488.
1977, Surface Sci. 62, 621.

Ishii, T., Naito, K. and Oshima, K., 1970, J. Nucl. Mat. 36, 288.

Johnson, W.S. and Gibbons, J.F., 1969, Projected Range Statistics in Semiconductors, dist. by Stanford University Bookstore.

Katz, J.J. and Rabinowitch, E., 1951, The Chemistry of Uranium (McGraw-Hill, New York), pp. 349-449.

Kelly, R., 1977, Rad. Eff. 32, 91.

Larson, A.C., Roof, R.B. and Cramer, D.T., 1964, Acta Cryst. 17, 555.

Lindhard, J., Nielsen, V. and Scharff, M., 1968, Mat. Fys. Medd. Dan. Vid. Selsk. 36, No. 10.

Marion, J.B., 1970, Classical Dynamics of Particles and Systems (Academic Press, New York), pp. 291-312.

Menzel, D., 1975, Surface Sci. 47, 370.

Northcliffe, L.C. and Schilling, R.F., 1970, Nuclear Data Tables A7, 233.

Oechsner, H., 1975, Appl. Phys. 8, 185.

Overbosch, E.G., Hurkmans, A. and Los, J., 1977, Surface Sci. 63, 417.

Rand, M.H. and Kubaschewski, O., 1963, The Thermochemical Properties of Uranium Compounds (Oliver and Boyd, Edinburgh), pp. 13-18.

Reynolds, D.C. and Middleton, A.E., 1952, AEC Report No. BMI-259.

Schram, B.L., DeHeer, F.J., Van der Wiel, M.J. and Kistemaker, J., 1965, Physica 31, 94.

Schram, B.L., Moustafa, H.R., Schutten, J. and DeHeer, F.J., 1966, Physica 32, 734.

Sigmund, P., 1969, Phys. Rev. 184, 383.
1972, Rev. Roum. Phys. 17, 823, 969 and 1079.

Sigmund, P., Matthies, M.T. and Phillips, D.L., 1971, Rad. Eff. 11, 39.

Steunenberg, R.K. and Vogel, R.C., 1961, in Stoller, S.M. and Richards, R.B. (eds.) Reactor Handbook: Volume II Fuel Reprocessing (Interscience, New York), pp. 251-254.

Thompson, D.A. and Johar, S.S., 1979, Appl. Phys. Lett. 34, 342.

Thompson, M.W., 1968, Phil. Mag. 18, 377.

Weissmann, R. and Sigmund, P. 1973, Rad. Eff. 19, 7.

Weller, R.A., 1978, Ph.D. Thesis, California Institute of Technology.

Weller, R.A. and Tombrello, T.A., 1978, Rad. Eff. 37, 83.

Winterbon, K.B., Sigmund, P. and Sanders, J.B., 1970, Mat. Fys. Medd. Dan. Vid. Selsk. 37, No. 14.

Ziegler, J.F., 1977, Helium: Stopping Power and Ranges in All Elemental Matter (Pergamon Press, New York).

Table 1

Results from the program to assess the errors induced by target misalignment. The geometry used for the calculation is shown in Fig. 11. The calculated distribution, initially produced by a flux with angular dependence $\cos^{B_o}\varphi$, was fit to the form $A\cos^{B}\theta$ and normalized so that a perfect measurement would give B = 1 and A = 2. A square simulated beam spot was used. The parameter r^2 is a measure of the goodness of fit; $r^2 = 1$ implies a perfect fit (see Section III.A.5).

Input Parameters: Foil radius = 1.43 cm

$B_o = 1$

TABLE 1

D_x (mm)	D_y (mm)	D_z (mm)	L (mm)	B	$\frac{A}{B+1}$	r^2
0.0	0.0	0.0	0.5	1.000	1.000	1.000
"	"	-2.0	2.0	0.570	0.972	1.000
"	"	-1.0	"	0.750	0.990	1.000
"	"	0.0	"	0.993	1.000	1.000
"	"	1.0	"	1.355	0.998	0.998
"	"	2.0	"	2.194	0.978	0.964
"	0.5	0.0	"	0.971	1.009	0.994
"	1.0	"	"	0.932	1.021	0.979
"	2.0	"	"	0.830	1.062	0.925
1.0	0.0	"	"	0.993	0.990	1.000
2.0	"	"	"	0.993	0.962	1.000
3.0	"	"	"	0.994	0.918	1.000
0.0	"	"	1.0	0.998	1.000	1.000
"	"	"	4.0	0.972	0.998	1.000
"	"	"	8.0	0.891	0.990	0.997

Table 2

Results from sticking fraction experiments. In 2A we show numbers of immediate interest, while in 2B we show the numbers on which the calculations are based. f is the fraction not sticking to the primary surface. B and the secondary track density at $\theta = 0^{o}$ were taken from a program fitting the track counts to the form $A \cos^{B} \theta$ (see Section III. B).

TABLE 2A

	Primary	Temperature (°C)	Ar Beam Energy (KeV)	^{235}U Fluence on Primary ($10^{13}/cm^2$)	B	f (%)
1	Al Foil - 1/25/77	23	80	4.32	.88	2.83
2	Al Foil - 7/29/77	23	"	1.76	.69	2.48
3	Al Foil - 11/28/77	23	"	2.22	.74	2.05
4	Al Foil - 11/28/77*	23	"	2.14	.74	2.30
5	Al Foil - 8/28/77	23	40	.958	.52	1.62
6	Al Film - 5/10/77	23	80	1.22	.52	2.55
7	Al Film - 5/10/77	152	"	1.28	1.05	2.17
8	Au Film - 4/25/78	23	"	3.60	.70	2.87
9	Au Film - 4/25/78	152	"	3.79	.71	1.27
10	Mica - 1/25/77	23	"	3.22	.86	3.02

*Also irradiated with sputtered ^{238}U.

TABLE 2B

	Primary Track Density ($10^6/cm^2$)	Primary Spot Area (cm^2)	Secondary Track Density at $\theta = 0^\circ$ ($10^5/cm^2$)	Standard Track Densities ($10^6/cm^2$) 0.10%	NBS-612
1	2.59	.22	2.78	1.02	1.41
2	.727	.18	.477	.702	.915
3	1.54	.20	.971	1.18	1.59
4	1.48	.17	.928	1.18	1.59
5	.334	.21	.293	.591	1.49
6	.918	.19	.503	1.27	1.47
7	.956	.20	.645	1.27	1.47
8	1.25	.18	2.29	.590	1.88
9	1.32	.19	1.14	.590	1.88
10	1.93	.20	1.98	1.02	1.41

Table 3

Results from electron microprobe studies of the uranium doped soda-lime glass target. Note the decrease in the sodium content in the irradiated spot (see Section III. C).

TABLE 3

	Composition (weight percent)				
	Na_2O	SiO_2	MgO	Al_2O_3	CaO
Unirradiated Glass	14.2	73.7	2.5	1.9	7.2
Edge of Beam Spot	11.2	75.0	3.0	2.1	7.3
Center of Beam Spot	6.9	78.6	3.3	2.1	8.1

Table 4

Relative sputtering yield data for ^{19}F incident at 45^{o}. The glass target was 0.3 atomic % ^{235}U, while the uranium foil target was 0.72 atomic % ^{235}U. The ^{235}U density per incident ion is quoted at the peaks of the angular distributions, which occur at approximately 90^{o} with respect to the beam direction. The standard glass used was NBS-612. In part A we show numbers of immediate interest, in part B we show the numbers from which those in 4A were calculated (see Section III.C).

TABLE 4A

	Target	Beam Energy (MeV)	Beam Current (particle nanoamps)	^{235}U Density/Incident Ion (10^{-5}/cm^2)
1	Glass	20	22	6
2	"	14	20	7
3	"	10	20	5
4	"	10	5	1
5	"	8	22	9
6	"	2	--	7
7	"	1	3	1
8	U Foil	10	100	4

TABLE 4B

	^{19}F Fluence/10^{14}	Standard Glass Track Density (10^5 /cm^2)	Track Density at Peak (10^4/cm^2)
1	4.4	1.6	1.8
2	"	"	2.0
3	"	"	1.5
4	"	16.	2.8
5	"	1.6	2.5
6	3.3	"	1.5
7	1.5	16.	1.4
8	6.3	"	17.

Table 5

Experimental sputtering yields for ^{19}F incident on UO_2 at normal incidence. In 5A we show numbers of immediate interest; in 5B we show the numbers from which those in 5A were calculated. The uranium yield is defined as the number of uranium atoms leaving the target per incident ion. In runs 1 through 3 we employed a pre-war foil* (0.72% ^{235}U atomic); in all other runs we employed a foil enriched to 99.7% (atomic) ^{235}U. The parameter B and the track density were determined from the program used to fit the track counts to the form $A \cos^B \theta$ (see Section III.A). The standard glass used was NBS-612 (see Section III.D).

Errors:	Track density at $\theta = 0^o$	± 2%
	B	±10%
	Standard glass track density	± 3%

*The adjective "pre-war" indicates that the isotopic content of the uranium has not been altered. The term alludes to World War Two during which the plant at Oak Ridge was built.

TABLE 5A

	Oxide Thickness (Å)	Beam Energy (MeV)	Beam Current (particle nanoamps)	B	Uranium Yield/10^{-3}
1	<500	2	5	0.5	40
2	"	10	40	1.2	10
3	"	20	15	0.7	8
4	500	5	25	0.9	2
5	"	10	25	1.0	9
6	700	2	23	0.4	9
7	"	10	33	0.4	3
8	"	15	10	0.5	3
9	"	20	25	0.4	2
10	"	20	13	0.5	3
11	"	30	9	0.4	2

TABLE 5B

	^{19}F Fluence/10^{13}	Track Density at $\theta = 0^{o}$ ($10^{5}/cm^{2}$)	Standard Glass Track Density ($10^{6}/cm^{2}$)
1	32.	.565	1.41
2	63.	.537	"
3	"	.268	"
4	6.3	9.51	1.61
5	"	5.85	"
6	6.6	2.07	.810
7	6.3	.562	"
8	"	1.42	1.47
9	"	.385	.810
10	"	1.10	1.47
11	"	.765	"

Table 6

Sigmund theory yields for uranium sputtered from UO_2 by ^{19}F. We have taken $\alpha = 0.1$ and $U = 5.4$ eV. We have used the Haff and Switkowski formula for binary sputtering (see Section II and III.D).

TABLE 6

Energy (MeV)	Uranium Yield
2	1×10^{-2}
5	6×10^{-3}
10	4×10^{-3}
15	3×10^{-3}
20	2×10^{-3}
30	2×10^{-3}

Table 7

Calculated values for the laboratory differential scattering cross section and for the final energy in the laboratory (KE_o) of the incident ^4He atom. A screened coulomb potential from the Lindhard theory was used (see Section III.E.2).

TABLE 7

E_o (MeV)	Angle (degrees)	^4He on ^{19}F		^4He on ^{238}U	
		KE_o (MeV)	$d\sigma/d\omega\|_{lab}$ (10^{-25} cm^2/Sr)	KE_o (MeV)	$d\sigma/d\omega\|_{lab}$ (10^{-23} cm^2/Sr)
1.8	135	.867	1.66	1.700	1.82
1.8	150	.810	1.37	1.691	1.52
2.0	135	.963	1.35	1.888	1.48
2.0	150	.900	1.11	1.878	1.24

Table 8

Results from Rutherford backscattering analysis of UF_4 with a ^4He beam. For UF_4 we expect F/U = 4.0 (see Section III.E.2).

TABLE 8

E_o (MeV)	Angle (degrees)	Fluorine Counts	Uranium Counts	F/U
1.8	135	2359	65268	3.98
1.8	150	2408	67087	3.98
2.0	135	2834	79686	3.91
2.0	150	2606	75196	3.88

Table 9

Results from low energy sputtering yield measurements. The first run (I-1) was performed under the conditions used in the high energy experiments: no sputter cleaning preceded it. All of the others were immediately preceded by cleaning runs. The elapsed time between the cessation of the cleaning run and the completion of the yield determination never exceeded 22 seconds. In calculating the number of monolayers removed, we assumed that we have 5.5×10^{14} molecules/cm^2. The uranium yield is the number of uranium atoms ejected per incident ion. The standard glass used was NBS-612. The parameter B and the track density at $\theta = 0^o$ were determined by the program that fits track counts to the form $A \cos^B \theta$ (see Section III.E.3 and Appendix A).

Errors:	Track Density at $\theta = 0^o$	± 2%
	B	± 5%
	Standard Glass Track Density	± 8%
	Neutron Fluence	±20%

TABLE 9A

Run	Pressure (10^{-8} torr)	Beam	Beam Current (particle nanoamps /cm^2)	Monolayers Removed	Uranium Yield
I-1	1.5	^{14}NH	30	.04	0.21
Cleaning	7.5	"	4500	3.0	--
I-2	"	"	4500	.03	0.16
Cleaning	"	"	4200	3.0	--
I-3	"	"	4200	.03	0.14
Cleaning	4.0	^{16}O	4200	3.3	--
II-1	"	"	4200	.03	0.17
Cleaning	25.	^{20}Ne	4500	5.2	--
II-2	"	"	4500	.05	0.26

TABLE 9B

Run	B	Fluence (10^{14} particles/cm^2)	Track Density at $\theta = 0^o$ (10^5 /cm^2)	Standard Glass Track Density (10^5 /cm^2)
I-1	.60	1.02	3.41	4.93
Cleaning	--	111.	--	
I-2	.92	1.05	3.12	"
Cleaning	--	111.	--	
I-3	.78	1.05	2.61	"
Cleaning	--	111.	--	
II-1	.91	1.05	3.30	4.88
Cleaning	--	111.	--	
II-2	.78	1.05	4.79	"

Table 10

Yields of uranium sputtered from UF_4 by high energy ^{19}F. The averages and standard deviations were calculated directly from the uranium yield column. In calculating the number of monolayers removed, we assumed that we have 5.5×10^{14} molecules/cm^2 and that four fluorine atoms leave the surface for every uranium atom sputtered. The standard glass used was NBS-612. The parameter B and the track density at $\theta = 0^o$ were determined from the program used to fit the track counts to the form $A \cos^B \theta$ (see Section III.E.4 and Fig. 32).

Errors:	Track Density at $\theta = 0^o$	± 2%
	B	± 5%
	Standard Glass Track Density	± 8%
	Neutron Fluence	±20%

TABLE 10A

	Energy (MeV)	Charge State	Uranium Yield	Average Yield	Standard Deviation
1	1.19	2	.697	.70	--
2	2.38	"	2.44	2.5	0.11
3	"	"	2.60		
4	4.75	"	6.53	5.6	1.0
5	"	"	4.46		
6	"	"	5.73		
7	"	3	8.17	7.1	1.5
8	"	"	6.10		
9	9.50	"	5.91	5.5	0.60
10	"	"	5.14		
11	"	"	4.68		
12	"	"	6.19		
13	"	"	5.33		
14	"	4	6.96	7.0	--
15	19.0	"	2.71	2.4	0.38
16	"	"	2.56		
17	"	"	2.45		
18	"	"	1.86		
19	"	"	2.04		
20	"	"	2.82		
21	28.5	5	1.78	1.8	--

TABLE 10B

	B	Monolayers Removed/10^{-2}	Track Density at $\theta = 0^{o}$ ($10^{5}/cm^{2}$)	Standard Glass Track Density ($10^{5}/cm^{2}$)
1	.71	4.2	3.92	4.92
2	.95	1.9	3.69	9.33
3	.72	8.0	7.33	4.92
4	.72	5.8	10.5	5.90
5	.72	2.1	3.64	9.40
6	.81	2.6	5.20	9.91
7	.81	6.6	6.94	5.20
8	.70	4.7	4.28	4.93
9	.81	5.3	10.1	5.90
10	.72	2.3	4.47	9.91
11	.77	4.8	5.00	5.26
12	.85	6.3	6.81	5.20
13	.73	5.6	5.25	4.93
14	.84	7.1	7.64	5.20
15	.74	6.3	11.1	9.29
16	.82	2.9	5.14	8.78
17	.79	2.7	4.82	8.78
18	.88	1.7	3.32	9.40
19	.63	1.6	2.60	9.33
20	.83	4.7	5.03	5.26
21	.83	4.7	5.07	5.26

Table 11

Temperature and pressure dependence of the uranium yields produced by bombarding UF_4 with ^{19}F at 9.5 MeV and 19 MeV. Note that these yields are stable between 70°C and 170°C. All of the runs, except those at 40°C and 210°C, are included in Table 10 (see Section III.E.4).

TABLE 11

Energy (MeV)	Target Temperature (°C)	Pressure (10^{-9} torr)	Uranium Yield	Average Uranium Yield
9.50	70	3	5.91	5.5
"	"	4	5.14	
9.50	150	5	6.19	5.4
"	160	5	5.33	
"	170	8	4.68	
19.0	40	30	1.4	1.4
19.0	70	8	2.56	2.3
"	"	8	2.45	
"	"	4	1.86	
19.0	120	8	2.71	2.4
"	"	4	2.04	
19.0	170	8	2.82	2.8
19.0	210	8	3.6	3.6

Table 12

Results from three runs in which UF_4 was bombarded with 19 MeV $^{19}F(+4)$. We show these yields to demonstrate the stability of the measurement against large increases in pressure and in the fluorine dose. The expected yield, taken from Table 10, is 2.4 ± 0.38. The track densities in the data bands were too high to allow a complete scan, so only a few hundred tracks were counted at the peak of each angular distribution. The yields quoted are subject to an uncertainty of perhaps ±50% (see Section III.E.4).

TABLE 12

Target Temperature (^{o}C)	Pressure (10^{-8} torr)	Monolayers Removed	Uranium Yield
205	15.	6.2	1.3
164	3.0	14.	3.0
37	3.0	6.5	1.4

Table 13

Numbers used to predict neutron fluences from the standard glasses. The Corning glass was used for fluences of about 10^{14} neutrons/cm^2, and NBS-612 was used for fluences of about 10^{16} neutrons/cm^2. In calculating the ^{235}U surface densities, we used a fission fragment range of 2.24×10^{-3} g/cm^2, which is subject to a large uncertainty (see Appendix A).

TABLE 13

Glass	Weight Fraction of Uranium	Isotope Fraction of ^{235}U	$^{235}U/cm^2$	Neutrons per Track
Corning 0.10%	8.32×10^{-4}	7.20×10^{-3}	1.70×10^{13}	1.01×10^{8}
NBS-612	$37.38 \pm 0.08 \times 10^{-6}$	2.392×10^{-3}	2.53×10^{11}	6.78×10^{9}

Table 14

Standard glass compositions by weight (see Appendix A).

TABLE 14

Glass	Component			
	SiO_2	Na_2O	CaO	Al_2O_3
Corning 0.10%	73%	17%	6%	4%
NBS-612	72%	14%	12%	2%

Figure 1

The energy spectrum, S(E), of ^{235}U sputtered from a uranium metal target (reprinted from the thesis by R.A. Weller (1978)). The vertical scale is arbitrary. The smooth curve is an empirical fit to the data, while the broken curve has the form $6.5\ E/(E+5.4)^3$ (see Section II).

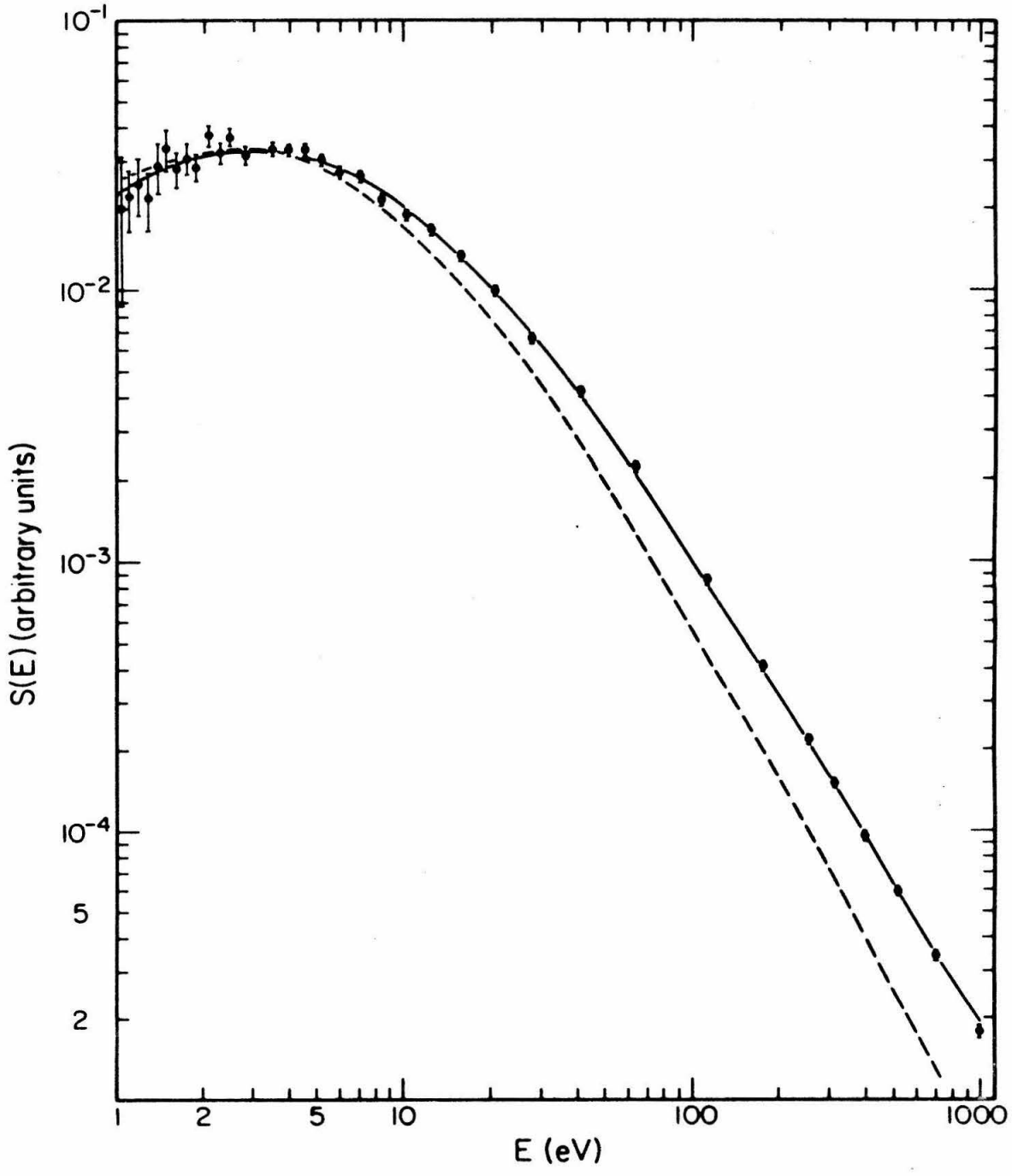

Figure 1

Figure 2

The primary ionization rate squared for fluorine (Z = 9). It expresses the energy dependence of the sputtering yield in the Haff model. For an explanation of its origin, see Figs. 3, 4 and 5 and the text (Section II).

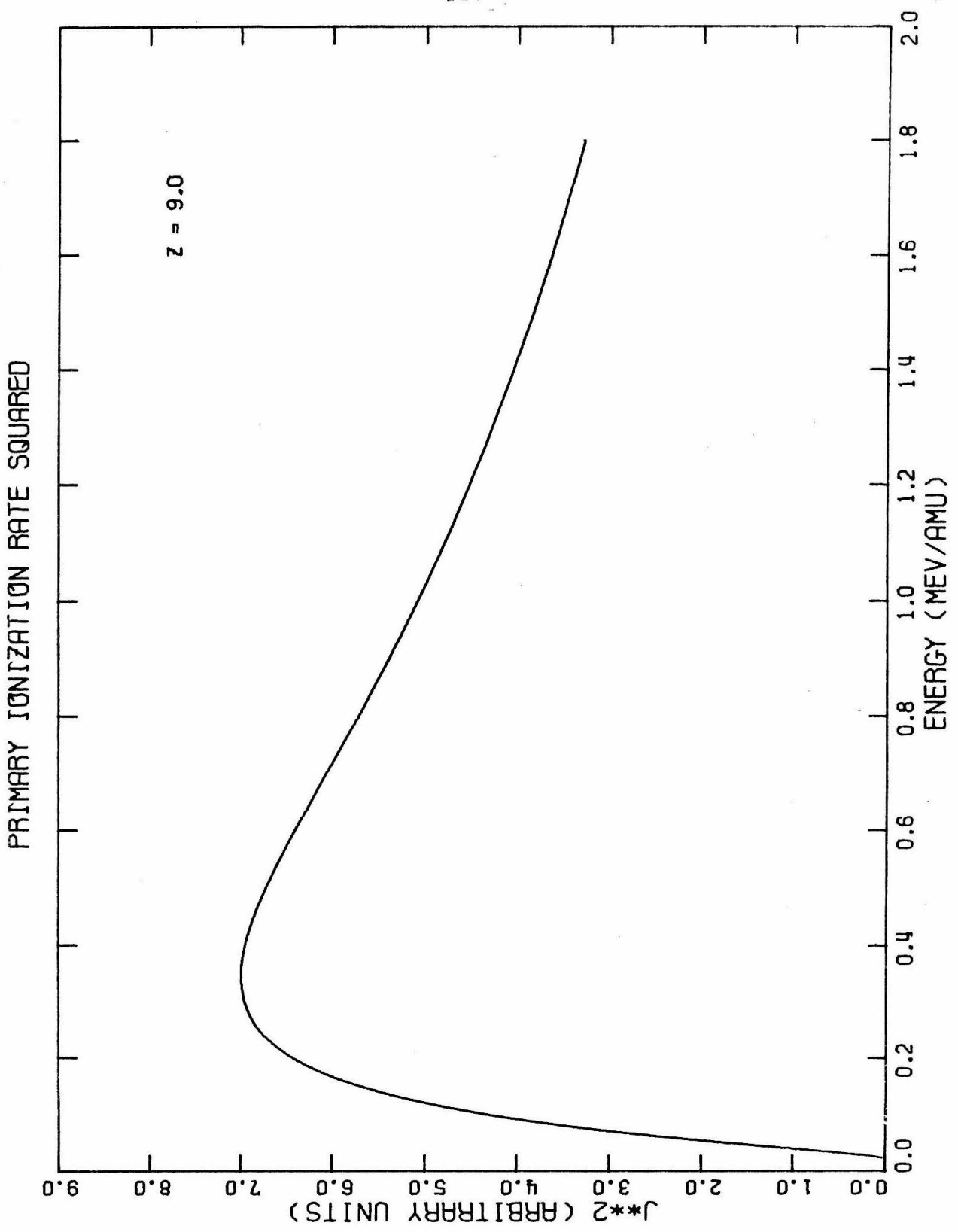
PRIMARY IONIZATION RATE SQUARED
J**2 (ARBITRARY UNITS)
ENERGY (MEV/AMU)
Z = 9.0
0.0
1.0
2.0
3.0
4.0
5.0
6.0
7.0
8.0
9.0
0.0
0.2
0.4
0.6
0.8
1.0
1.2
1.4
1.6
1.8
2.0

Figure 2

Figure 3

The equilibrated charge of fluorine passing through a solid as predicted by Heckman, Hubbard and Simon (1963):

$$\overline{Z} = Z \left[1 - 10^{-\frac{1}{3}(137\beta/Z^{0.55})}\right]$$

(see Section II).

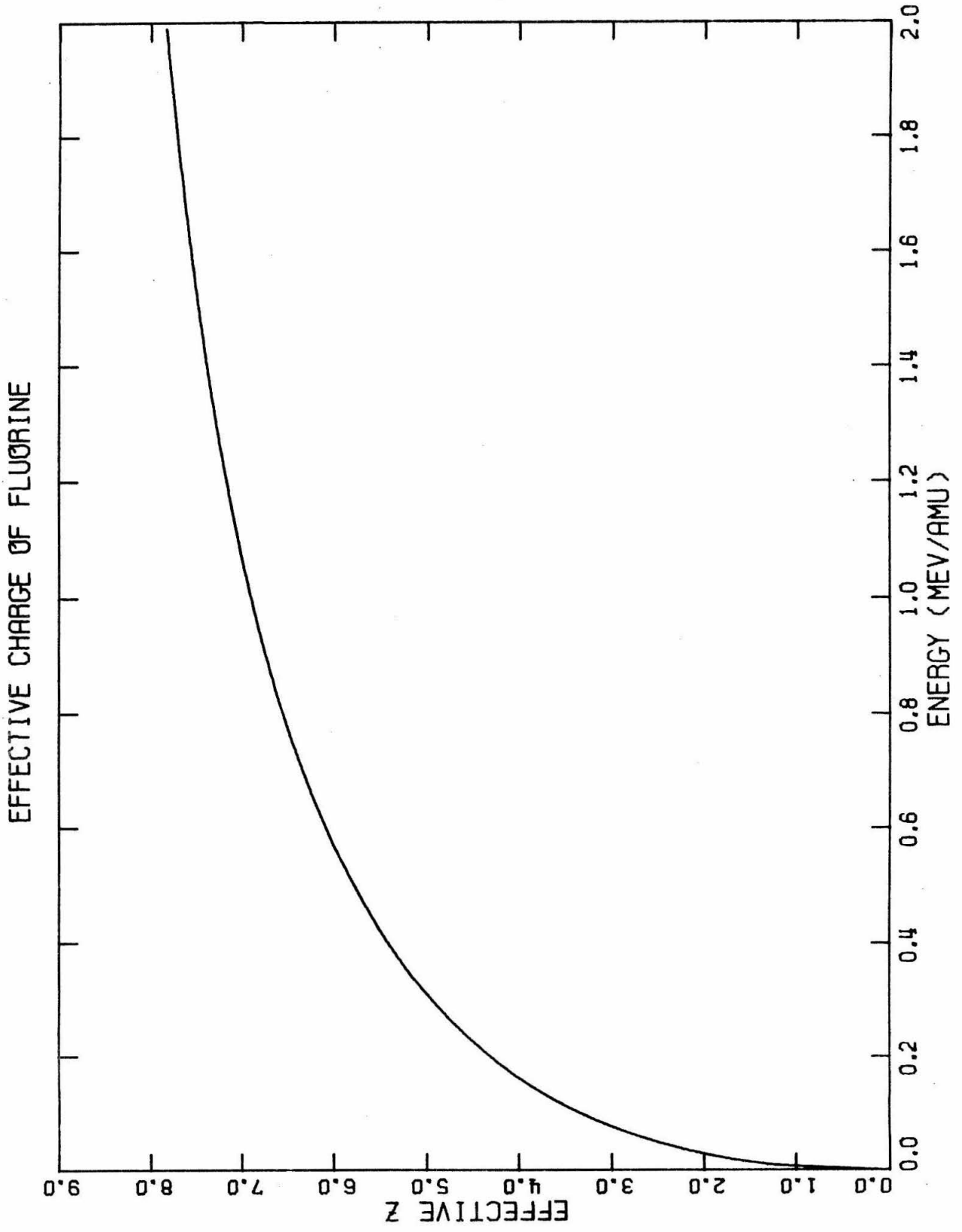
EFFECTIVE CHARGE OF FLUORINE
EFFECTIVE Z
0.0
1.0
2.0
3.0
4.0
5.0
6.0
7.0
8.0
9.0
ENERGY (MEV/AMU)
0.0
0.2
0.4
0.6
0.8
1.0
1.2
1.4
1.6
1.8
2.0

Figure 3

Figure 4

A fit to the ionization cross section data for ^{40}Ar from the work of Schram et al. (1965 and 1966) and DeHeer et al. (1966). Data from ionization by protons is used at low energies, and data from ionization by electrons is used at high energies. The original electron energies have been multiplied by m_p/m_e to produce a consistent energy scale. The fit is of the form

$$J_p = \frac{A}{E_p} \ln(B E_p)$$

where $B = 4.5 \times 10^{-2}$/keV (see Section II).

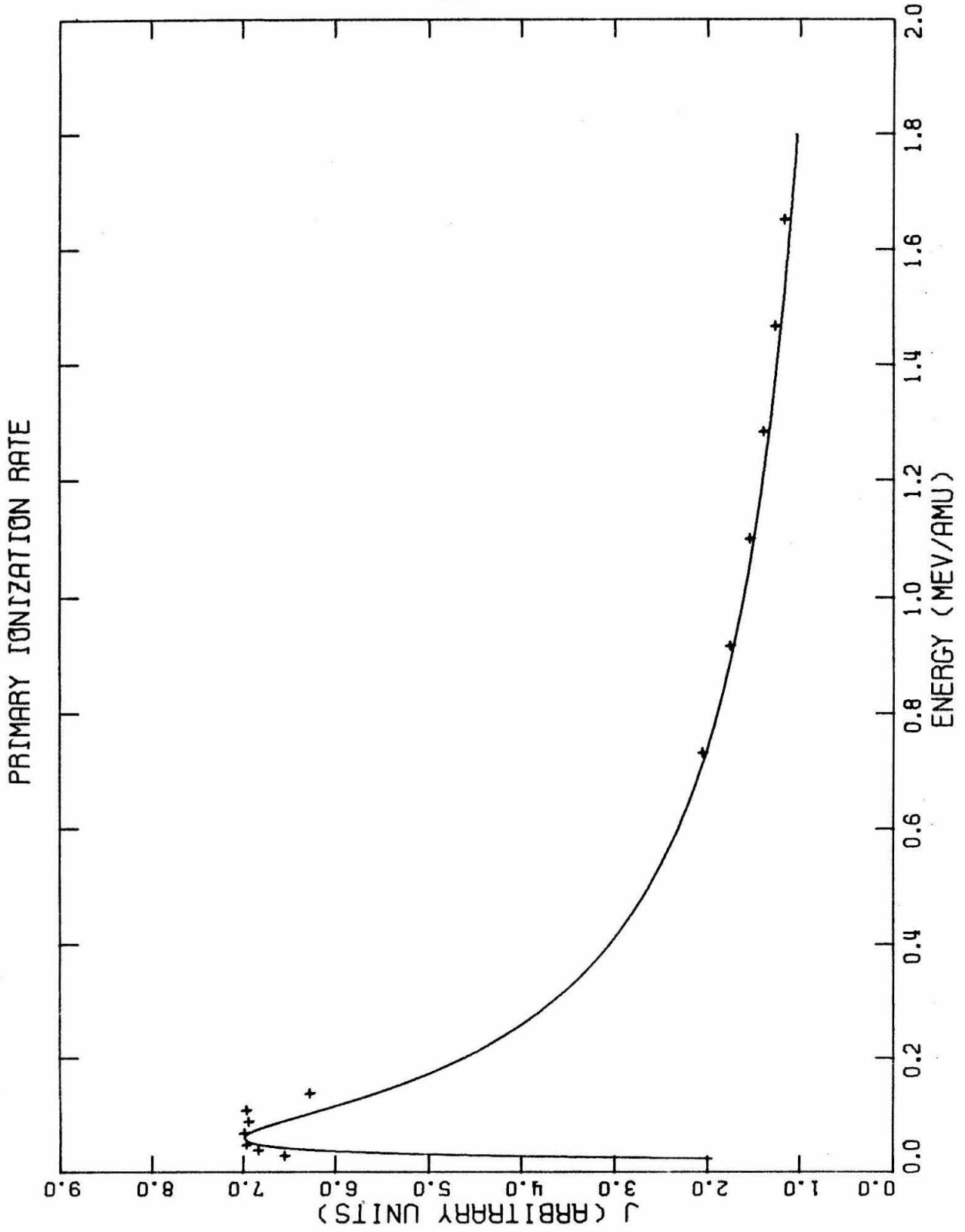
PRIMARY IONIZATION RATE
J (ARBITRARY UNITS)
0.0
1.0
2.0
3.0
4.0
5.0
6.0
7.0
8.0
9.0
0.0
0.2
0.4
0.6
0.8
1.0
1.2
1.4
1.6
1.8
2.0
ENERGY (MEV/AMU)

Figure 4

Figure 5

Primary ionization rate for fluorine, which is equal to $\overline{Z}^2 J_p$ (see Section II).

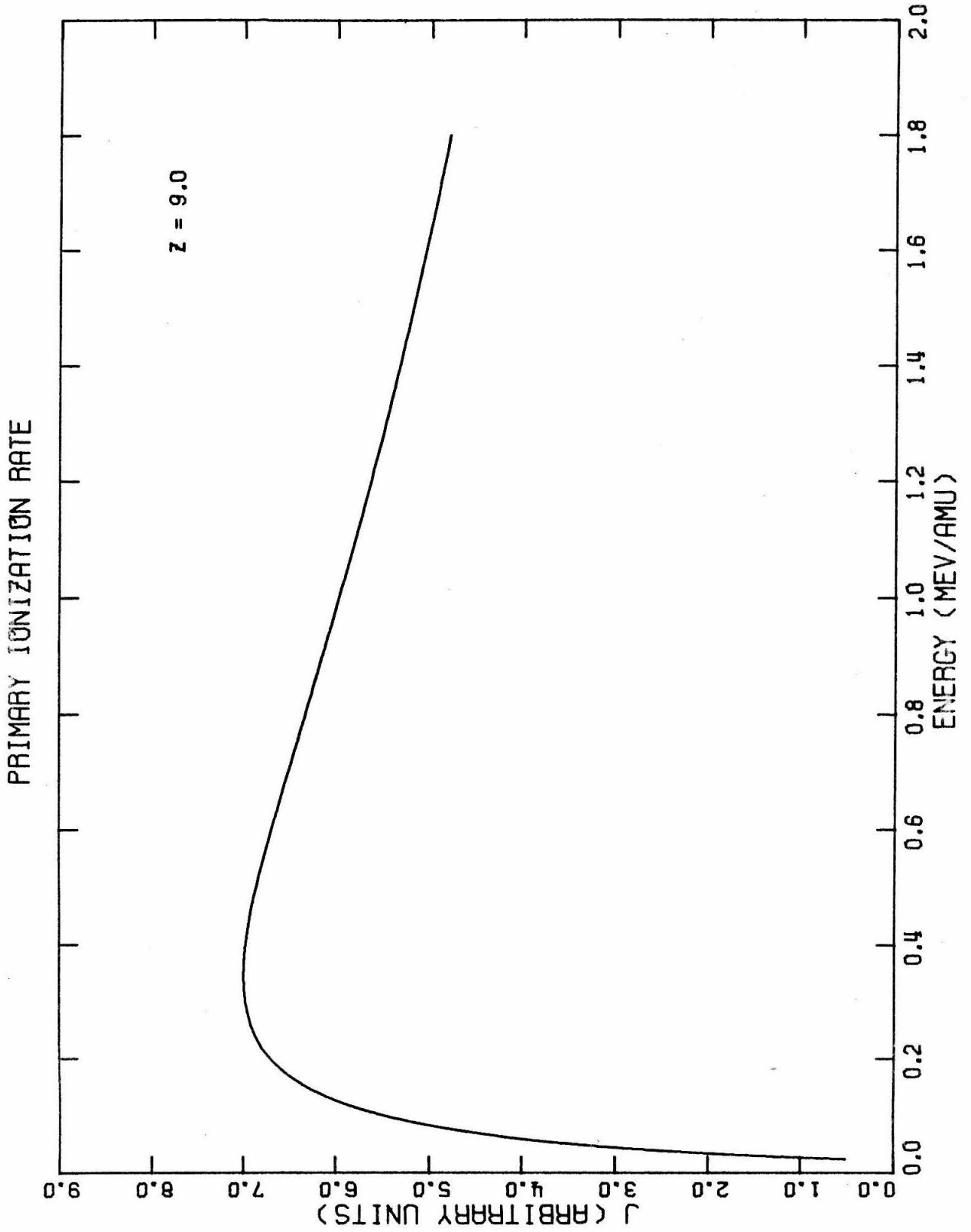
PRIMARY IONIZATION RATE
Z = 9.0
J (ARBITRARY UNITS)
0.0
1.0
2.0
3.0
4.0
5.0
6.0
7.0
8.0
9.0
ENERGY (MEV/AMU)
0.0
0.2
0.4
0.6
0.8
1.0
1.2
1.4
1.6
1.8
2.0

Figure 5

Figure 6

Schematic of the Frank-Condon process as it applies to induced desorption. An atom bound to the surface is promoted from its ground state to one of the two excited states. If the energies of the excited atoms are greater than the energies of the states at infinity, they will escape with the energy spectra shown to the left (see Section II).

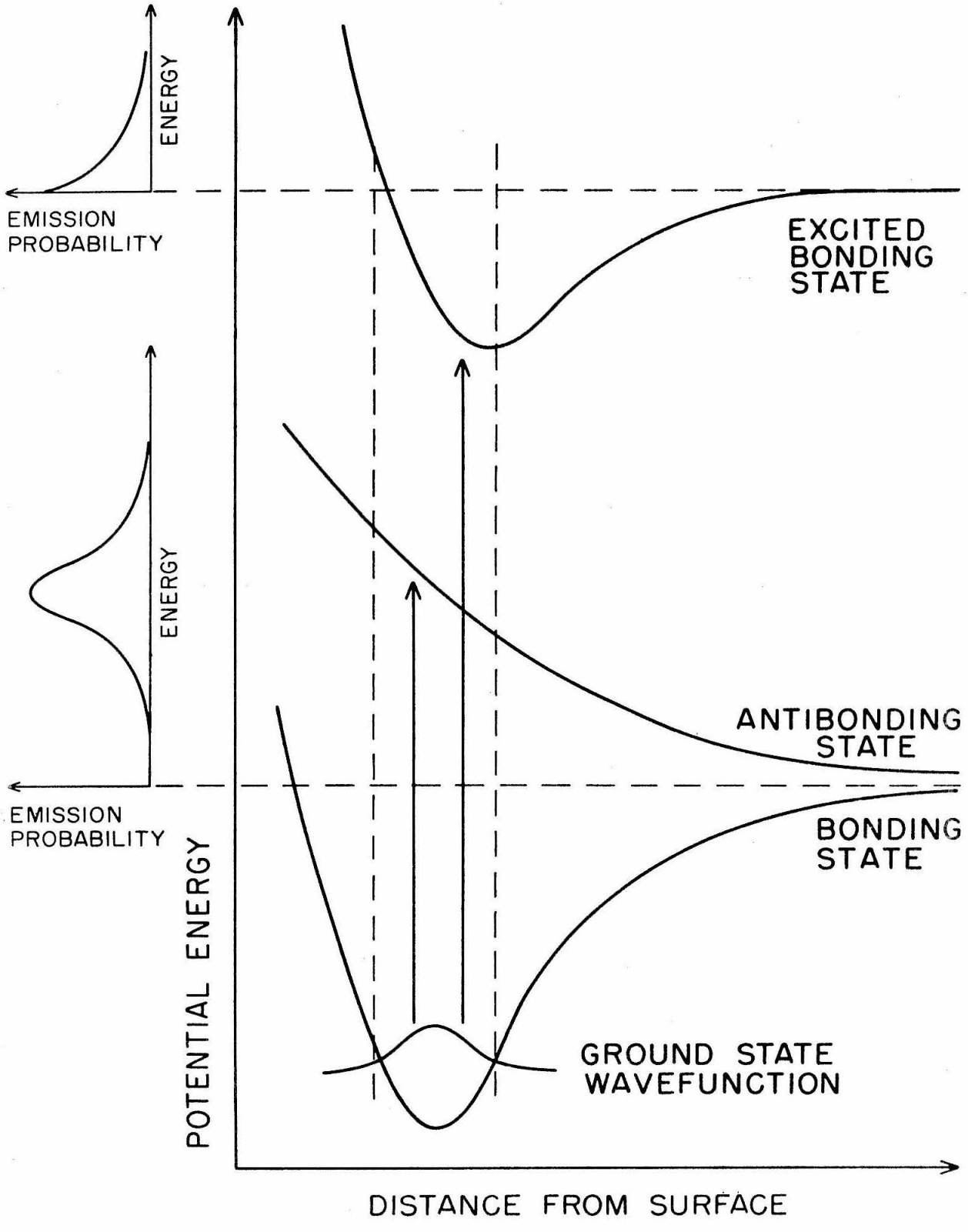
ENERGY
EMISSION PROBABILITY
EXCITED BONDING STATE
ENERGY
ANTIBONDING STATE
EMISSION PROBABILITY
BONDING STATE
GROUND STATE WAVEFUNCTION
POTENTIAL ENERGY
DISTANCE FROM SURFACE

Figure 6

Figure 7

Behavior of measured sputtering yield for three chamber pressures: P_1, P_2, P_3. For a given pressure, the target becomes cleaner as the temperature increases. The temperature region corresponding to the flat plateau produces accurate yields. If the temperature rises too high, an exponential increase in the measured yield sets in as the target begins to sublime (see Section II).

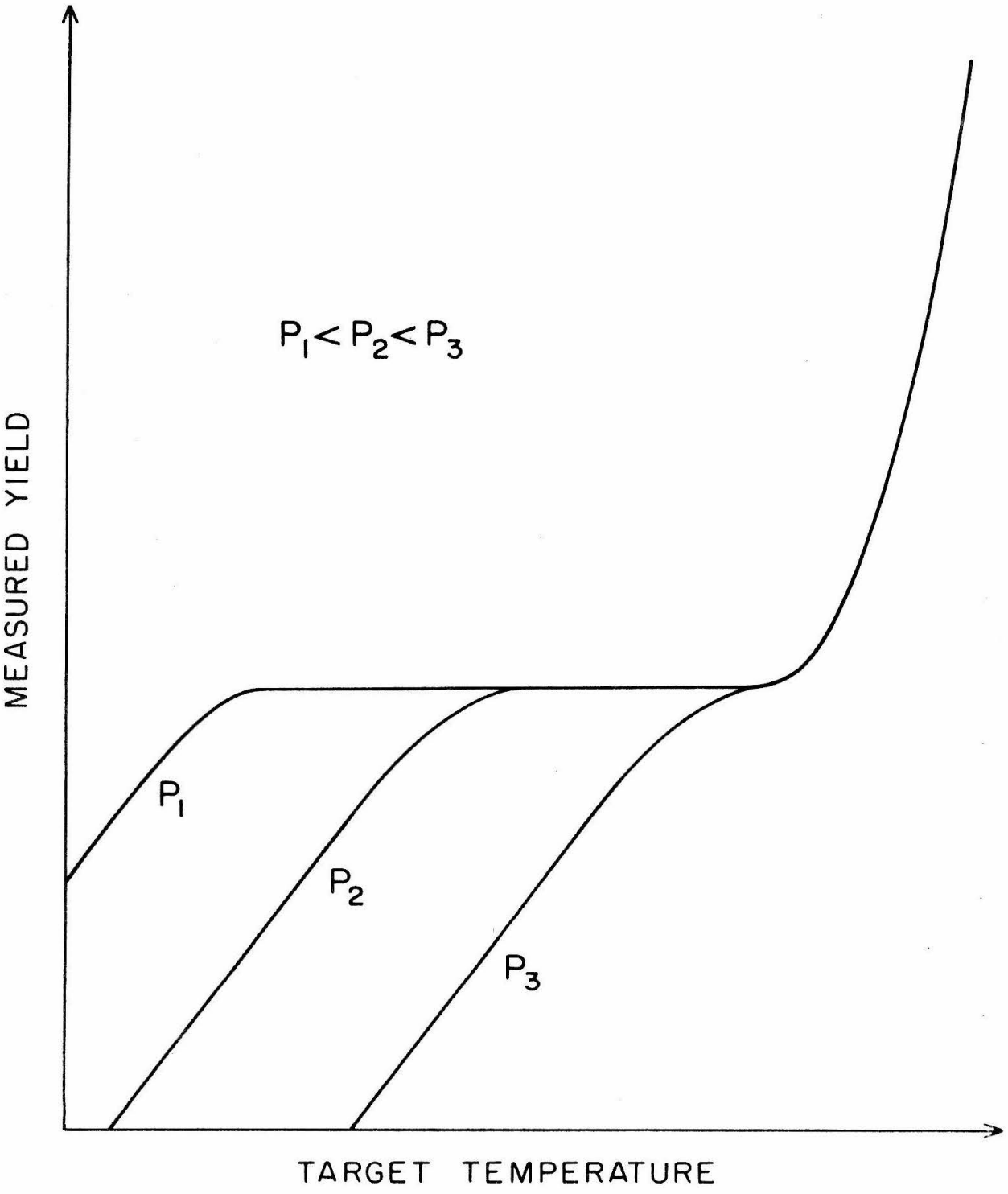

Figure 7

Figure 8

Schematic drawings of the three major types of experiments performed for this dissertation. In all of them ^{235}U is sputtered from a target and collected on high purity aluminum (see Section III.A).

SPUTTERING YIELD EXPERIMENT: HIGH AND LOW ENERGY

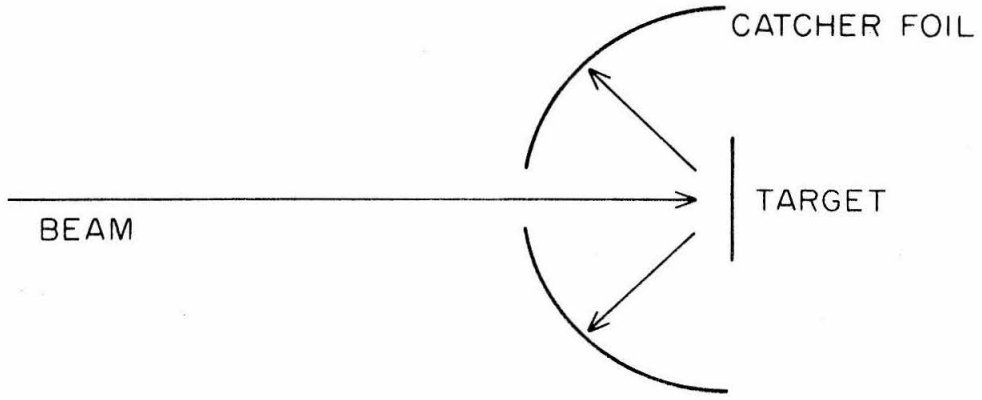

STICKING FRACTION EXPERIMENT

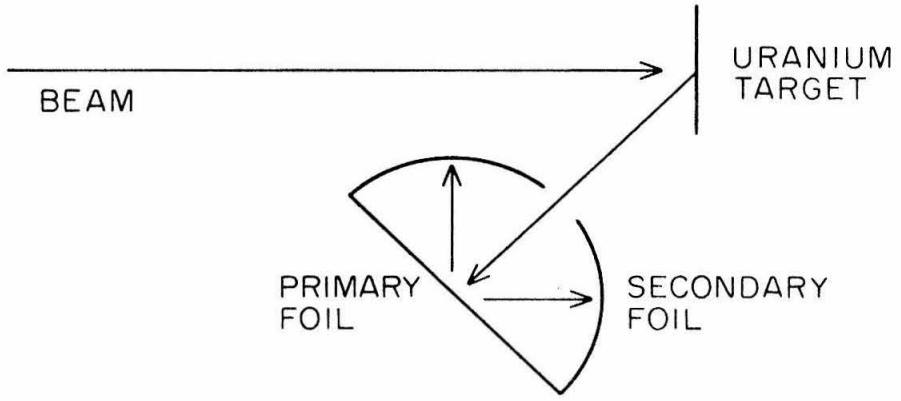

ENERGY SPECTRUM EXPERIMENT

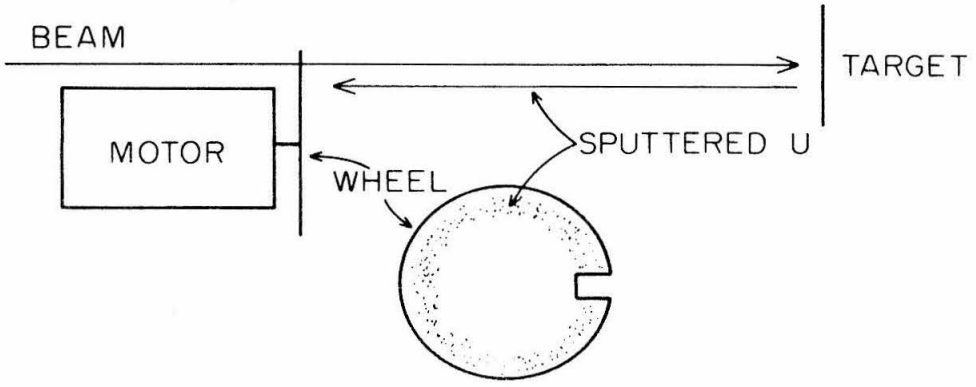

Figure 8

Figure 9

The relationship between the catcher foil geometry and the configuration of the data bands on the mica. The catcher foil holder is shown in Figs. 21 and 22. The partitions on the holder allow three separate irradiations for one foil, which results in three data bands on the mica (cross-hatched areas). The gaps at the centers of the bands are due to the square holes through which the beam passes. The cross at the upper left corner of the mica serves as a reference point for setting the stage micrometers. In scanning the mica, the coordinates of the frames scanned are recorded. Eventually, the x-coordinate translates into the angle θ (see Section III. A).

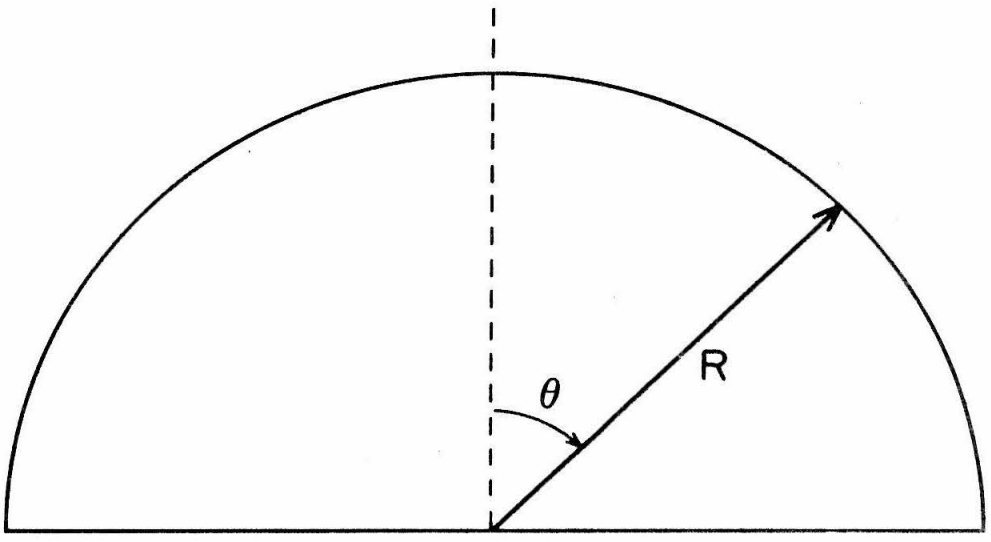

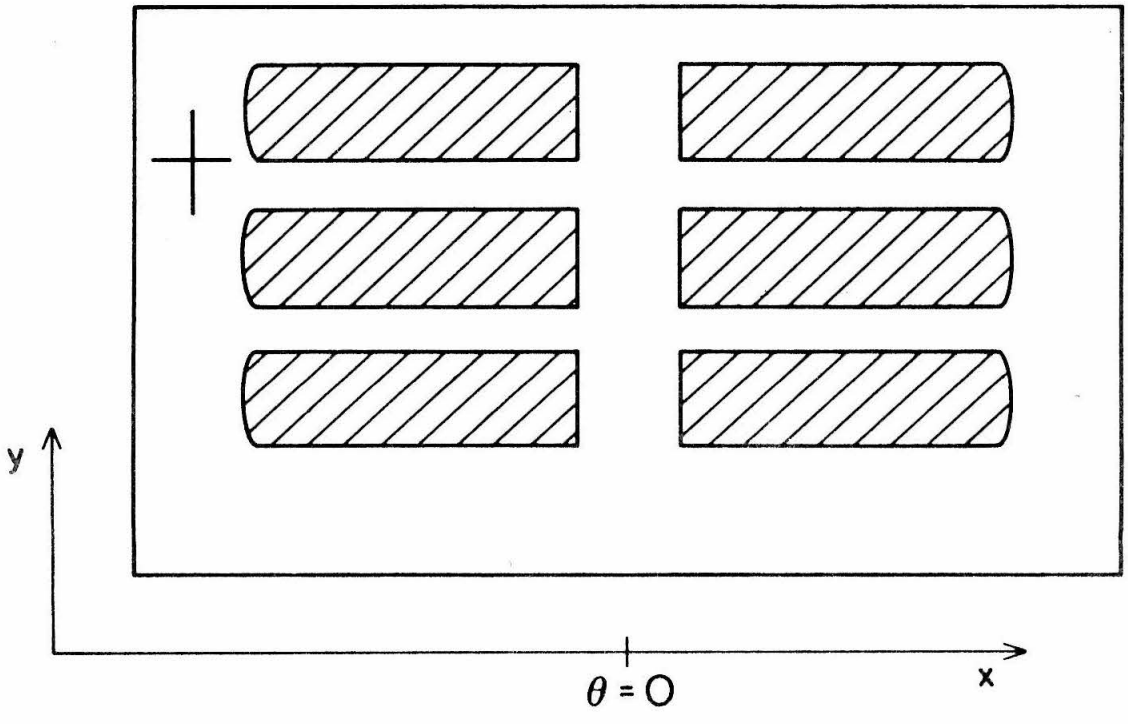

Figure 9

Figure 10

Schematic chamber configuration used for the UF_4 yield measurements. In the glass and UO_2 experiments, the target did not have a heater or thermocouple. The functions performed by the various parts of the chamber are described in the text. A picture of the chamber is shown in Fig. 20 (see Section III. A).

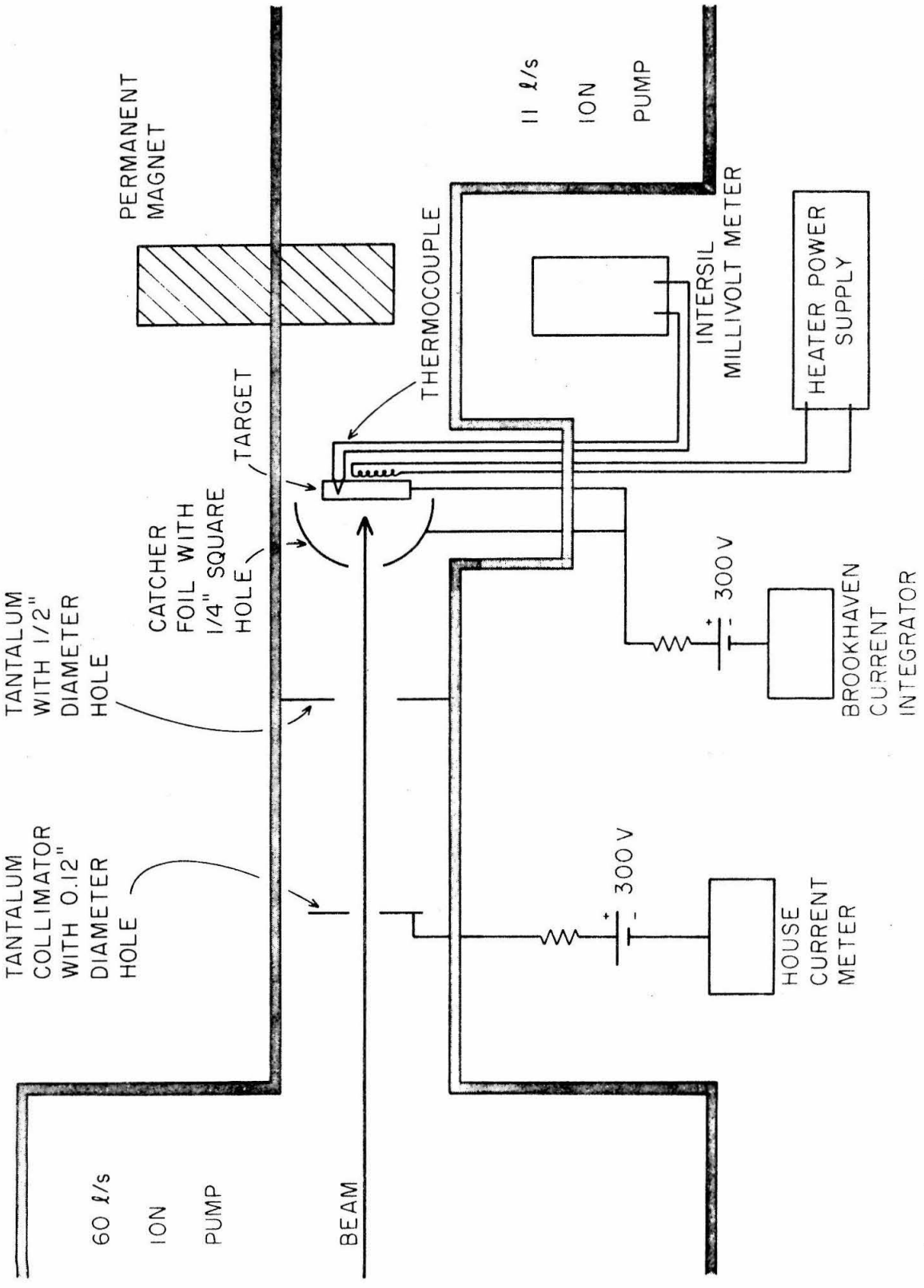
PERMANENT MAGNET
11 ℓ/s ION PUMP
THERMOCOUPLE
INTERSIL MILLIVOLT METER
HEATER POWER SUPPLY
TARGET
CATCHER FOIL WITH 1/4" SQUARE HOLE
TANTALUM WITH 1/2" DIAMETER HOLE
300 V
BROOKHAVEN CURRENT INTEGRATOR
TANTALUM COLLIMATOR WITH 0.12" DIAMETER HOLE
300 V
HOUSE CURRENT METER
60 ℓ/s ION PUMP
BEAM

Figure 10

Figure 11

Geometry for the computer program used to assess the error induced by target misalignment. We simulated the beam spot with a rectangular array of source points (shown below) each of which emitted particles with the distribution $\cos^{B_o}\varphi$. The vector $\vec{D}$ expresses the displacement of the beam spot from the correct position (see Section III. A).

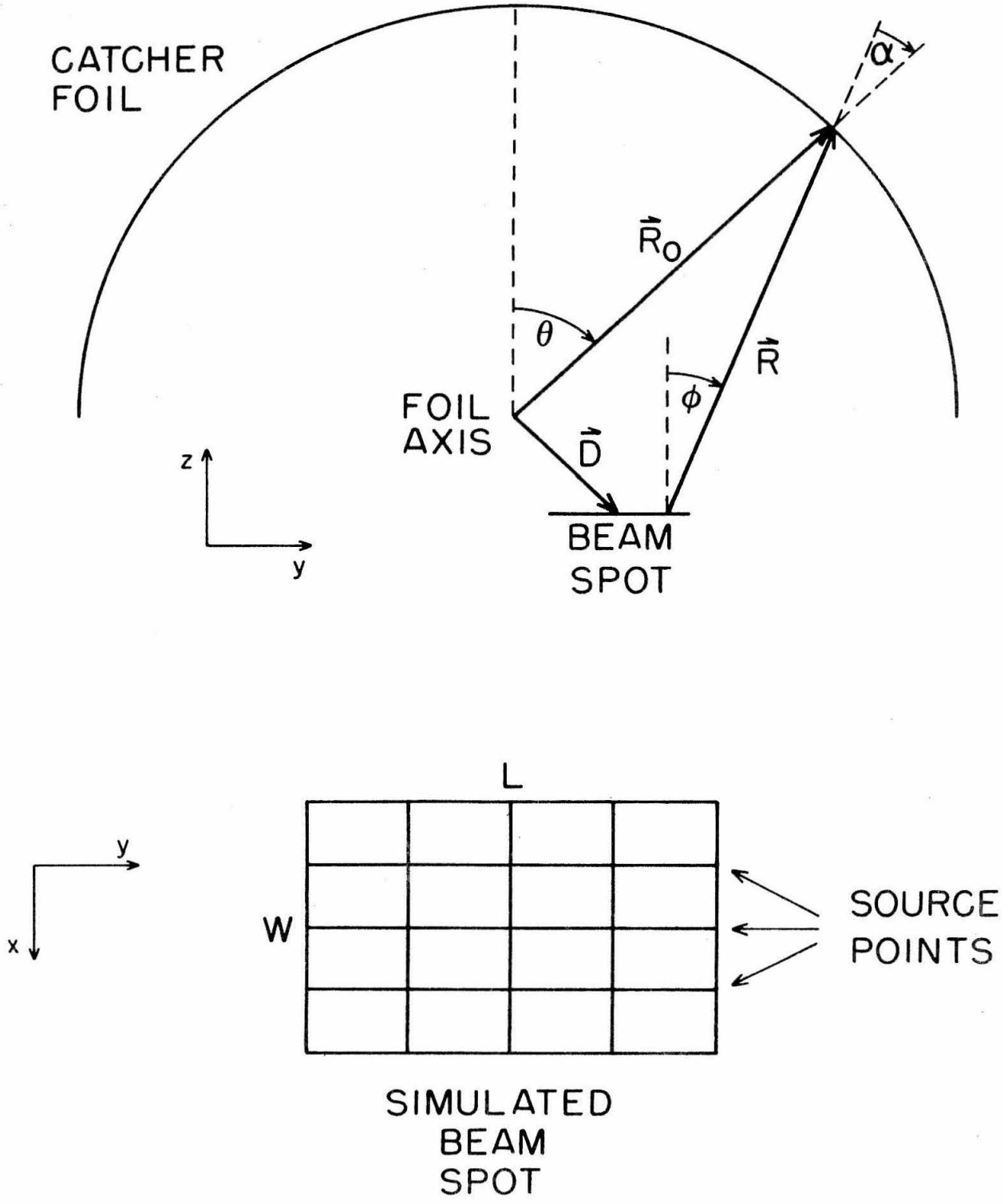
CATCHER
FOIL
α
$\vec{R}_o$
θ
$\vec{R}$
φ
FOIL
AXIS
$\vec{D}$
z
y
BEAM
SPOT
L
y
x
W
SOURCE
POINTS
SIMULATED
BEAM
SPOT

Figure 11

Figure 12

Results from the computer program used to assess the error induced by target displacement. The crosses represent points calculated by integrating the response from the source points. The continuous line is a fit of the form $A\cos^{B}\theta$. The parameter A was renormalized to 1 in the graph. A square beam spot was used (see Section III. A).

Input parameters: Foil radius R_o = 1.43 cm

Spot width L = 0.20 cm

B_o = 1.0

Displacement $\vec{D}$ = (0.0, 0.0, 0.0) cm

Output parameters: B = 0.993

A/(B + 1) = 1.000

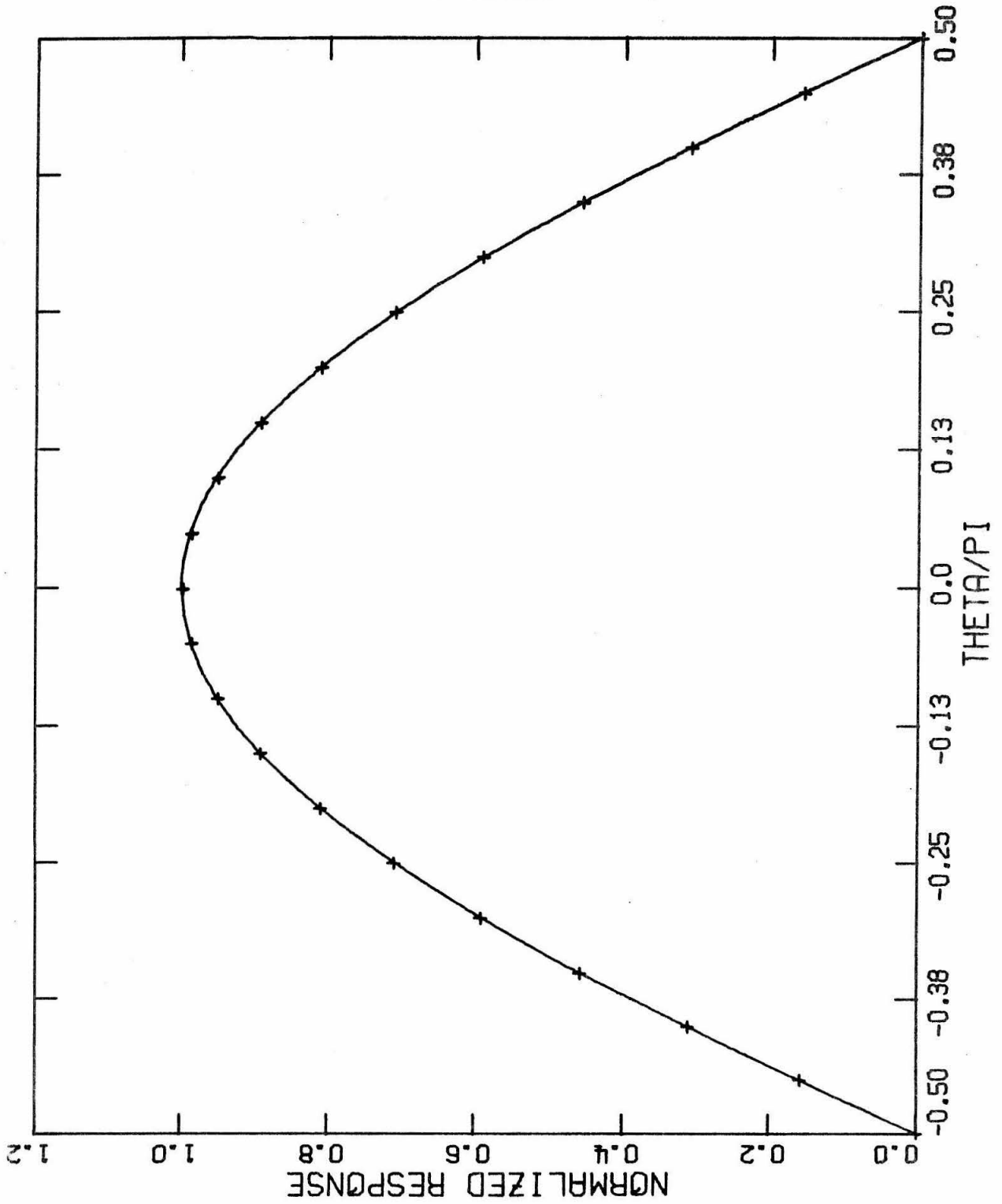
NORMALIZED RESPONSE
0.0
0.2
0.4
0.6
0.8
1.0
1.2
THETA/PI
-0.50
-0.38
-0.25
-0.13
0.0
0.13
0.25
0.38
0.50

Figure 12

Figure 13

Results from the computer program to assess the error induced by target displacement. The crosses represent points calculated by integrating the response from the source points. The continuous line is a fit of the form $A\cos^{B}\theta$. The parameter A was renormalized to 1 in the graph. A square beam spot was used (see Section III. A).

Input parameters: Foil radius R_o = 1.43 cm

Spot width L = 0.20 cm

B_o = 1.0

Displacement $\vec{D}$ = (0.0, 1.0, 0.0) cm

Output parameters: B = .932

A/(B + 1) = 1.021

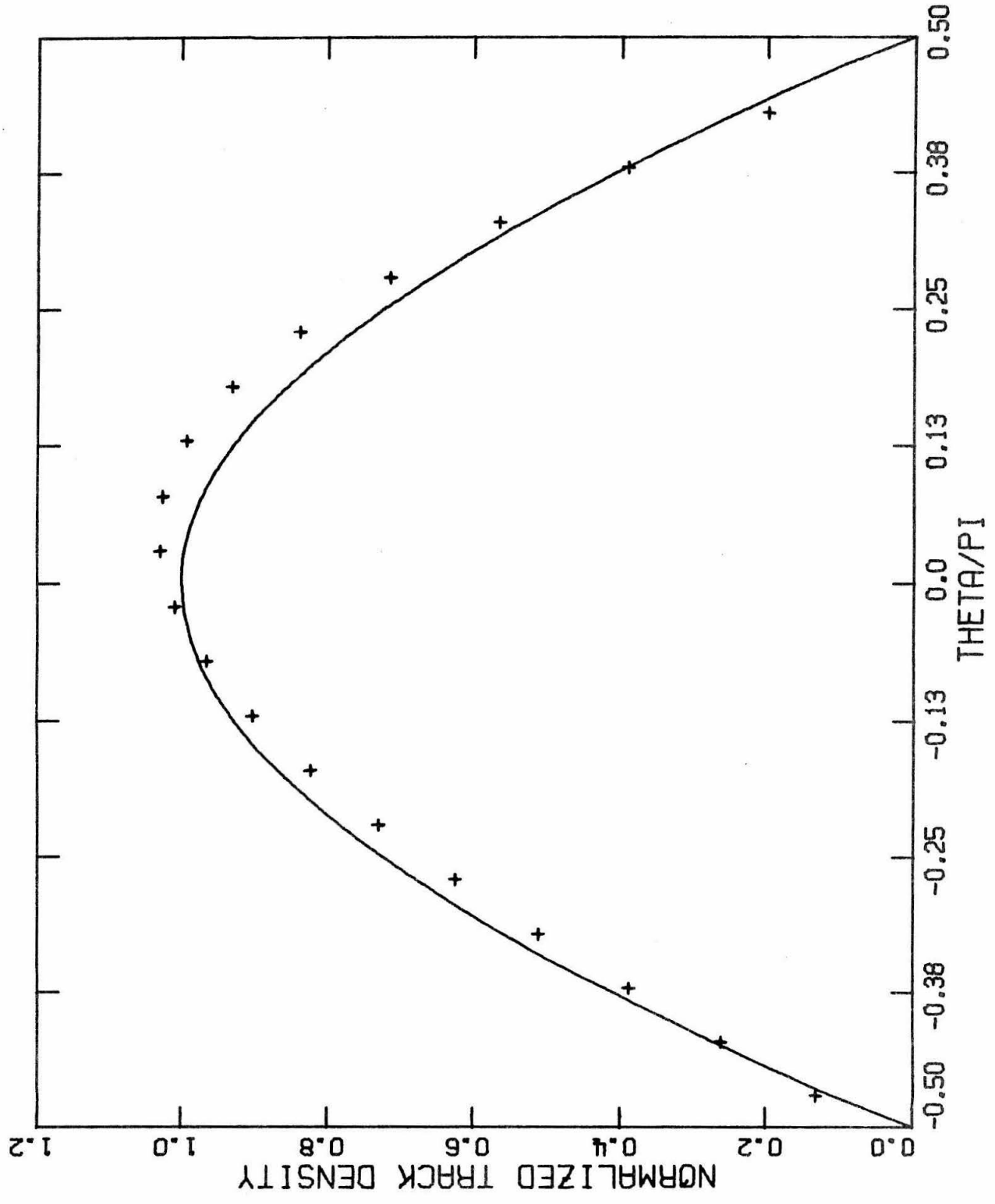
NORMALIZED TRACK DENSITY
0.0
0.2
0.4
0.6
0.8
1.0
1.2
THETA/PI
-0.50
-0.38
-0.25
-0.13
0.0
0.13
0.25
0.38
0.50

Figure 13

Figure 14

Schematic drawing of the experimental apparatus for the sticking fraction experiments. The top figure displays the arrangement inside the cylinder used to hold the cages. Each cage contained a primary-secondary assembly like the one below, though the heater was included in only two of the runs. By using two uranium foils and two shields, we could irradiate the cages separately (see Section III. B).

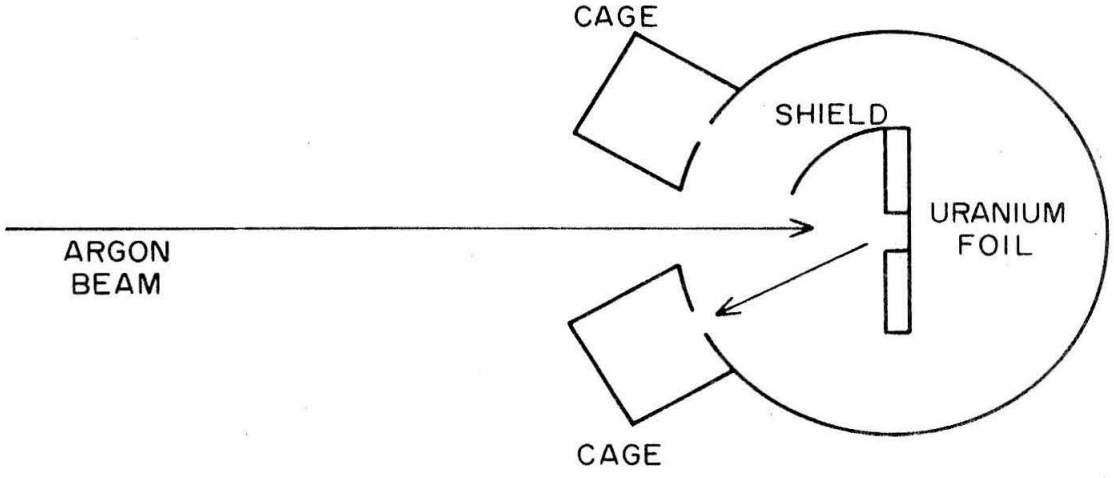
CAGE
SHIELD
URANIUM
FOIL
ARGON
BEAM
CAGE

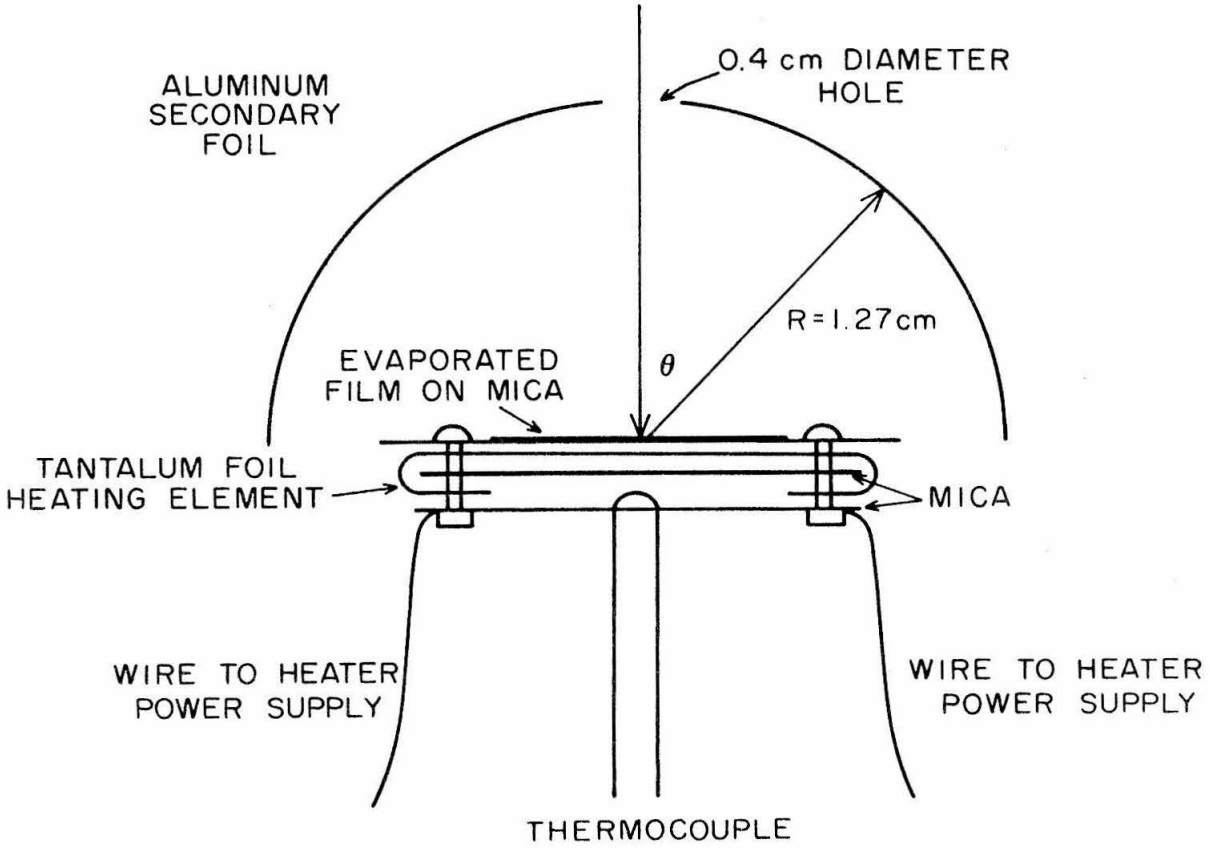
ALUMINUM
SECONDARY
FOIL
0.4 cm DIAMETER
HOLE
R=1.27cm
θ
EVAPORATED
FILM ON MICA
TANTALUM FOIL
HEATING ELEMENT
MICA
WIRE TO HEATER
POWER SUPPLY
WIRE TO HEATER
POWER SUPPLY
THERMOCOUPLE

Figure 14

Figure 15

UHV chamber used for the sticking fraction experiments (see Section III. B).

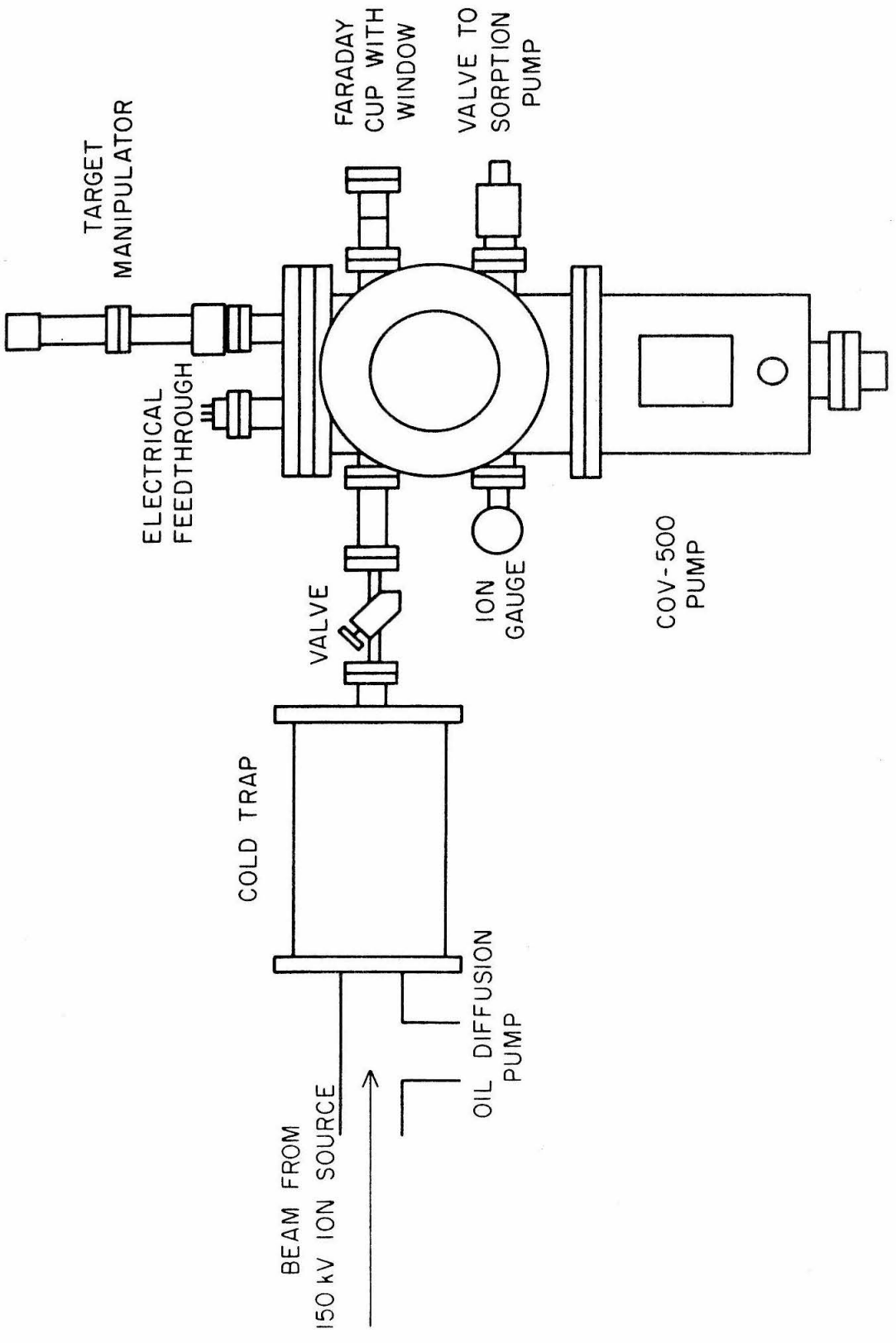
TARGET MANIPULATOR
FARADAY CUP WITH WINDOW
VALVE TO SORPTION PUMP
ELECTRICAL FEEDTHROUGH
VALVE
ION GAUGE
COV-500 PUMP
COLD TRAP
OIL DIFFUSION PUMP
BEAM FROM 150 kV ION SOURCE

Figure 15

Figure 16

Angular distribution of sputtered ^{235}U scattering from an aluminum foil with an oxidized surface at 23°C. At the peak, each point represents about 770 tracks, which implies a statistical error of ± 4%. The fit is of the form $A\cos^{B}$. B = 0.69 ± .02. The uncertainty in A is ± 1% (see Section III. B).

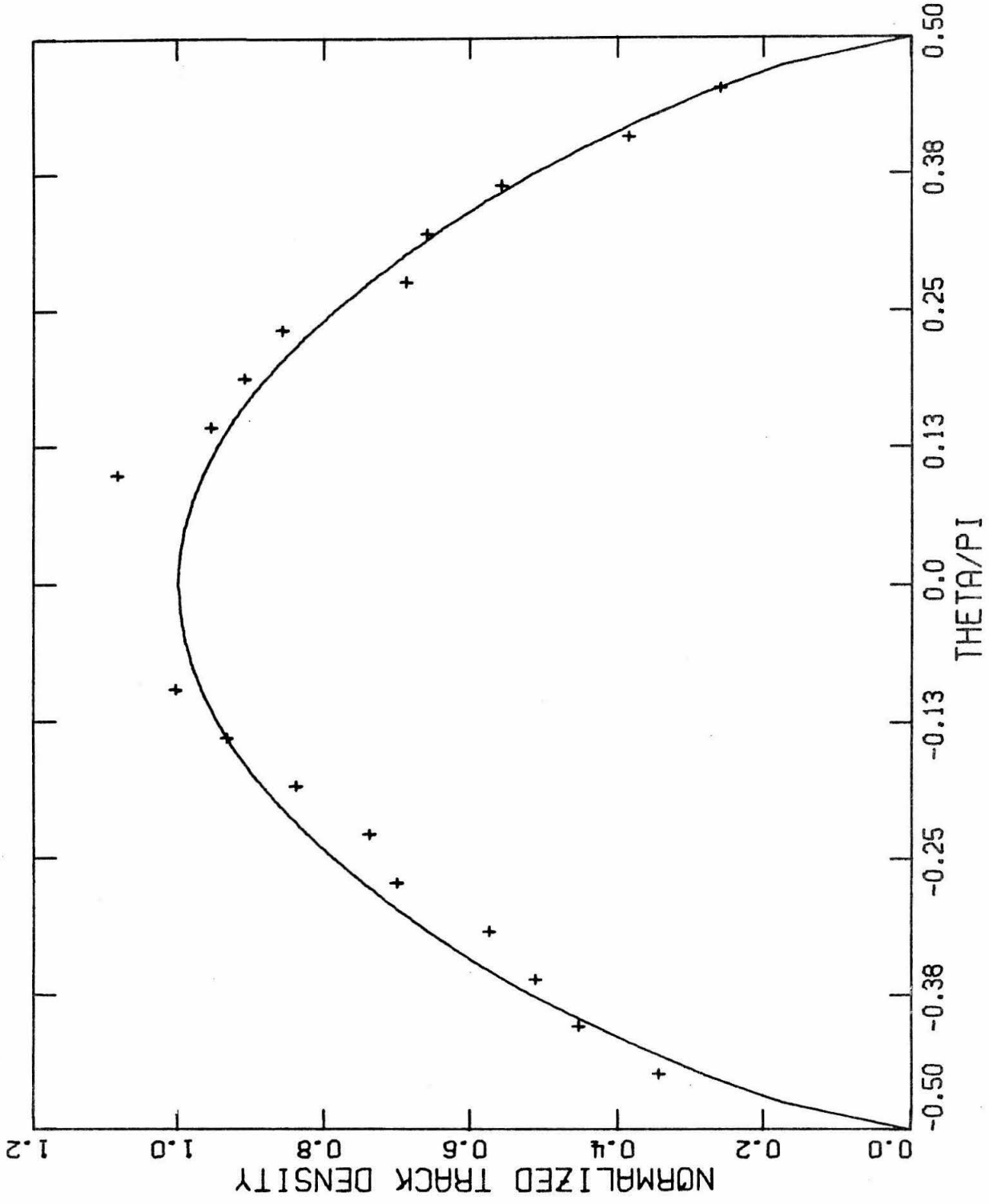
NORMALIZED TRACK DENSITY
0.0
0.2
0.4
0.6
0.8
1.0
1.2
THETA/PI
-0.50
-0.38
-0.25
-0.13
0.0
0.13
0.25
0.38
0.50

Figure 16

Figure 17

Angular distribution of sputtered ^{235}U scattering from an evaporated aluminum film with an oxidized surface at 23°C. At the peak, each point represents about 90 tracks, which implies a statistical error of ± 11%. The fit is of the form $A\cos^{B}\theta$. B = 0.52 ± .05. The uncertainty in A is ± 3% (see Section III.B).

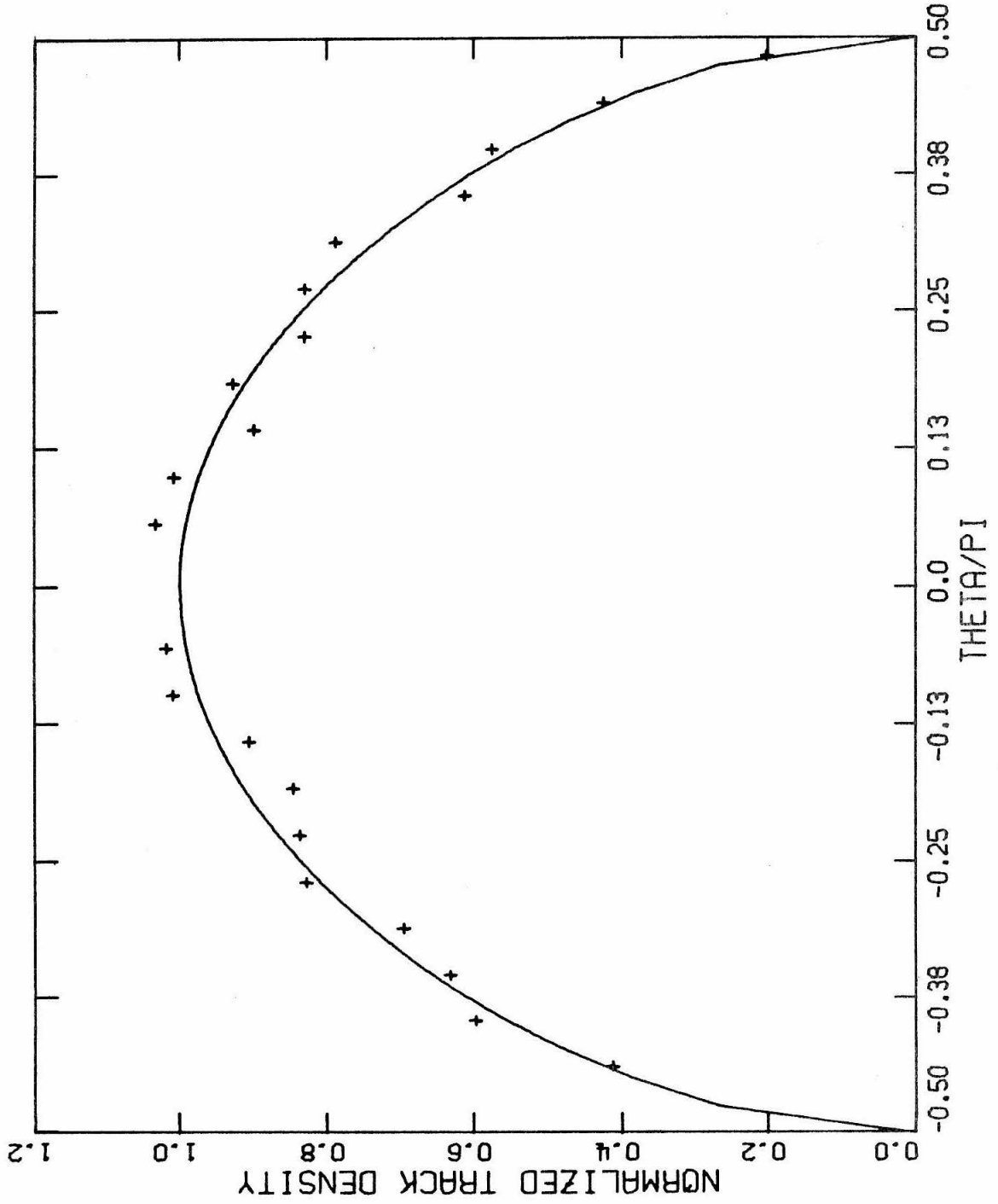
NORMALIZED TRACK DENSITY
0.0
0.2
0.4
0.6
0.8
1.0
1.2
THETA/PI
-0.50
-0.38
-0.25
-0.13
0.0
0.13
0.25
0.38
0.50

Figure 17

Figure 18

Angular distribution of sputtered ^{235}U scattering from an evaporated aluminum film with an oxidized surface at 152°C. At the peak, each point represents about 120 tracks, which implies a statistical error of ±9%. The fit is of the form $A\cos^{B}\theta$. B = 1.05 ± .07. The uncertainty in A is ± 3% (see Section III.B).

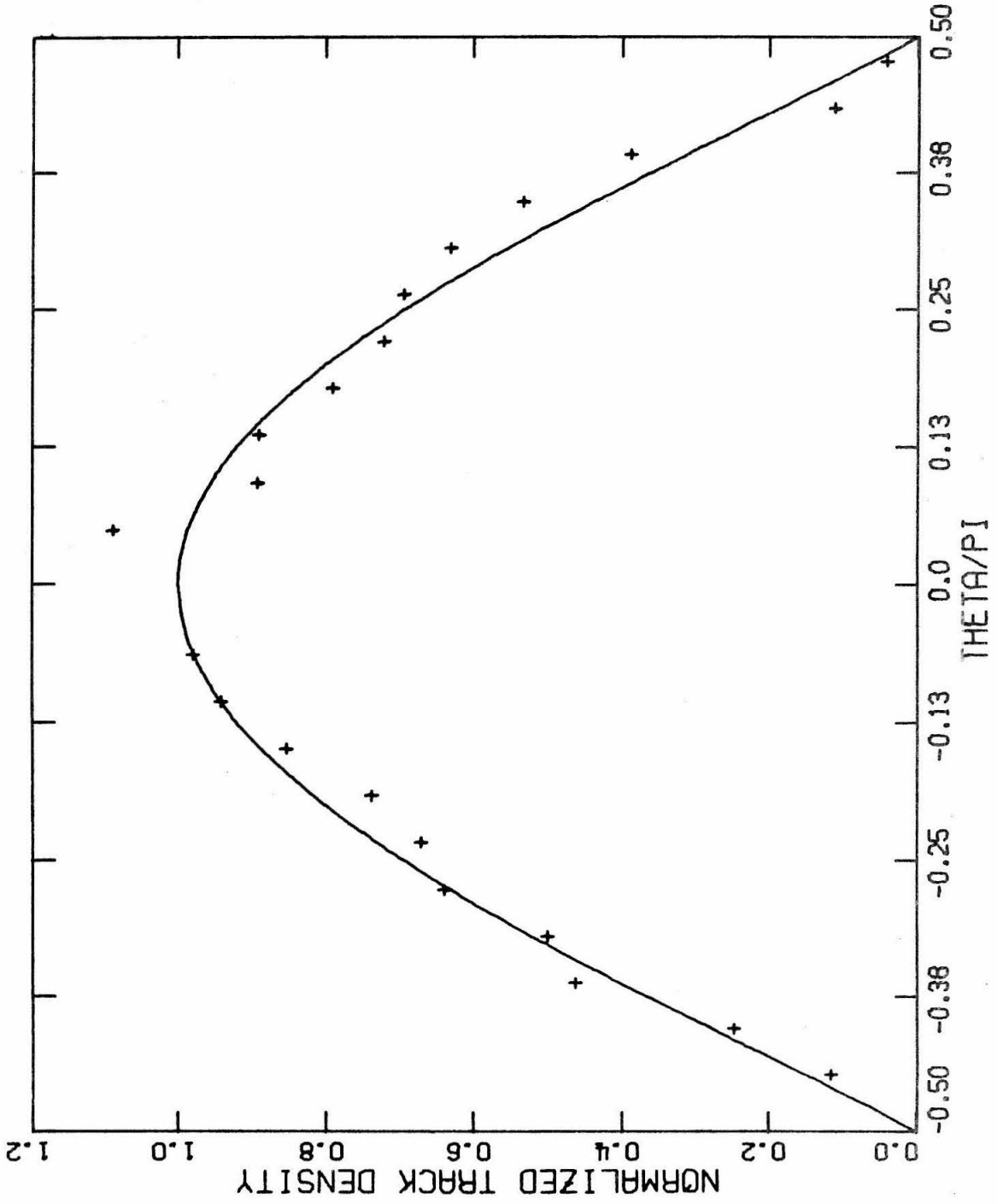
NORMALIZED TRACK DENSITY
0.0
0.2
0.4
0.6
0.8
1.0
1.2
THETA/PI
-0.50
-0.38
-0.25
-0.13
0.0
0.13
0.25
0.38
0.50

Figure 18

Figure 19

Chamber used for high energy sputtering yield experiments (see Section III.C).

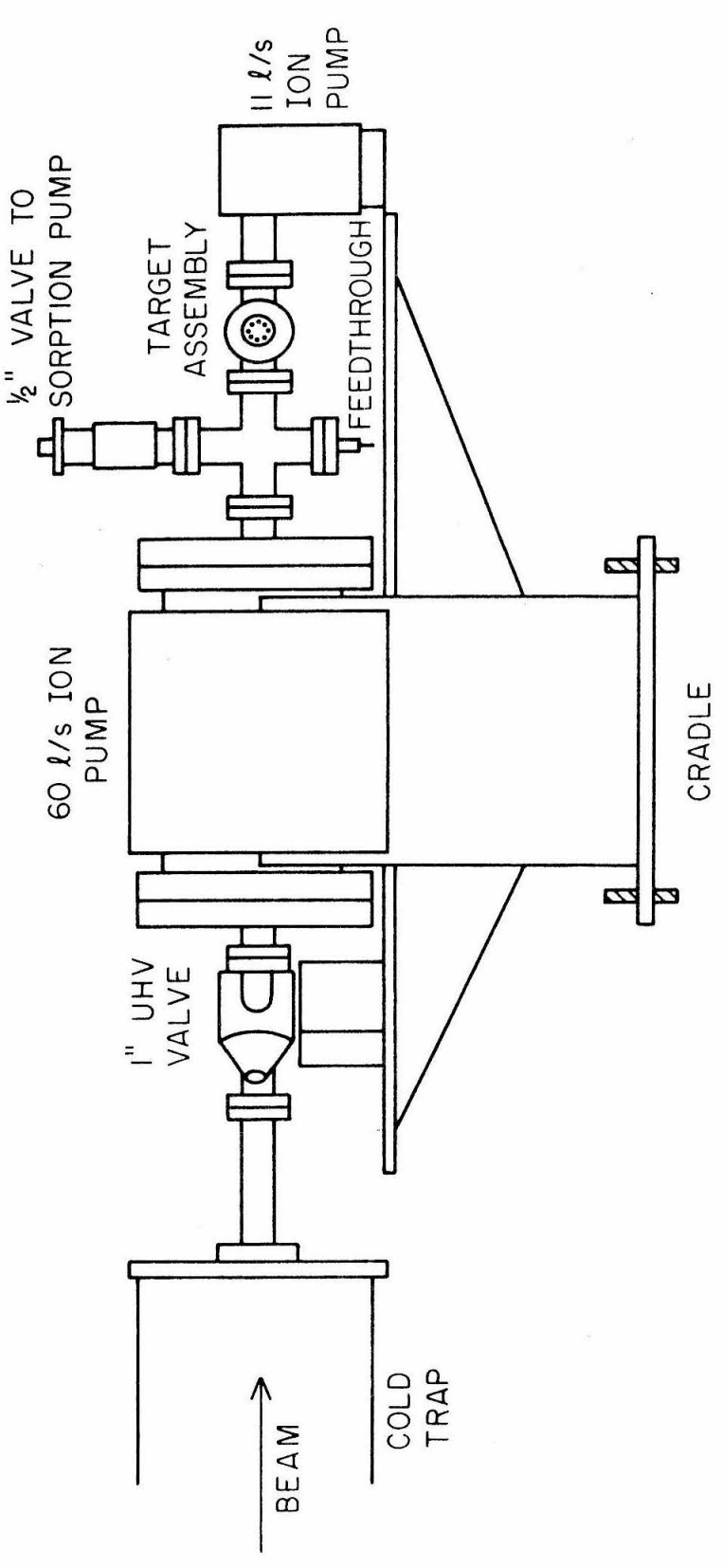
11 ℓ/s ION PUMP
½" VALVE TO SORPTION PUMP
TARGET ASSEMBLY
FEEDTHROUGH
60 ℓ/s ION PUMP
CRADLE
1" UHV VALVE
BEAM
COLD TRAP

Figure 19

Figure 20

Photograph of chamber shown in Fig. 19. The Bennington Flag was a gift from the management of a local Armenian restaurant on July 4, 1976 (see Section III.C).

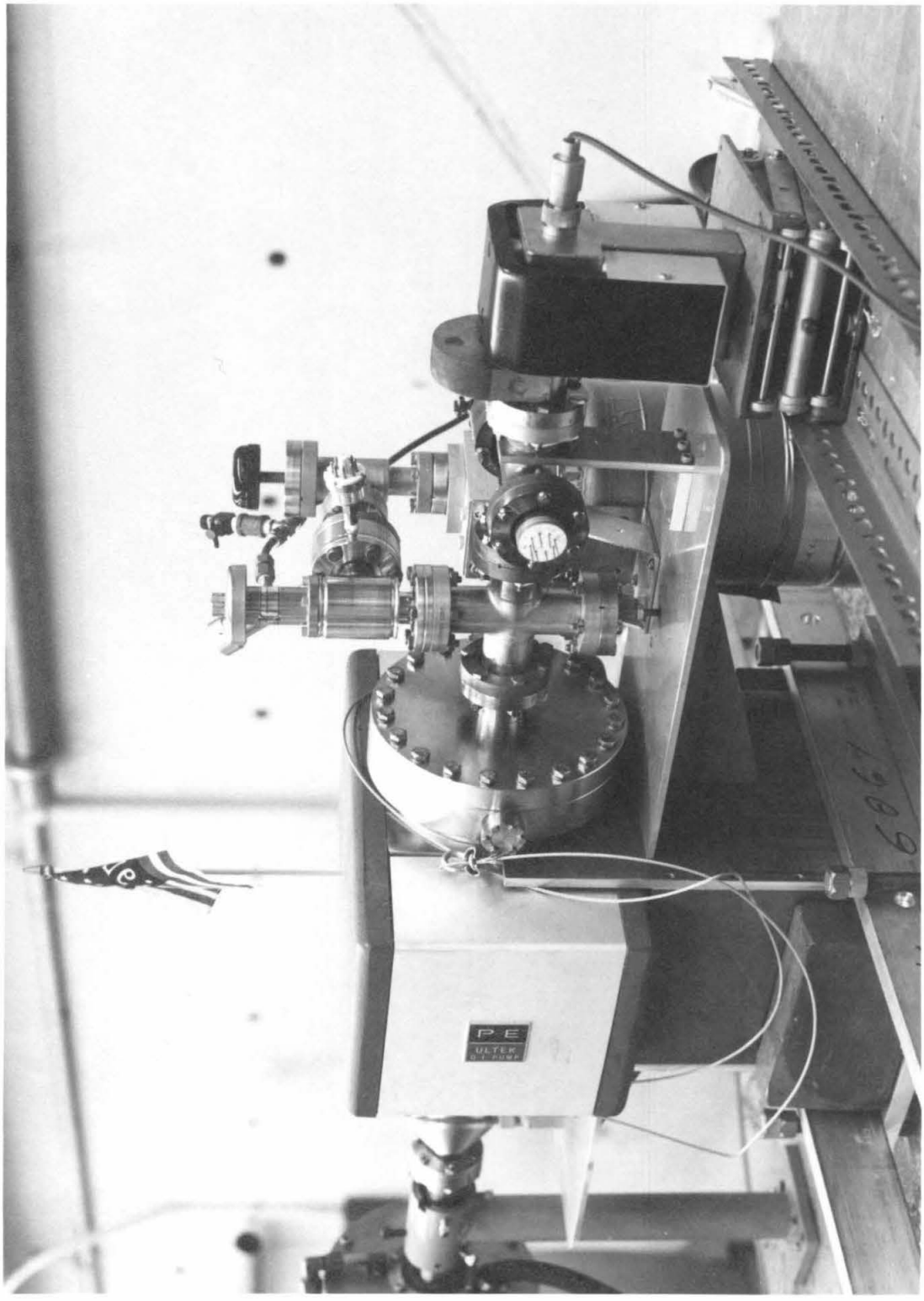

Figure 20

Figure 21

Photograph of catcher foil holder used in the sputtering yield determinations. The ceramic piece on top insulates the holder from the bellows. The spring is used to electrically connect the catcher foil to the outside (see Section III. C).

Figure 22

Figure 22

Photograph of catcher foil holder with catcher foil. The three square holes allow the beam to pass through. The scale reads in centimeters (see Section III.C).

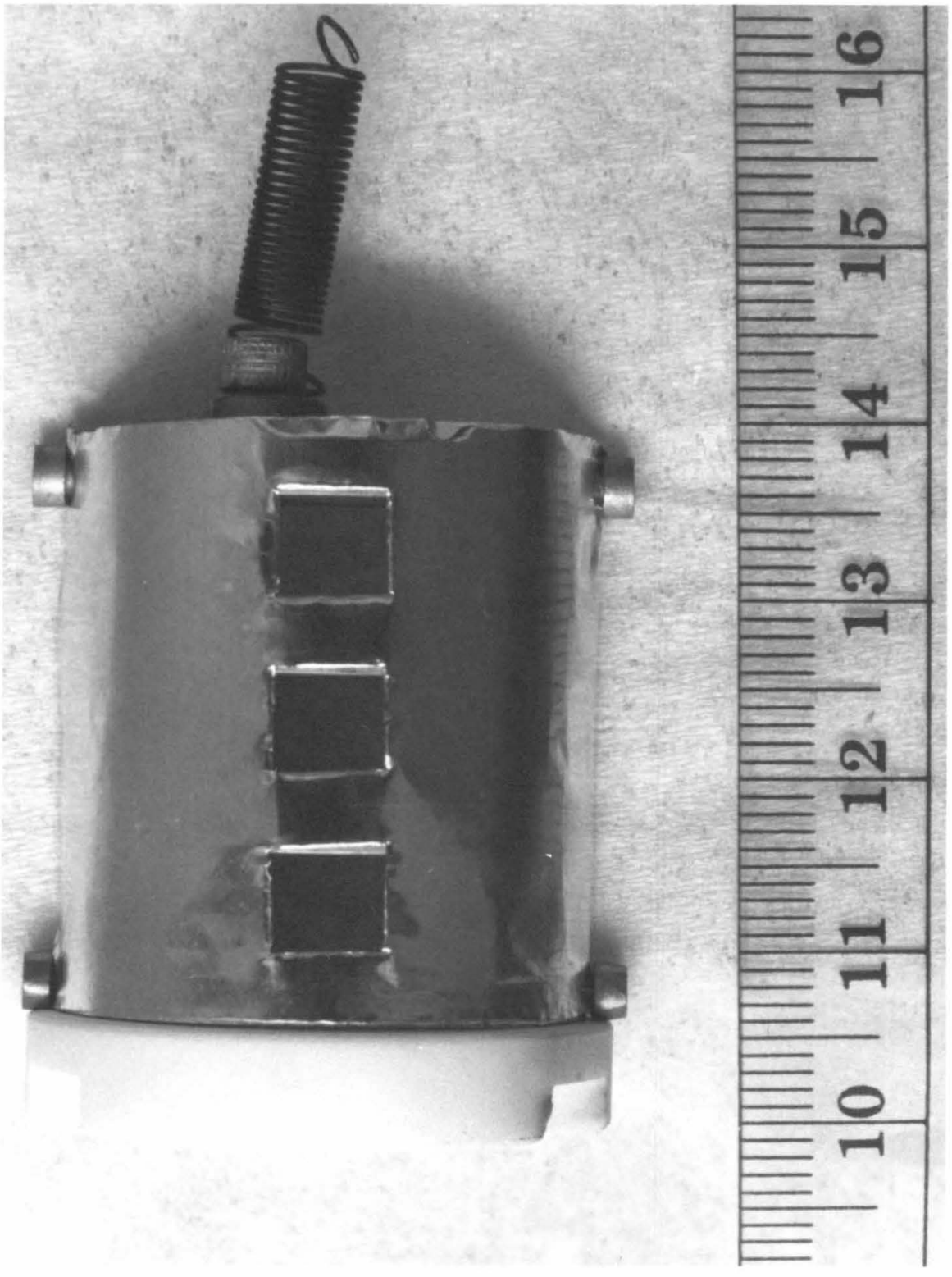

Figure 22

Figure 23

Angular distribution produced by 20 MeV ^{19}F incident on the glass target at 45^{o}. This is run #1 (see Table 4 and Section III. C).

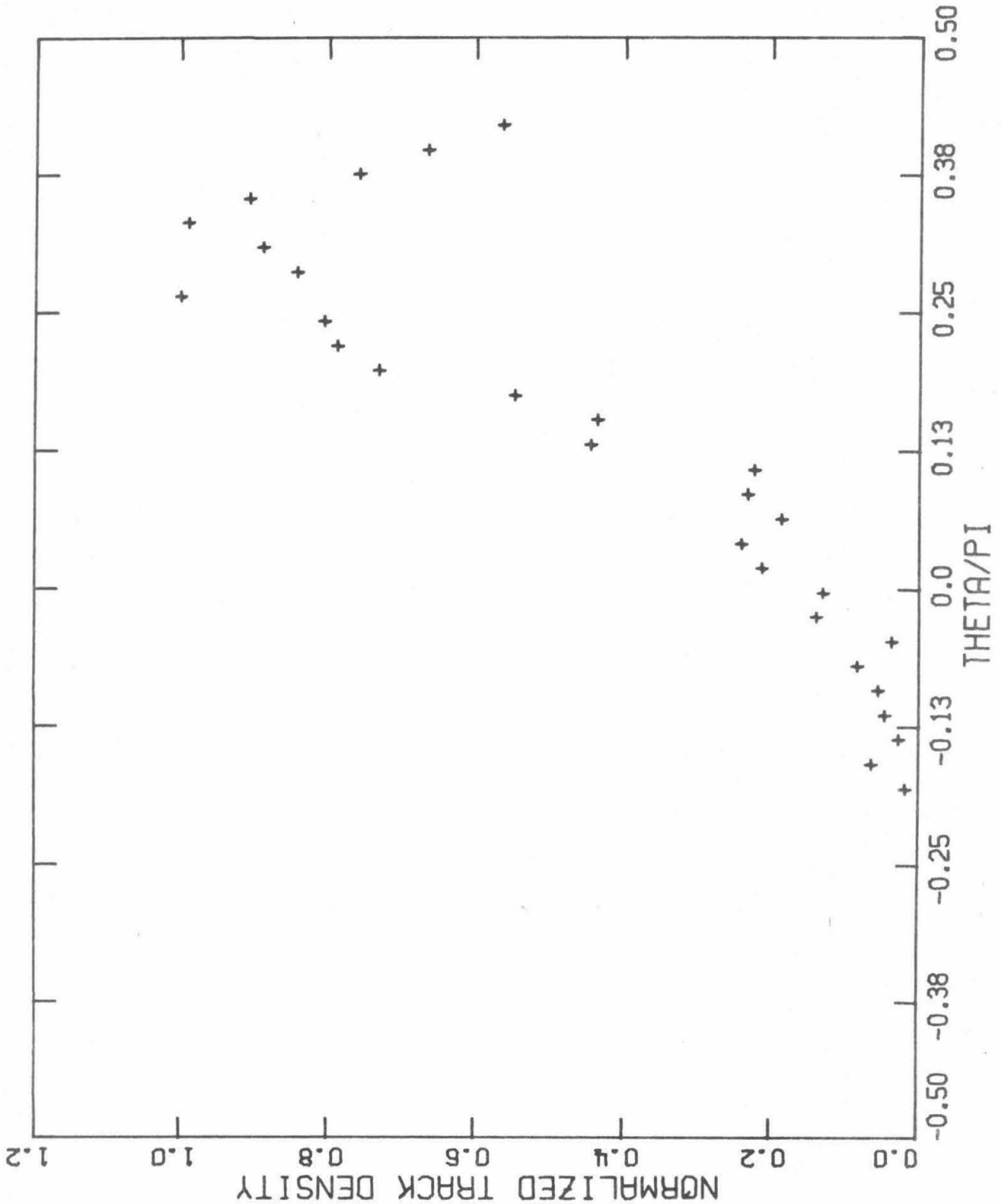
NORMALIZED TRACK DENSITY
0.0
0.2
0.4
0.6
0.8
1.0
1.2
THETA/PI
0.50
0.38
0.25
0.13
0.0
-0.13
-0.25
-0.38
-0.50

Figure 23

Figure 24

Angular distribution produced by 8 MeV ^{19}F incident on the glass target at 45^{o}. This is run #5 (see Table 4 and Section III. C).

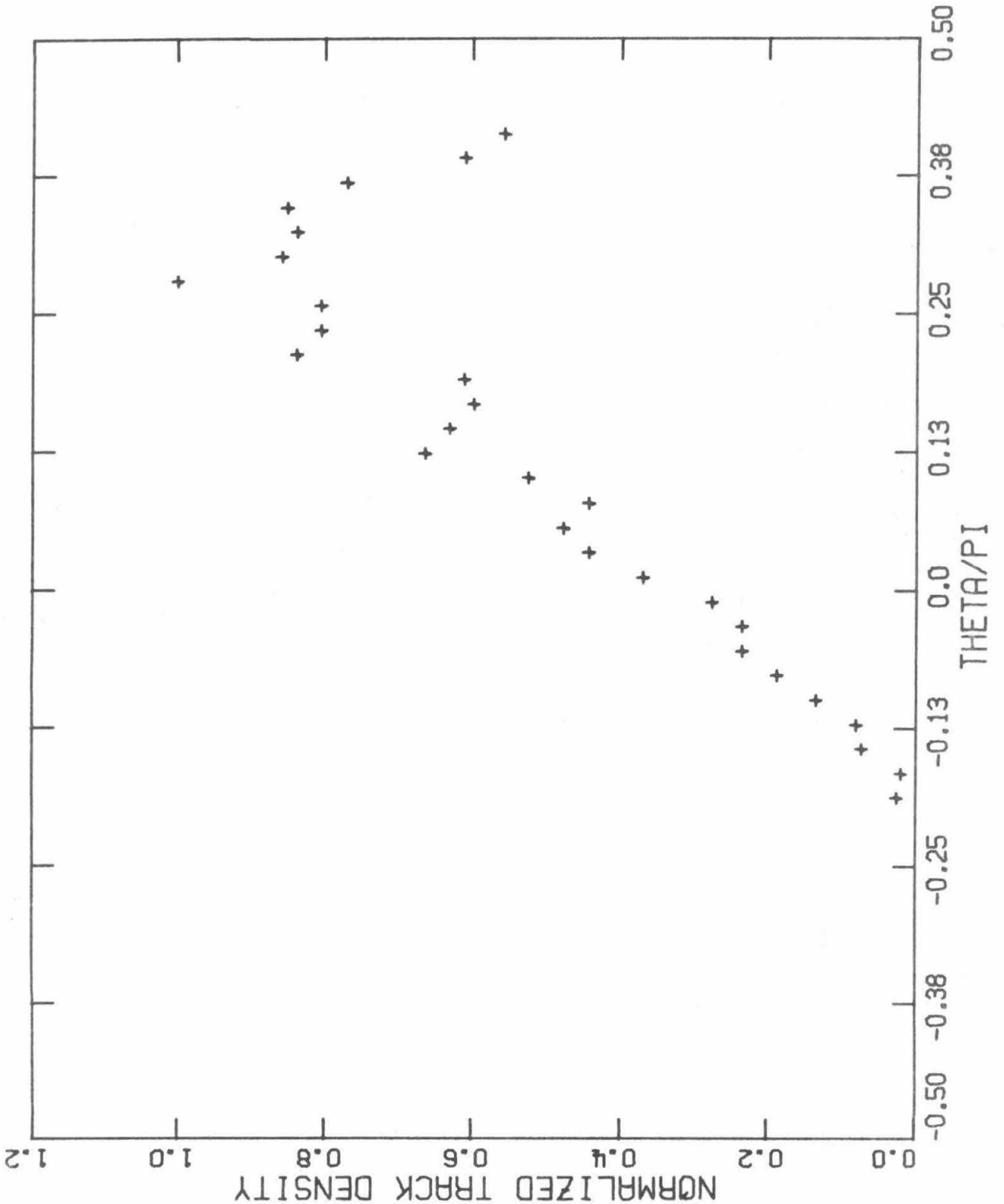
NORMALIZED TRACK DENSITY
0.0
0.2
0.4
0.6
0.8
1.0
1.2
THETA/PI
-0.50
-0.38
-0.25
-0.13
0.0
0.13
0.25
0.38
0.50

Figure 24

Figure 25

Angular distribution produced by 10 MeV ^{19}F incident on a pre-war uranium foil at 45^{o}. This run #8 (see Table 4 and Section III. C).

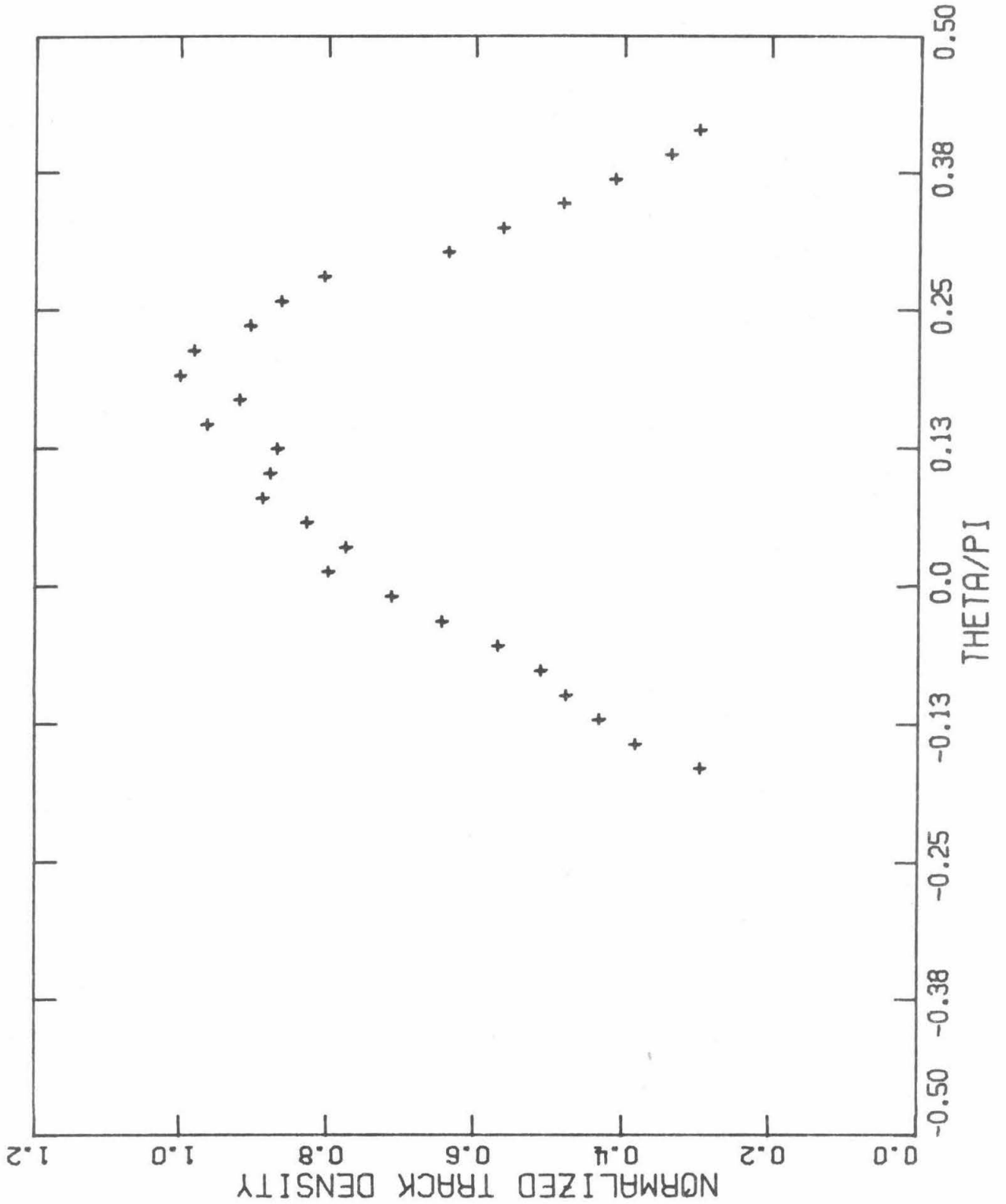
NORMALIZED TRACK DENSITY
0.0
0.2
0.4
0.6
0.8
1.0
1.2
THETA/PI
-0.50
-0.38
-0.25
-0.13
0.0
0.13
0.25
0.38
0.50

Figure 25

Figure 26

Angular distribution produced by 10 MeV ^{19}F incident on the glass target at 45^{o}. This is run #4 (see Table 4 and Section III.C).

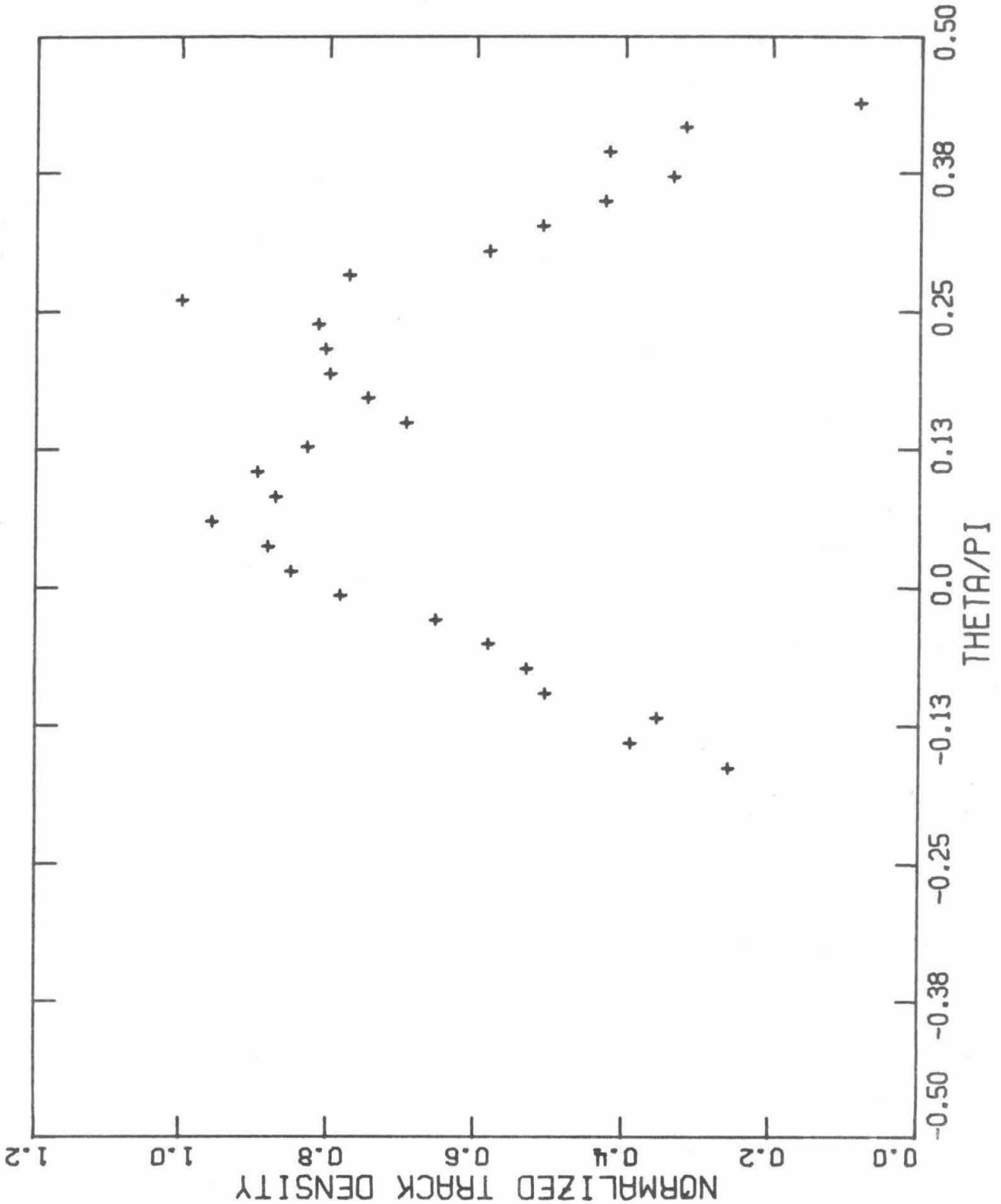
NORMALIZED TRACK DENSITY
0.0
0.2
0.4
0.6
0.8
1.0
1.2
THETA/PI
0.50
0.38
0.25
0.13
0.0
-0.13
-0.25
-0.38
-0.50

Figure 26

Figure 27

Energy spectrum of 1.8 MeV ^{4}He scattered from a UF_4 target. The large peak on the right corresponds to the uranium; the peak on the left corresponds to the fluorine (see Section III.E.2).

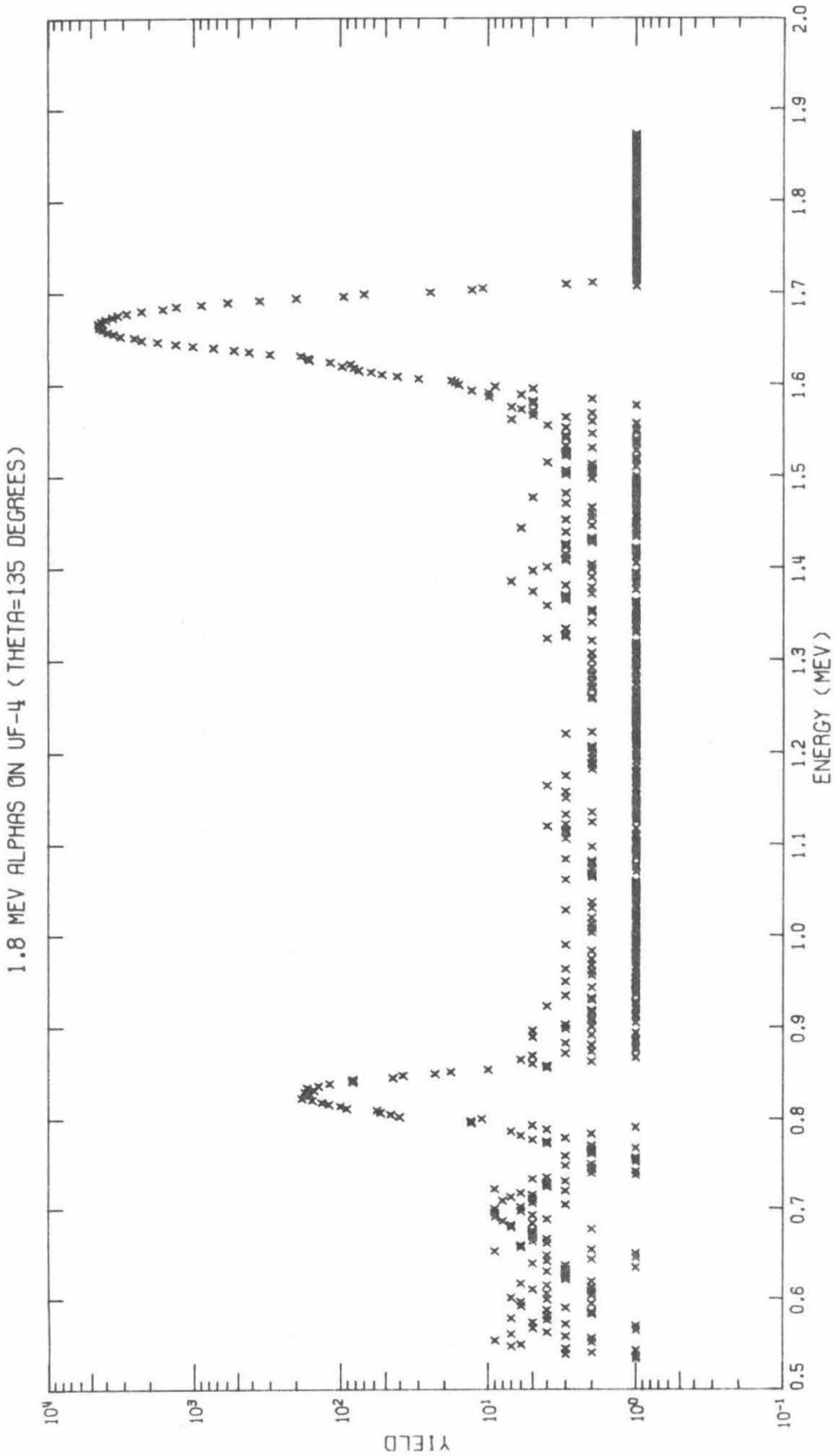
1.8 MEV ALPHAS ON UF-4 (THETA=135 DEGREES)
YIELD
ENERGY (MEV)
10^4
10^3
10^2
10^1
10^0
10^{-1}
0.5
0.6
0.7
0.8
0.9
1.0
1.1
1.2
1.3
1.4
1.5
1.6
1.7
1.8
1.9
2.0

Figure 27

Figure 28

Chamber used for low energy yield measurements with the 150 kV ion source. Current integration was performed in the manner illustrated in Fig. 10 (see Section III.E.3).

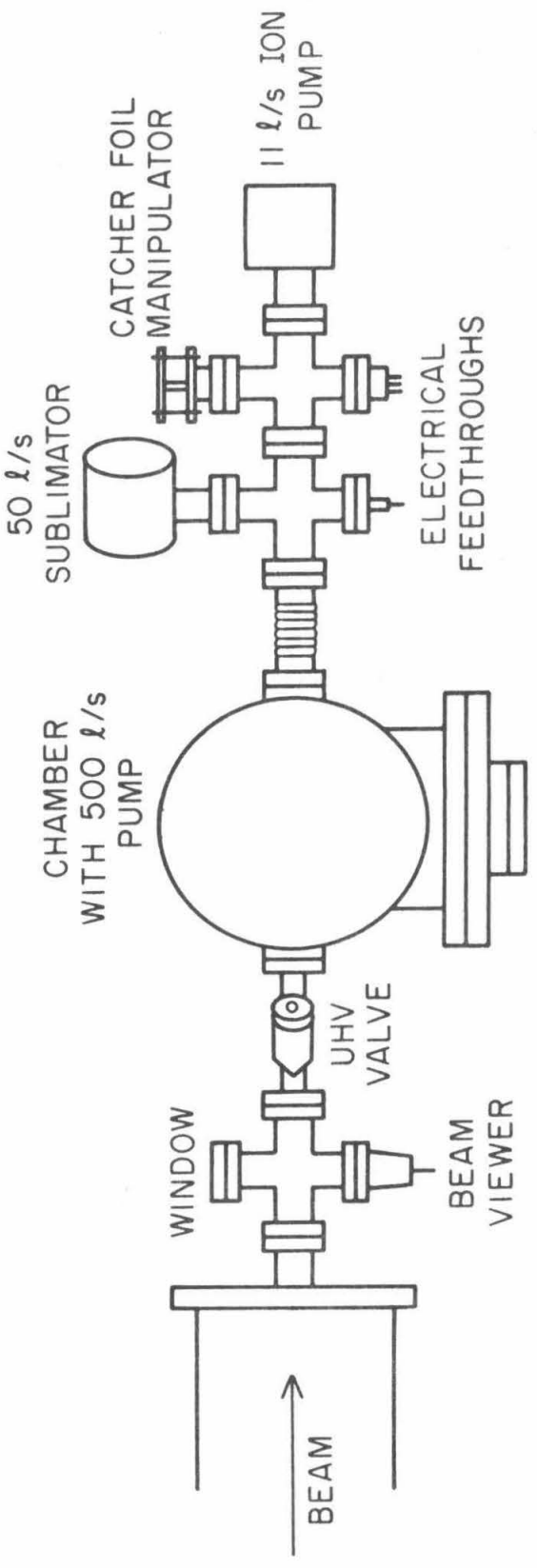
11 ℓ/s ION PUMP
CATCHER FOIL MANIPULATOR
50 ℓ/s SUBLIMATOR
ELECTRICAL FEEDTHROUGHS
CHAMBER WITH 500 ℓ/s PUMP
UHV VALVE
WINDOW
BEAM VIEWER
BEAM

Figure 28

Figure 29

Photograph of the target assembly for UF_4 sputtering. The UF_4 film is on the shiny front surface of the copper block (note that the reflection of the support post can be seen). Fig. 30 is a schematic drawing of this target (see Section III.E.3).

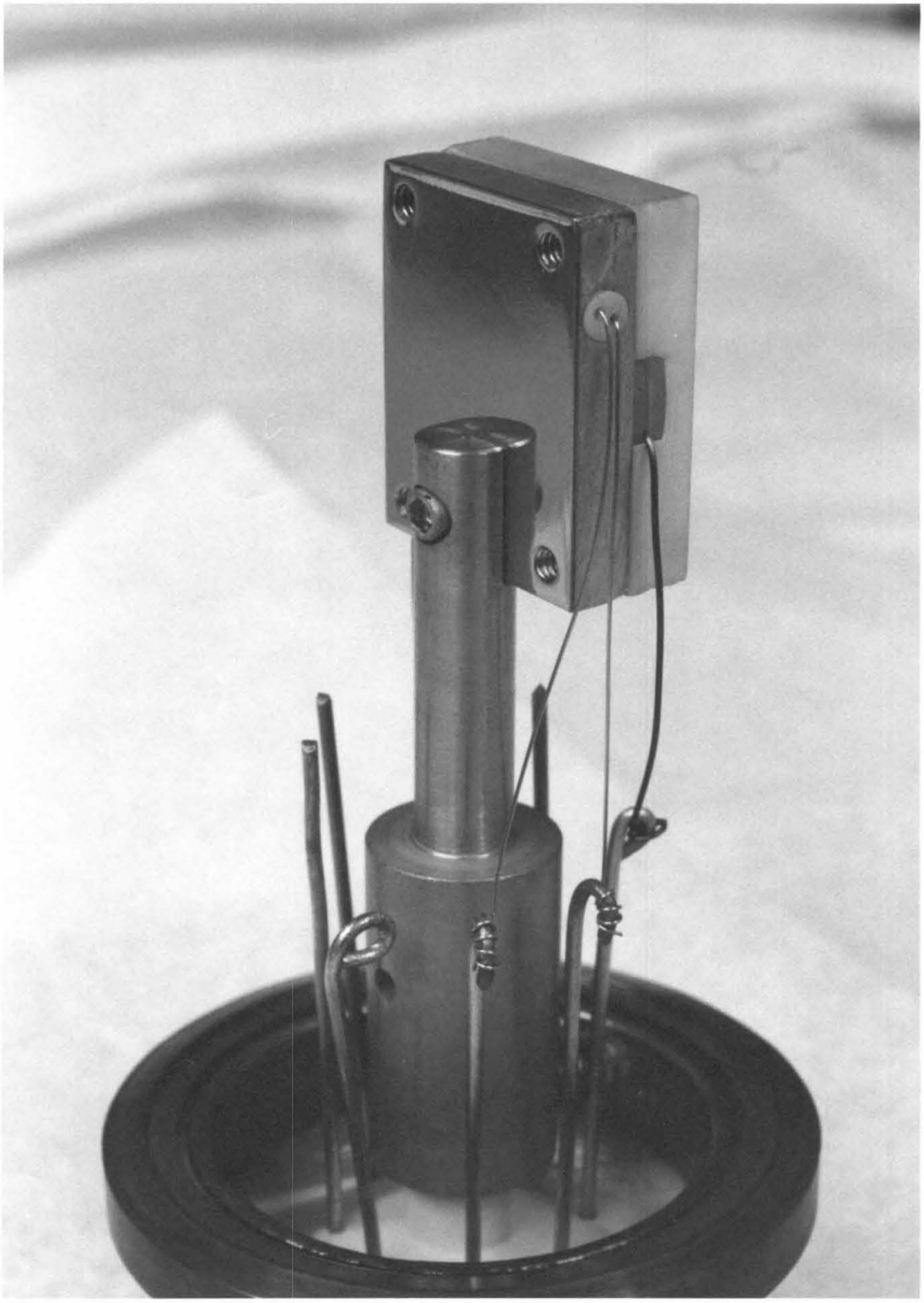

Figure 29

Figure 30

Schematic drawing of the target for UF_4 sputtering shown in Fig. 29. The thermocouple and tungsten heater are electrically insulated from the copper block. Charge is collected from the target with a connection to the support post, which is not visible in the drawing (see Section III.E.3).

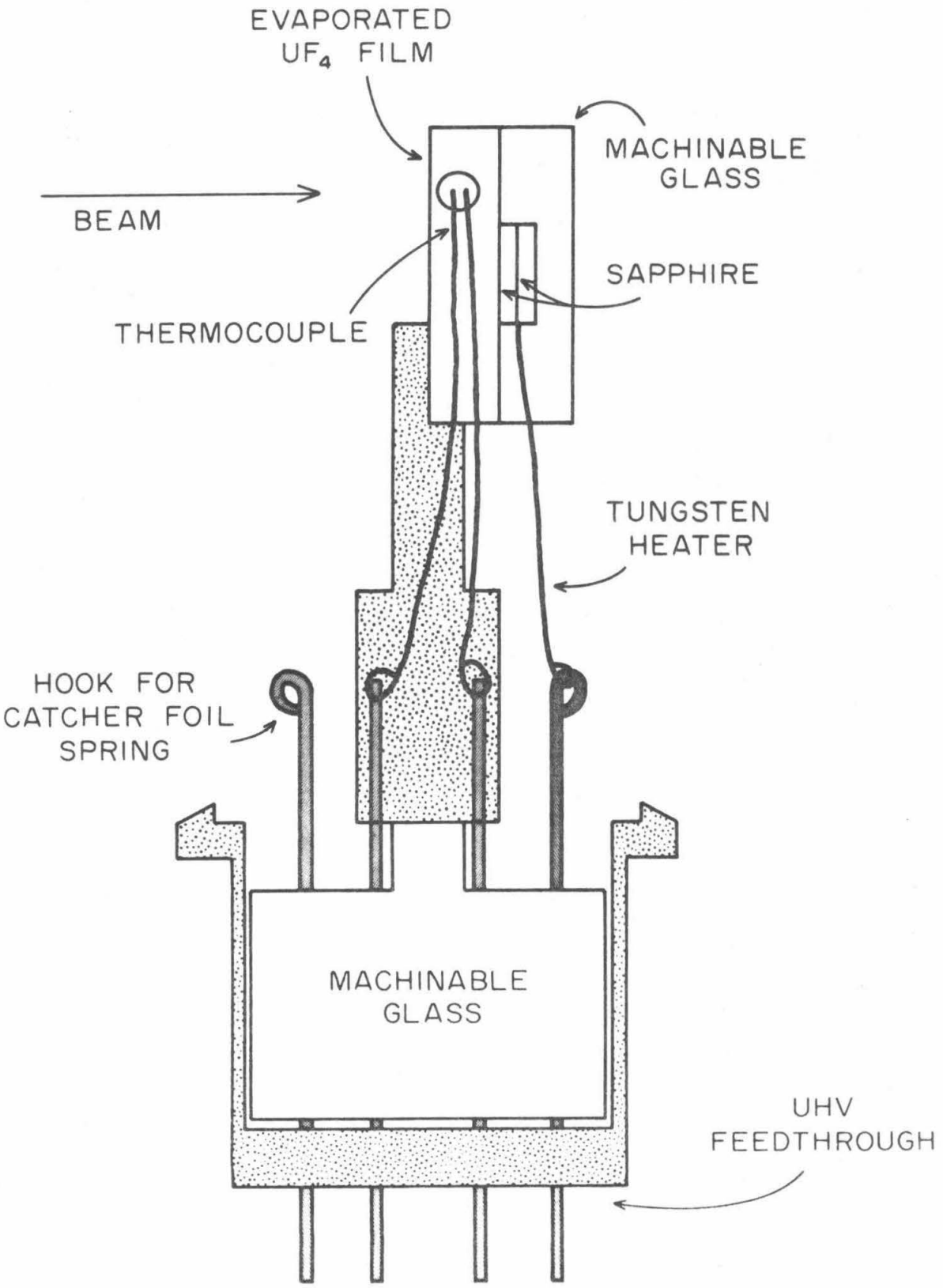
EVAPORATED
UF4 FILM
MACHINABLE
GLASS
BEAM
SAPPHIRE
THERMOCOUPLE
TUNGSTEN
HEATER
HOOK FOR
CATCHER FOIL
SPRING
MACHINABLE
GLASS
UHV
FEEDTHROUGH

Figure 30

Figure 31

Angular distribution of ^{235}U atoms sputtered from a UF_4 film with 4.75 MeV $^{19}F(+3)$. This run produced a uranium yield of 8.2, the highest we ever observed. The fit is $\cos^{.81}\theta$, which was probably flattened somewhat by target misalignment. The scatter in the data is typical of the results from the UF_4 targets (see Section III.E.4).

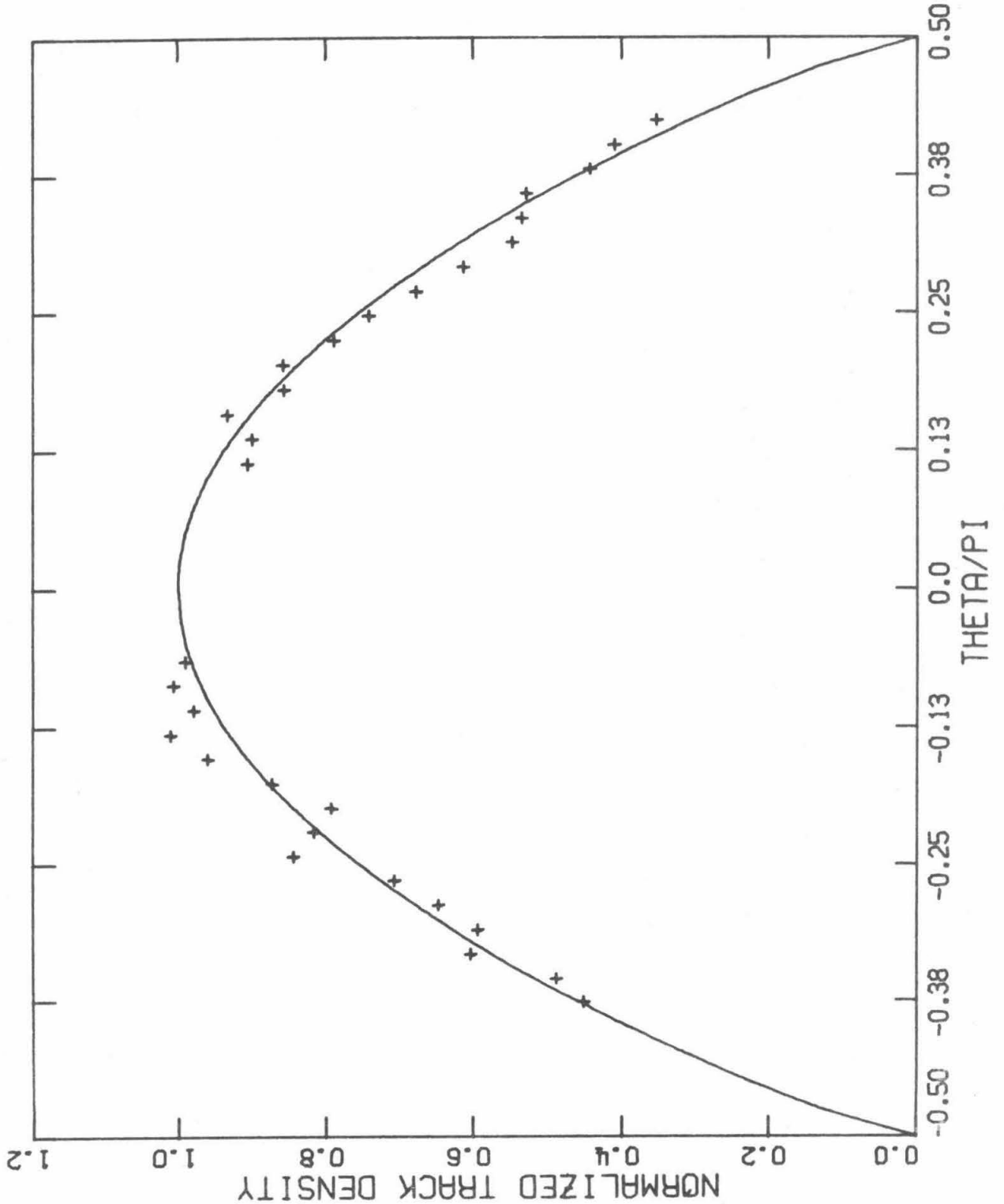
NORMALIZED TRACK DENSITY
0.0
0.2
0.4
0.6
0.8
1.0
1.2
THETA/PI
-0.50
-0.38
-0.25
-0.13
0.0
0.13
0.25
0.38
0.50

Figure 31

Figure 32

Sputtering yield of uranium produced by ^{19}F incident on UF_4. The electronic stopping curve was calculated from the tables of Northcliffe and Schilling (1970) with the Bragg rule. The numbers used are shown in Table 10. The numbers beside the data points indicate the charge state of the incident beam. The error bars correspond to the standard deviations of the measured yields in those cases for which more than one run was performed. The points without error bars represent single runs (see Section III.E.4).

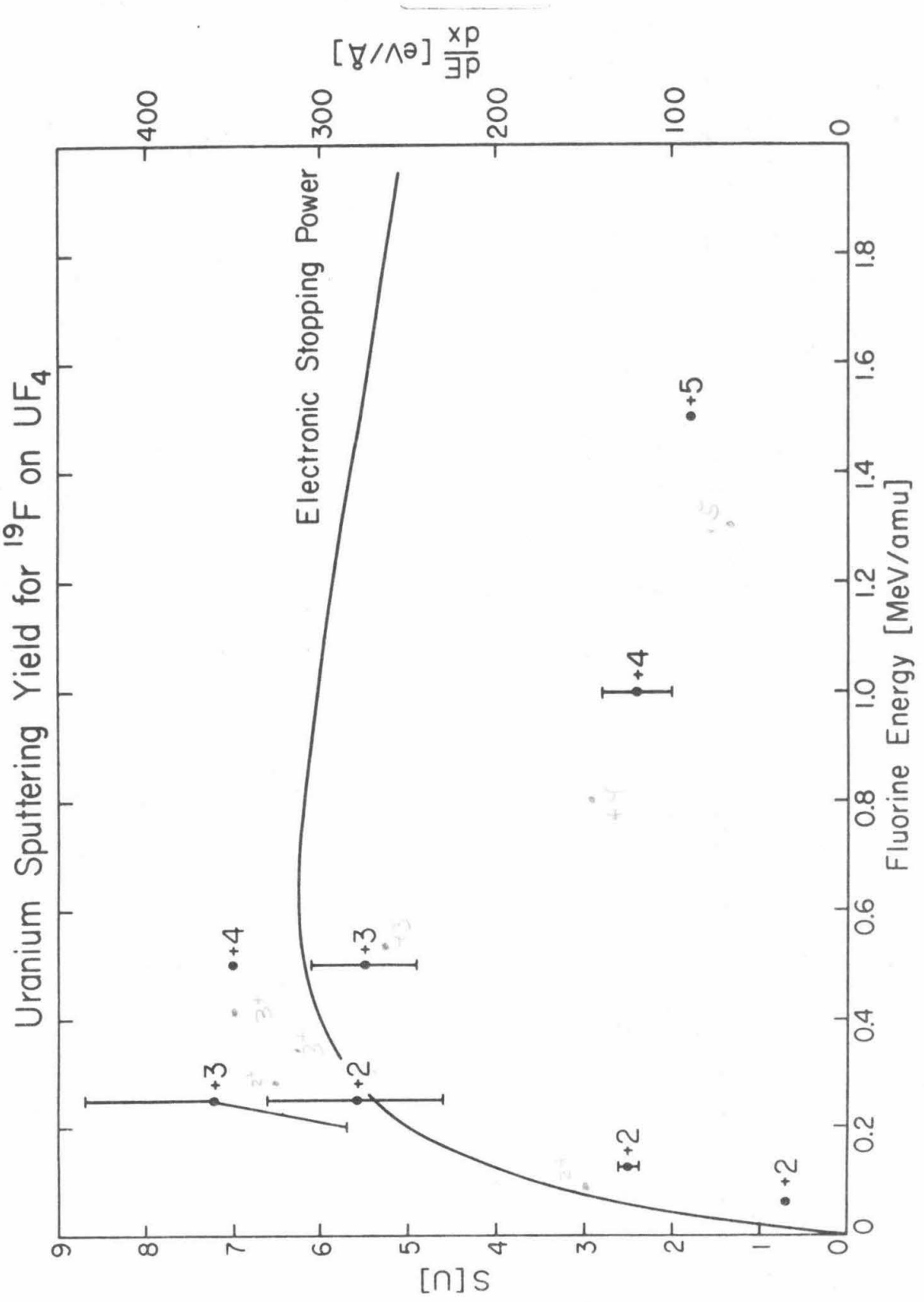
Uranium Sputtering Yield for ^{19}F on UF_4
Electronic Stopping Power
S[U]
$\frac{dE}{dx}$ [eV/Å]
Fluorine Energy [MeV/amu]
+2
+3
+4
+5

Figure 32

Figure 33

UHV chamber used in the energy spectrum experiments. The target was mounted on the bellows, and a sliding contact allowed the beam current to be collected from the electrical feedthrough. The 11 l/s ion pump was used in Run II only (see Section III.E.5).

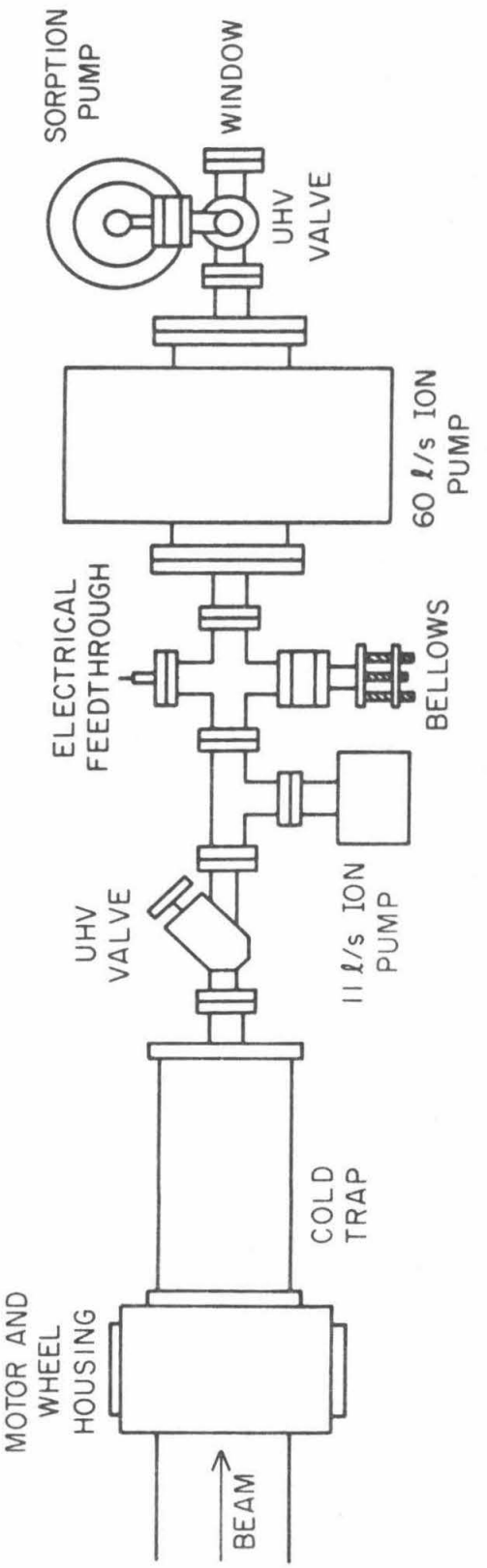
SORPTION PUMP
WINDOW
UHV VALVE
60 ℓ/s ION PUMP
ELECTRICAL FEEDTHROUGH
BELLOWS
UHV VALVE
11 ℓ/s ION PUMP
COLD TRAP
MOTOR AND WHEEL HOUSING
BEAM

Figure 33

Figure 34

Arrival time spectrum for the UF_4 target irradiated with +300 V bias on the target. The wheel had two slots, which produce two identical spectra. If we assume that the counts in the two peaks correspond to atoms accelerated by the target potential, then we obtain a charged fraction of 47%. The yield is expressed in arbitrary units. The energy spectrum produced by this arrival time spectrum is shown in Fig. 38 (see Section III.E.5).

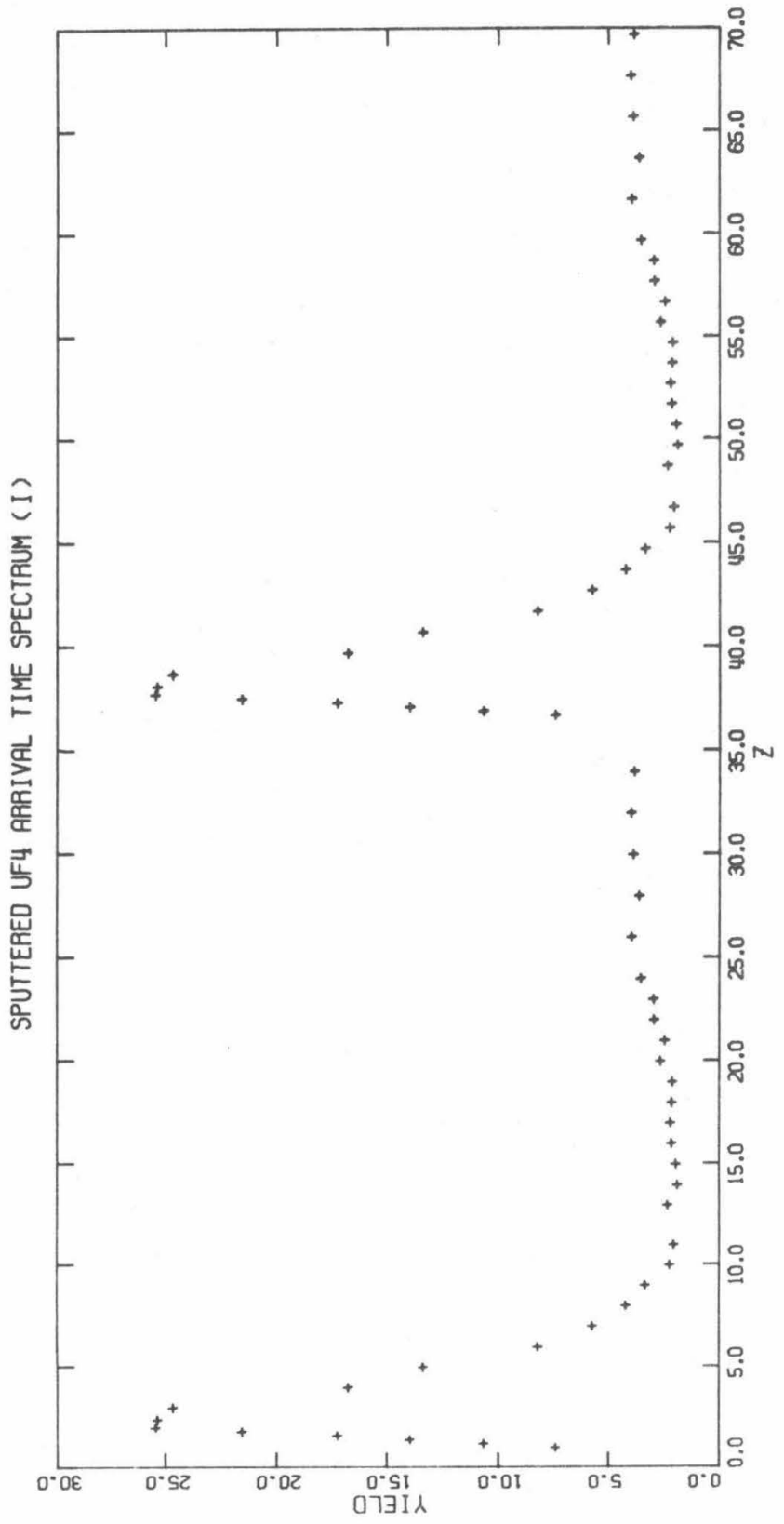
SPUTTERED UF4 ARRIVAL TIME SPECTRUM (I)
YIELD
0.0
5.0
10.0
15.0
20.0
25.0
30.0
Z
0.0
5.0
10.0
15.0
20.0
25.0
30.0
35.0
40.0
45.0
50.0
55.0
60.0
65.0
70.0

Figure 34

Figure 35

Arrival time spectrum for the UF_4 target irradiated with no bias on the target. The wheel used had only one slot. The yield is expressed in arbitrary units. The corresponding energy spectrum is displayed in Fig. 39 (see Section III.E.5).

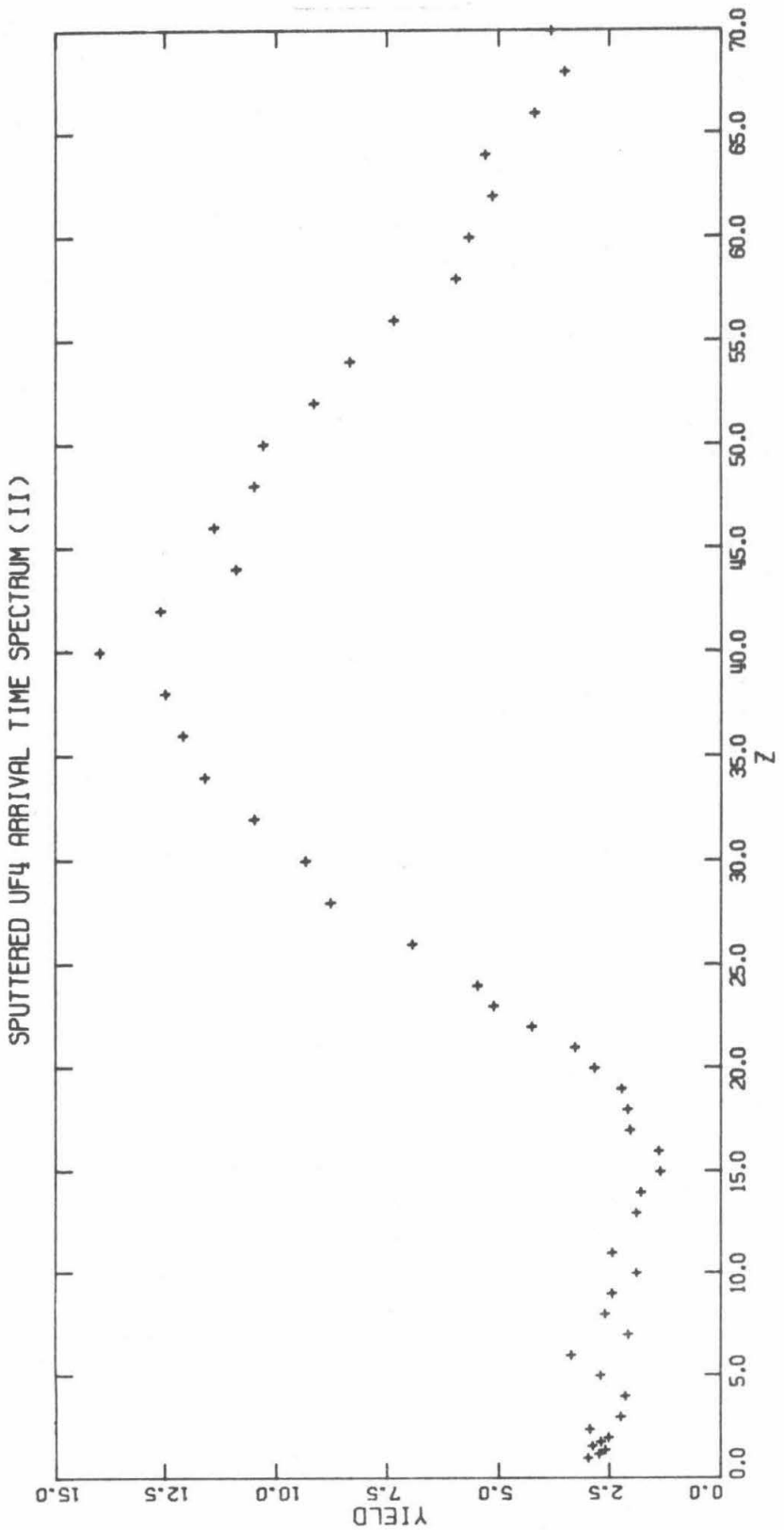
SPUTTERED UF4 ARRIVAL TIME SPECTRUM (II)
YIELD
0.0
2.5
5.0
7.5
10.0
12.5
15.0
Z
0.0
5.0
10.0
15.0
20.0
25.0
30.0
35.0
40.0
45.0
50.0
55.0
60.0
65.0
70.0

Figure 35

Figure 36

Energy spectrum for Run I in which the target was biased at +300 V. The shoulder corresponding to the energies above 10 eV was produced by the accelerated particles (see Section III.E.5).

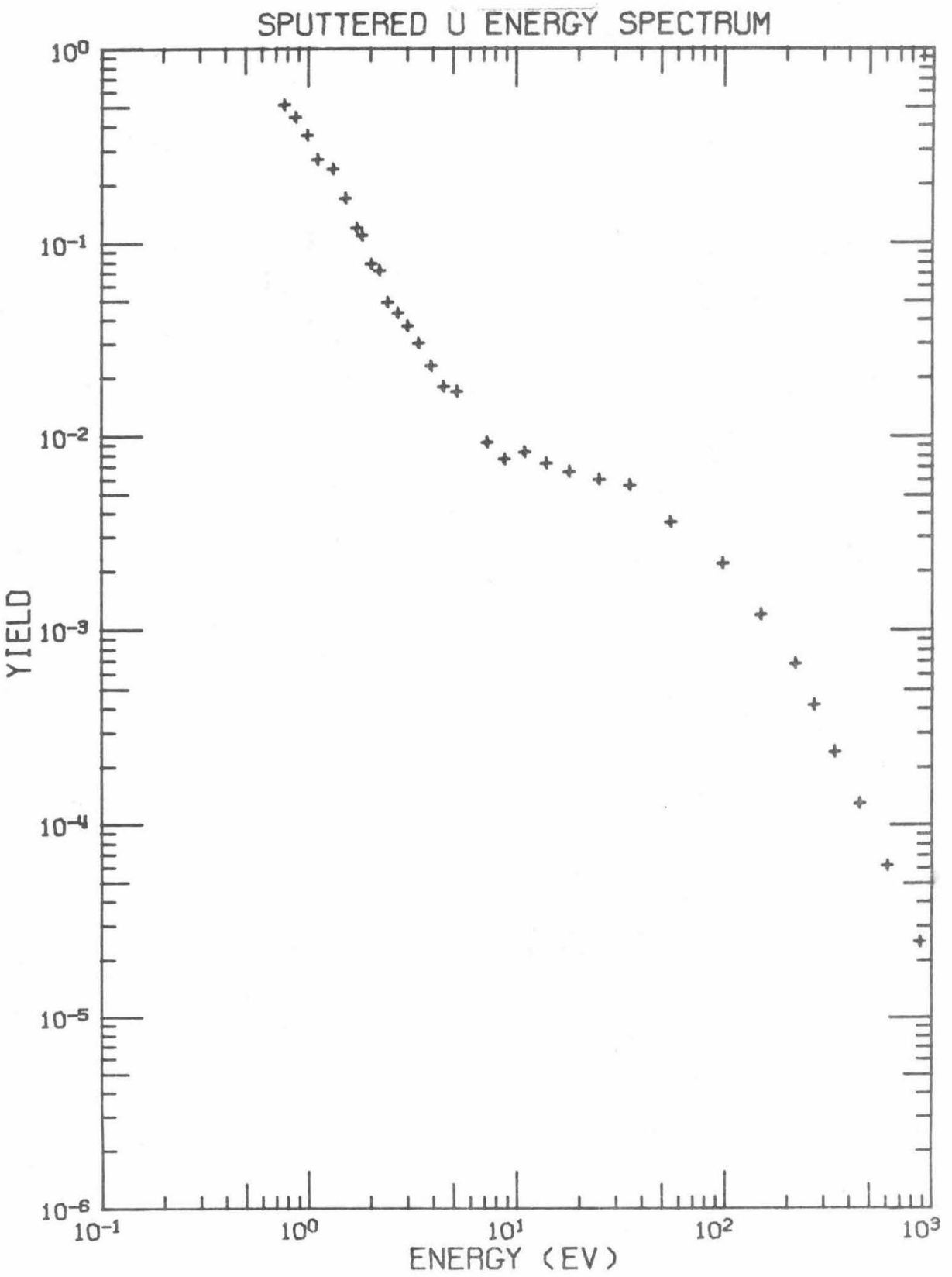
SPUTTERED U ENERGY SPECTRUM
YIELD
ENERGY (EV)
10^0
10^-1
10^-2
10^-3
10^-4
10^-5
10^-6
10^-1
10^0
10^1
10^2
10^3

Figure 36

Figure 37

Energy spectrum from Run II in which the target was not biased. The points at energies above 5 eV are not reliable. We believe that the yield was enhanced by very low energy particles produced by the beam pulse from the previous cycle of the wheel (see Section III.E.5).

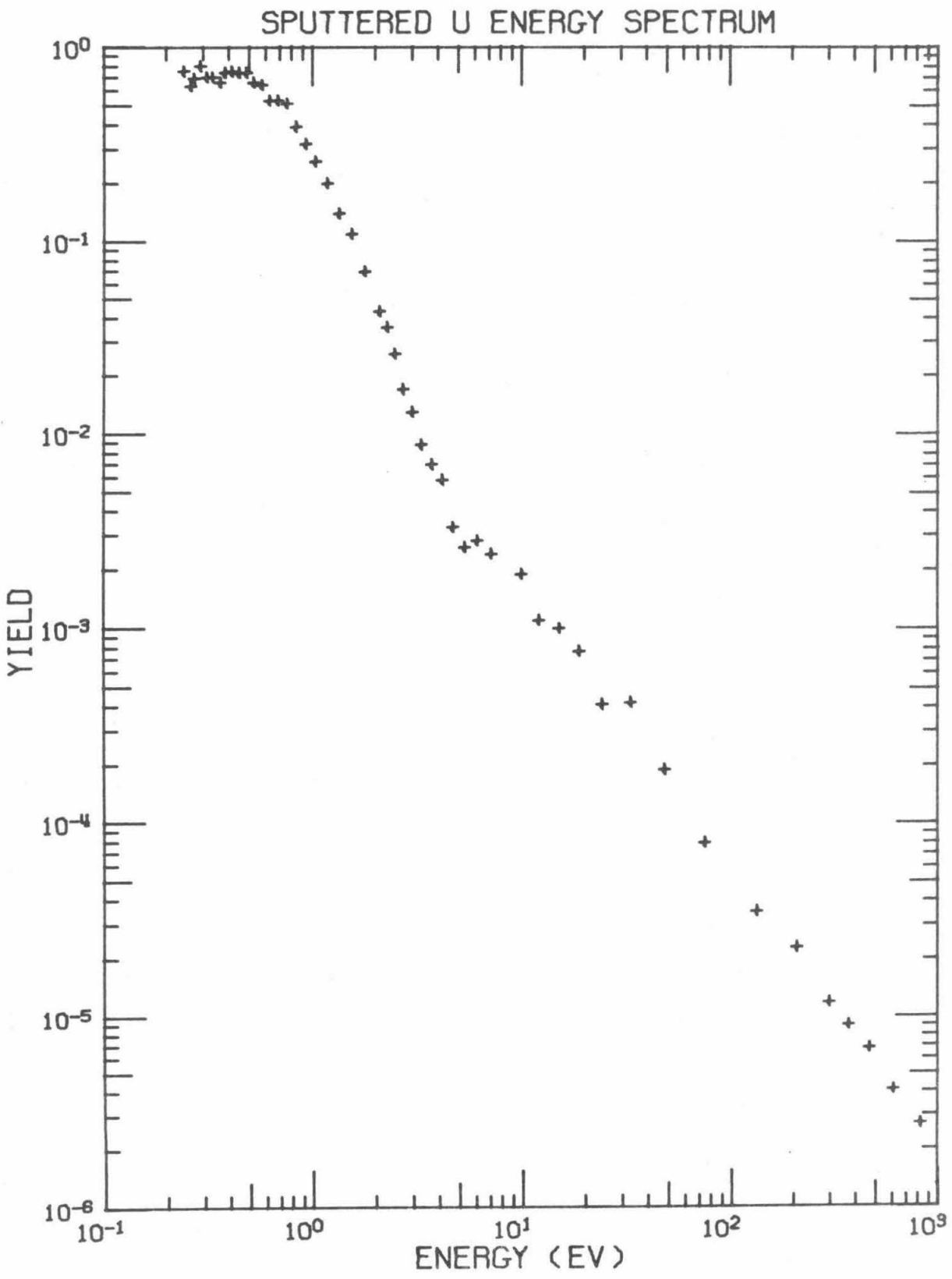
SPUTTERED U ENERGY SPECTRUM
YIELD
ENERGY (EV)
10^0
10^-1
10^-2
10^-3
10^-4
10^-5
10^-6
10^-1
10^0
10^1
10^2
10^3

Figure 37

Figure 38

A two parameter fit to the data from Run II using the Maxwell-Boltzmann distribution:

$$1.7 \times 10^{7} \; E^{\frac{1}{2}} \exp(-E/.62 \text{ eV}) ,$$

which corresponds to 7000°K (see Section III.E.5).

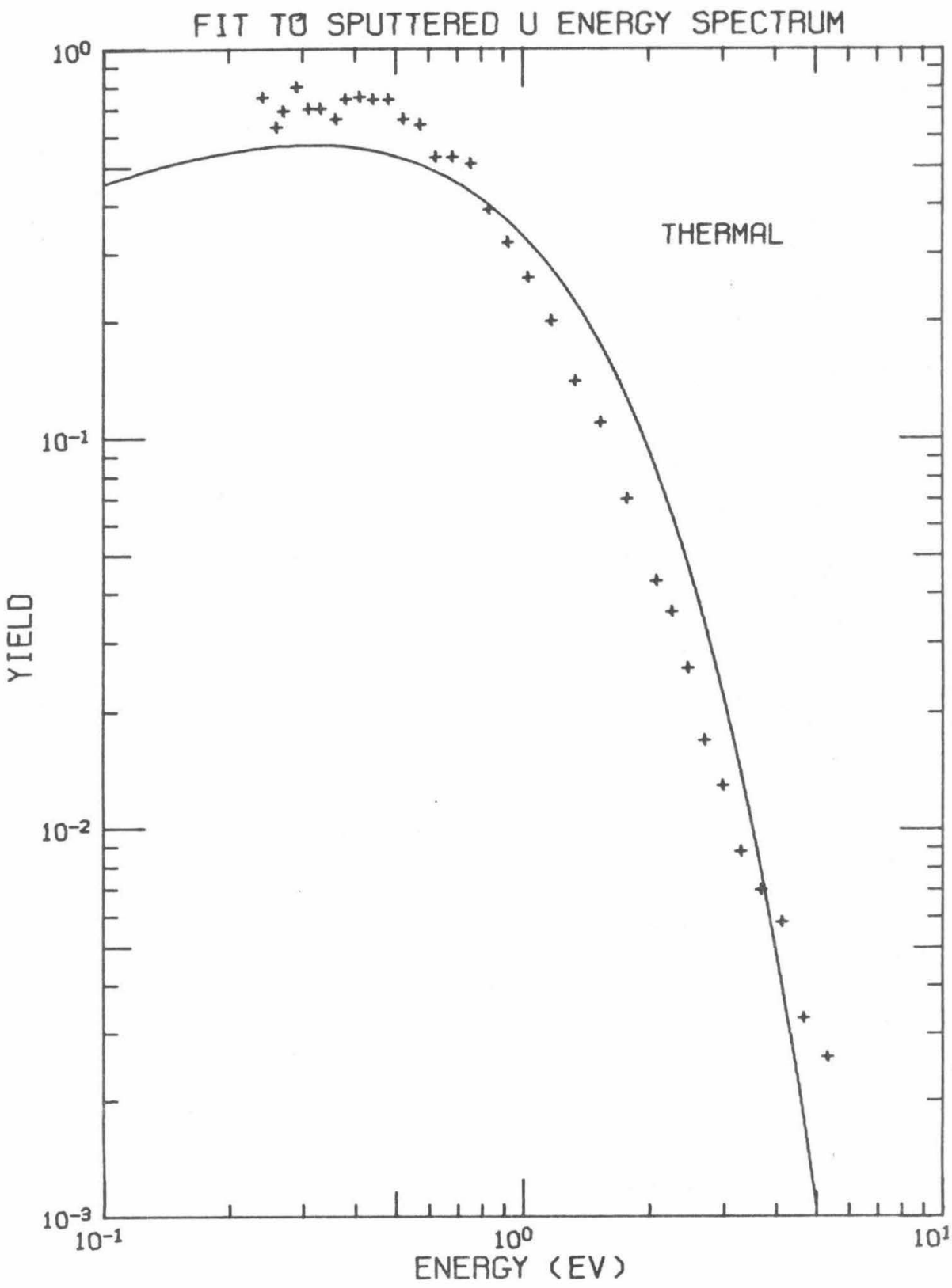
FIT TØ SPUTTERED U ENERGY SPECTRUM
THERMAL
YIELD
ENERGY (EV)
10^0
10^-1
10^-2
10^-3
10^-1
10^0
10^1

Figure 38

Figure 39

A three parameter fit to the data from Run II using the collision cascade distribution:

$$3.1 \times 10^{8} \frac{E}{(E + 1.2\ eV)^{6.1}}$$

(see Section III.E.5).

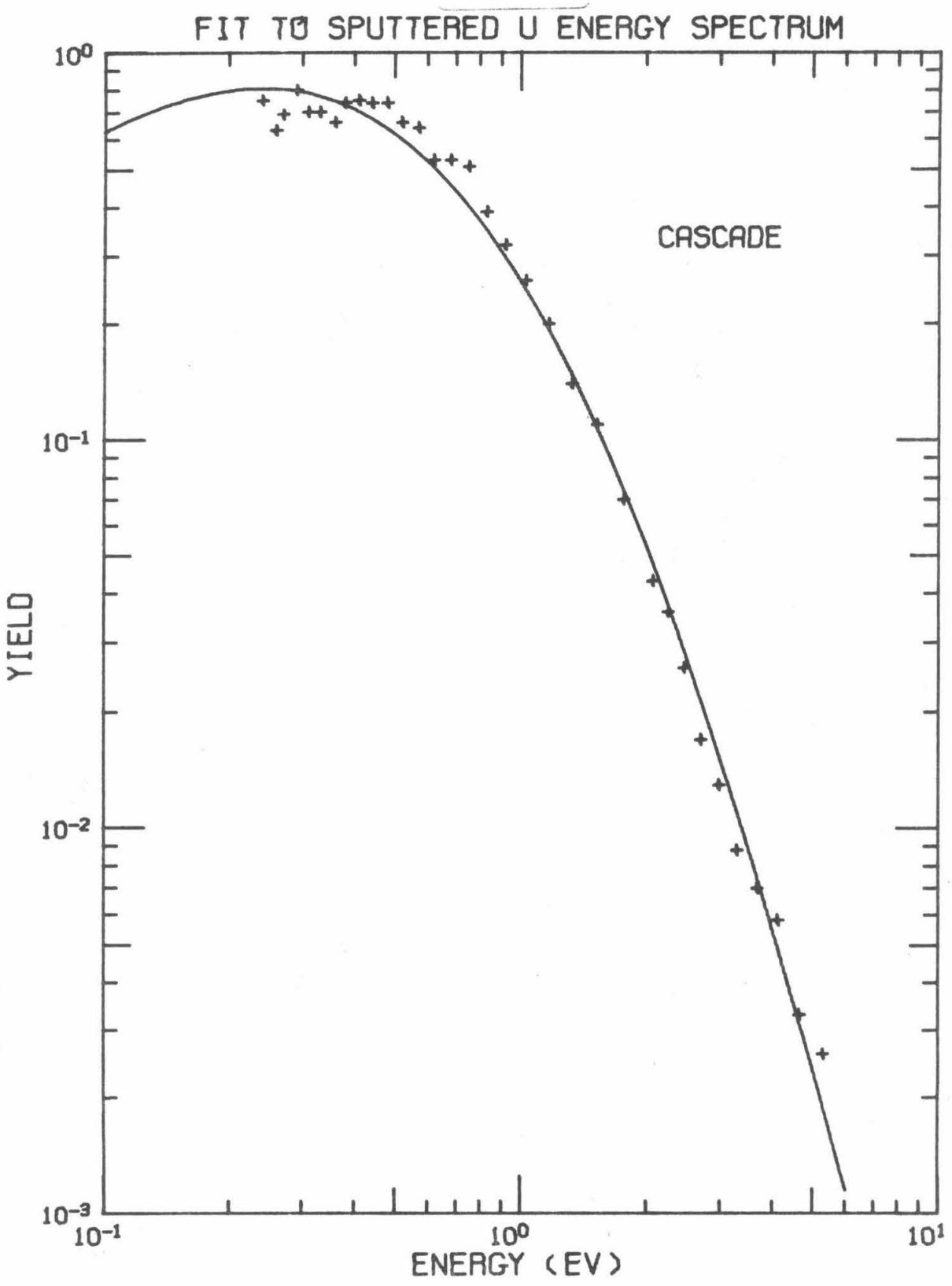
FIT TO SPUTTERED U ENERGY SPECTRUM
CASCADE
YIELD
ENERGY (EV)
10^{0}
10^{-1}
10^{-2}
10^{-3}
10^{-1}
10^{0}
10^{1}

Figure 39